GROWTH AND CHARACTERIZATION OF ORGANIC AND SEMI-ORGANIC NONLINEAR OPTICAL SINGLE CRYSTALS

A dissertation submitted to the Department of Physics of Bangladesh University of Engineering and Technology in partial fulfillment of the requirements for the award of the degree of Doctor of Philosophy (Ph.D.) in Physics

by

Ferdousi Akhtar
Roll No. P10061406F
Session: October 2006

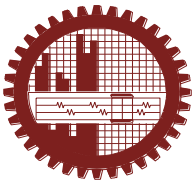

Department of Physics
Bangladesh University of Engineering and Technology
Dhaka – 1000

October 2011

CANDIDATE'S DECLARATION

It is hereby declared that this thesis or any part of it has not been submitted elsewhere for the award of any degree or diploma.

_____

Signature of the Candidate

Name of the Candidate: **Ferdousi Akhtar**

DEDICATED

TO

My Mother

Acknowledgements

I am extremely delighted to express my indebtedness and deepest sense of gratitude to my supervisor **Prof. Dr. Jiban Podder**, Department of Physics, Bangladesh University of Engineering and Technology (BUET), Dhaka, for his keen interest, sincere help, indispensable guidance, and constant encouragement throughout the progress of this research work.

I am very much grateful to **Prof. Dr. Md. Mostak Hossain,** Head, Department of Physics, BUET, for showing keen interest and useful discussions in various stages of this work.

I am also grateful to **Prof. Dr. Nazma Zaman**, **Prof. Dr. Md. Abu Hashan Bhuiyan, Prof. Dr. Md. Feroz Alam Khan, Prof. Dr. A. K. M. Akther Hossain, Associate Prof. Mrs. Fahima Khanam and Dr. Afia Begam**, Department of Physics, BUET, Dhaka, for their valuable suggestions, kind co-operation and inspiration in various experimental parts of this research work.

I express my indebtedness to **Dr. Dilip Kumar Saha, C.S.O., Mr. Harinarayan Das, S.O. and Mr. Md. Al-Mamun, S.O.**, Materials Science Division, Atomic Energy Center, Dhaka, for their generous help in taking XRD patterns and EDX spectra.

I am very much grateful to **Dr. A. K. M. Abdul Hakim**, Materials Science Division, AECD. I am also grateful to the Department of MME, BUET and the department of PP&PDC, BCSIR for their helpful assistance in utilizing some facilities.

I am thankful to all other teachers of the Department of Physics, BUET for showing interest in this thesis work. I am very much thankful to all staff of the department of Physics, BUET, for their sincere co-operation to my research work.

I am very happy to extend my sincere thanks to my husband **Prof. Dr. Rezaul Karim Siddique**. Department of Physics, American International University Bangladesh (AIUB) and my affectionate child **Faizah Siddique** for their patience and co-operation during the period of this research work. They have sacrificed many pleasant moments for me during this period.

I am thankful to all Ph. D. and M. Phil. students in the Department of Physics, BUET, Dhaka, for their valuable discussions, suggestions and kind co-operation in various experimental parts of this research work.

Finally, I am thankful to the authority of BUET to accept this research proposal and providing financial support to carry out this research work and to all honorable members of the doctoral committee for giving valuable suggestions and guidance through out this research work.

Abstract

Crystals of Ammonium Dihydrogen Phosphate (ADP), Potassium Dihydrogen Phosphate (KDP), Potassium Acid Phthalate (KAP) and Amino Acid L-alanine (LA) are the best nonlinear optical (NLO) materials increasingly being used for second harmonic generation, frequency doubling of Neodium : Yttrium-aluminium garnet (Nd-YAG) laser and also in electro-optical applications. The typical functions of these materials are to modulate carrier waves, to amplify and to rectify signals and acts as very fast switch. Though KDP and ADP have all essential qualities but these suffer from relatively low electro-optic coefficients. The electro-optic coefficient of these crystals mainly originates from their P-O bonds. The electro-optic properties of these crystals can be improved by the replacement of K^+ by NH_3^+ or COO^- ion of the LA materials. LA has a Zwitterionic nature of the molecule ($^+NH_3 – C_2H_4 – COO^-$), which favors the way for possessing high electro-optic parameters and good mechanical and thermal stability of the crystals. The KAP is a noncentrosymmetric molecular ionic crystal. It is widely used in the field of X-ray spectroscopy as monochromator and also as analyzer. So it would be a good approach for improving the electro-optic properties of the LA doped ADP, KDP and KAP crystals.
The growth of pure LA and LA doped ADP, KDP and KAP crystals with different concentrations (such as 0.3, 0.5, 0.7 and 1.0 mol% of LA) by slow evaporation method at room temperature are discussed. The solubility of pure LA, pure and LA doped ADP, KDP and KAP was determined at different fixed temperatures (viz. 30, 35, 40, 45 and 50 ^0C) in a constant temperature bath maintained with an accuracy of ±0.01 ^0C. It is found that the solubility is increased with temperature but it is decreased with doping concentration. The metastable zone width of pure LA first decreased and then increased with increasing temperature. A colorless large size crystal with dimensions 17 x 5 x 3 mm^3 of pure LA was harvested in 30 days. Large size (such as 25 x 10 x 5 mm^3) transparent pure and doped ADP, KDP and KAP crystals have been grown in 35 days by a slow solvent evaporation method. The grown crystals were subjected to characterize structurally, optically, thermally, mechanically and electrically by various experimental studies.

The structural investigations were performed by Fourier Transform Infrared (FTIR) Spectroscopy, Energy Dispersive X-ray (EDX) Spectroscopy and powder X-ray Diffraction (XRD). Functional groups of pure and doped crystals were confirmed by FTIR analysis. The presence of the elements as atomic percent in the pure and doped crystals was confirmed by EDX analysis. The XRD studies confirmed the structure of all grown crystals. The presence of LA doping has marginally altered the lattice parameters without affecting the basic structure of crystals.

UV-Visible studies for pure and doped crystals have sufficient transmission in the entire visible region. The transmittance of doped crystals was increased with doping concentration of LA. The good transmission of the crystals in the entire visible region suggests the suitability for second harmonic generation devices. Optical quality of the crystals was studied by UV-Visible spectroscopy. The values of optical parameters were calculated from transmittance data.

The thermal behavior of the grown crystals was investigated by Differential thermal analysis (DTA) and Thermogravimetric analysis (TGA). DTA and TGA results reveal that the substitution of amino acid dopants slightly increases the decomposition temperature of all the selected crystals. The thermal studies also reveal that the LA doped crystals are thermally stable compared to the pure crystals. Different thermodynamic parameters of pure LA were calculated from the TGA data.

DC electrical conductivity of the crystals was measured at various temperatures ranging from 35 to 140 ^{0}C by conventional two probe method. AC electrical conductivity and dielectric properties of pure and doped KDP crystals were measured by LCR meter at various temperatures ranging from 35 to 140 ^{0}C at constant frequency 1 kHz. DC electrical conductivity of pure LA, pure and doped ADP and KAP increases with temperature and also with doping concentration. AC electrical conductivity of pure and doped KDP crystals increases with temperature and decreases with doping concentration. Dielectric constant and dielectric loss of pure and doped KDP crystals were decreased with temperature and also with doping concentration.

Mechanical microhardness of the grown crystals was studied by the Vicker's microhardness indentation measurements. Microhardness measurements were made using

a Leitz microhardness tester fitted with a diamond pyramidal indenter. The applied load was varied from 25 to 100 g for a constant indentation period of 7 s for all indentations. It is observed that the Vicker's Hardness number of the crystals decreases with increasing load and the pure crystals are harder than doped crystals.

The surface morphology such as crystal symmetry and lattice defects of the pure and doped crystals was studied by etching 10 s in water. When a surface is etched, well defined etch patterns were produced at the dislocation sites. Etching studies revealed the growth mechanism and to assess the perfection of the grown crystals of pure and doped ADP, KDP, KAP and pure LA crystals.

LIST OF CONTENTS

3. GROWTH AND CHARACTERIZATION OF PURE L-ALANINE CRYSTAL

4. GROWTH AND CHARACTERIZATION OF L-ALANINE DOPED AMMONIUM DIHYDROGEN PHOSPHATE (ADP) CRYSTALS

5. GROWTH AND CHARACTERIZATION OF L-ALANINE DOPED POTASSIUM DIHYDROGEN PHOSPHATE (KDP) CRYSTALS

6. GROWTH AND CHARACTERIZATION OF L-ALANINE DOPED POTASSIUM ACID PHTHALATE (KAP) CRYSTALS

7. SUMMARY AND SUGGESTIONS FOR FUTURE WORK

LIST OF FIGURES

LIST OF TABLES

LIST OF SYMBOLS AND ABBREVIATIONS

SYMBOLS

C	Concentration of solution
C^*	Equilibrium concentration of the solution
ΔG	Change in Gibbs free energy
ΔG_s	Change in surface free energy
ΔG_v	Change in volume free energy
P	Polarization
n	Refractive index
$\chi^{(1)}$, $\chi^{(2)}$, $\chi^{(3)}$	First, second, and third order nonlinear susceptibility tensors
r	Radius of the spherical nucleus
γ	Interfacial tension
r^*	Radius of the critical nucleus
V	Molar volume of the crystal
K	Boltzmann's constant
T	Temperature of the solution in K
S	Super saturation ratio
i^*	Number of molecules in the nucleus
r_c	Critical nucleus size
t_{ind}	Induction period
C_0	Solubility limit

ABBREVIATIONS

MSZW	Metastable Zone width
NLO	Non Linear Optical
SHG	Second Harmonic Generation
THG	Third Harmonic Generation
SFM	Some Frequency Mixing
Nd-YAG	Neodymium doped Yttrium Aluminium Garnet
FTIR	Fourier Transform Infrared Spectroscopy
XRD	X-ray Diffraction
EDX	Energy Dispersive X-ray
UV-Vis-NIR	Ultraviolet – Visible – Near Infrared
DTA	Differential Thermal Analysis
TGA	Thermogravimetric Analysis
LA	L-alanine
ADP	Ammonium Dihydrogen Phosphate
KDP	Potassium Dihydrogen Phosphate
KAP	Potassium Acid Phthalate

Chapter 1

AN INTRODUCTION TO NONLINEAR OPTICAL CRYSTALS AND LOW TEMPERATURE SOLUTION GROWTH TECHNIQUE

Chapter 1

AN INTRODUCTION TO NON LINEAR OPTICAL CRYSTALS AND LOW TEMPERATURE SOLUTION GROWTH TECHNIQUE

1.1 Introduction

The beauty of crystals has always been fascinating. The enchanting colors, the smooth surfaces with scintillating reflections of light, the definite and varied shapes with sharp edges, the deep transparency of some perfect crystals, all together aroused the aesthetic sense of the man who used that as an ornament. Parallel with the growth of other sciences, grew the curiosity of mankind to understand, more quantitatively the characteristics of nonlinear optical (NLO) crystal. The utility of crystals were extended from the bounds of ornaments to several useful applications in optical, electrical and opto-electronic devices. The fantasy of their external beauty was understood more thoroughly through the natural laws of mathematics, physics and chemistry. The contents of the crystal and their insides were explored, analyzed and understood by modern methods of diffraction as well as with the help of spectroscopic techniques. The external shapes, planes and colors were correlated with the internal atomic content and their arrangements in unequivocal terms. Thus grew a science: the study of "crystal growth and characterization".

Crystal is a homogeneous solid with a definite chemical composition and ordered atomic arrangement, bounded by naturally-formed plane faces. In the crystal the atoms are arrange in such a way that their positions are exactly periodic. Crystals are classified into two categories: single crystals and polycrystals.

A single crystal is constructed by the infinite repetition of identical structural units. In the simplest crystals such as copper, silver, iron, aluminum and the alkali metals, the structural unit is a single atom. The perfect ordering in the single crystals gives rise to

many of the physical properties of crystals such as ferromagnetism, birefringence, piezo-electricity etc.

A poly crystal is an aggregate of crystals which might or might not be of different kinds, generally irregularly shaped and interlocked together at the boundaries of contact. Organic NLO materials with high non linear susceptibilities have in-adequate transparency, poor optical quality, and lack of robustness, high laser damage threshold and inability to grow into large size have impeded the use of single crystal organic materials in practical device applications.

Inorganic materials have excellent mechanical and chemical properties but are often of limited use because they possess low nonlinear coefficients or difficult and expensive to grow. Semi-organic crystals have the potential for combining the high optical nonlinearity and chemical flexibility of organics with the physical ruggedness of inorganic materials.

1.2 Nonlinear Optical Materials

Nonlinear optical (NLO) materials have acquired new significance with the advent of a large number of devices utilizing semiconductor and solid-state laser sources. The NLO materials have vast applications for obtaining tunable laser beams from fixed wavelength or tunable laser sources by the principle of harmonic generation. Second harmonic generation (SHG) and third harmonic generation (THG) and some frequency mixing (SFM) can be used for frequency up conversion. Physicists and engineers have been on the look out for new materials which have larger second harmonic coefficients and larger figures of merit [2, 8].

Inorganic crystals like KDP, ADP, KTP and β-BaB_2O_4 are the best nonlinear optical materials increasingly being used for the SHG, frequency doubling of Nd-YAG laser and also in electro-optical applications. The supersonic crystals like silicates, germinates, phosphates and tungstates built of octahedral and tetrahedral form a major group of fast ionic conductors after the discovery of a 3-dimensional ionic conductor [14].

Organic crystals show a complex range of phase behavior, photo and thermal stability, solubility and morphology. The rapid development of optical communication systems has led to a demand for NLO materials of high structural and optical quality. The most widely encountered crystals for this type of application are urea, thiourea, MNA, POM etc [5]. The perfect organic crystal should have high efficiency, low absorption edge cut-off and high damage threshold.

The advantages of organic nonlinear materials are:

i) High second-order nonlinear optical efficiency
ii) High damage threshold
iii) Birefringence used for phase matching

There are a number of properties, particularly relevant to the crystal growth, which is common to many organic materials. Firstly, the intermolecular forces are comparatively weak, being predominantly Vander Waals forces or permanent dipole-dipole interactions. Due to the technological importance of these nonlinear crystals, the need for high quality organic crystals has grown dramatically in the last decade [13].

Enormous studies have been devoted to inorganic crystals in comparison to the organic crystals, where problems arise due to the polar nature of the nonlinear optical material. The growth of crystals is problematic due to the solvent and solute interaction. A comparison of general crystal growth characteristics of organic and inorganic crystals is shown in Table 1.1.

Table 1.1 Characteristics of organic and inorganic single crystals

Characteristics	Organic crystals	Inorganic crystals
Chemical nature	Covalently bonded molecules	Salts composed of charged inorganic ions
Solubility	Soluble in a wide variety of organic solvents	Soluble in water
Sensitivity to pH and ionic strength	None	Sensitive
Thermal properties	Stable up to melting point between 50^0-150^0C	Highly thermally stable
Size of the crystal	0.1-100 mm^3, from common crystal growth methods	No size limit for many inorganic compounds
X-ray diffraction quality	Good-moderate, excellent	Excellent
Mechanical strength	Fair-good	Extremely good

1.3 Basic Principle of Linear and Nonlinear Optics

In a dielectric material the influence of an electric field causes changes in the spatial distribution of the electrons and the nuclei. These distortions create electric diploes, which in turn manifest as polarization.

The resultant electric dipole moment per unit volume is called polarization. At very low external fields, polarization P is directly proportional to the electric field:

$$P = \varepsilon_0 \chi E$$

Where ε_0 is the permittivity of free space, and χ denotes the linear susceptibility tensor, related to the refractive index n by the following equation

$$n^2 = 1 + \chi$$

The oscillating input electromagnetic field forces the dipoles to oscillate, and these induced oscillating dipoles re-radiate. However, at intense electric fields, the induced polarization is no longer linearly proportional to the field. As a result, the re-radiation

from the oscillating dipoles differs in amplitude and phase with respect to the incident sinusoidal electric field. As a consequence, the reradiated wave contains, in addition to the fundamental frequency, different other frequencies as well.

The nonlinear response of the dielectric can be expressed as follows:

$$P_i = \varepsilon_0 (\chi_{ij}^{(1)} E_j + \chi_{ijk}^{(2)} E_j E_k + \chi_{ijkl}^{(3)} E_j E_k E_l + - - -)$$

Where $\chi^{(1)}$, $\chi^{(2)}$ and $\chi^{(3)}$, etc. are the first, second, third order, etc. nonlinear susceptibility tensors.

The magnitude of the tensor components rapidly decreases with increasing rank of nonlinearity ($\chi^{(1)} : \chi^{(2)} : \chi^{(3)} \approx 1 : 10^{-8} : 10^{-16}$). Thus it is not surprising that the exploitation of most of the nonlinear optical effects was not possible prior to the invention of lasers.

The linear term is responsible for the refractive index, dispersion, birefringence and absorption. $\chi^{(2)}$ in the quadratic term describes second harmonic generation, optical mixing, and optical parametric oscillation. $\chi^{(3)}$ in the cubic term is responsible for the occurrence of phenomena such as stimulated Raman scattering, third harmonic generation, phase conjugation, and optical bistability.

$$P = \varepsilon_0 (\chi^{(1)} E \cos \omega t + \chi^{(2)} (E \cos \omega t)^2 + \chi^{(3)} (E \cos \omega t)^3 + —)$$

Suppose we assume that a monochromatic electromagnetic (e.m.) radiation (E cos ωt) is incident on a material, and the frequency of this e.m. radiation is higher than that of the ionic vibrations. In that case the e.m. wave exerts force mainly on the valence electrons of the medium and results in polarization that is dependent on the electric field as follows. This equation can be written as,

$$P = \varepsilon_0 (\chi^{(1)} E \cos \omega t + \chi^{(2)} \frac{E^2}{2} (1 + \cos 2\omega t) + \chi^{(3)} \frac{E^3}{4} (\cos 3\omega t + 3 \cos \omega t) + -)$$

The first term of the above equation is a linear term and corresponds to an oscillation that follows the incident light and thus reradiates the e.m. wave at the same frequency. The

higher order terms indicate the oscillation at integral multiples of the input frequency and hence result in the harmonics of the fundamental input frequency.

1.4 Role of Impurities in Crystal Growth Mechanism

When a solute crystallizes from its supersaturated solution, the presence of a third component can often have a dramatic effect on the crystal growth kinetics and habit form of the crystalline phase. Such a third component is referred to here as an impurity. Different impurities have different effects on the crystal growth.

*Some impurities can suppress growth entirely, some may enhance growth.

*Some may exert a highly selective effect, acting only on certain crystallographic faces.

*Some are adsorbed onto growing crystal surfaces.

*Adsorption of impurities onto the crystal changes the relative surface free energies of the faces.

*Low concentration of impurities is effective and exhibits a marked specificity in their action ($10^{-9} < X < 10^{-3}$ mole concentration).

*Some impurities may change in growth kinetics.

*Some impurities may modify the habit of the crystalline phase.

1.5 Crystal Growth Techniques

Classification of methods of growth is based on the nature of the starting material. When the starting material is in a solution form, the controlled evaporation of the saturated solution will give rise to single crystals only. When the actual vapor pressure of the crystal is maintained at that temperature, then it is possible to grow crystals even if the material is in the vapor form, where the vapor is supersaturated. Melt growth is widely employed for the preparation of congruently melting materials because of the high growth rates which can be used coupled with the high crystalline perfection attainable. Growing crystal from the melt is more widely used than the solution and the vapour

techniques. Growth by chemical reaction of gases or growth from another solid phase is possible by a polymorphic phase change. In the case of compound single crystals, the stoichiometry needs must be considered and it is possible as epitaxial layers of thickness anywhere from sub-micron to hundreds of microns.

Different methods of growing crystals vary from one another in their growth temperature. For crystals grown from low temperature aqueous solution, the temperature does not exceed 90^0C and for super heated aqueous solution it reaches up to 800^0C. For crystals growth from salt melts called molten salt growth or flux growth, the temperature ranges from 1200^0C to 1300^0C but sometimes goes up to 1500^0C. The different techniques of crystal growth may be classified as given in the following table.

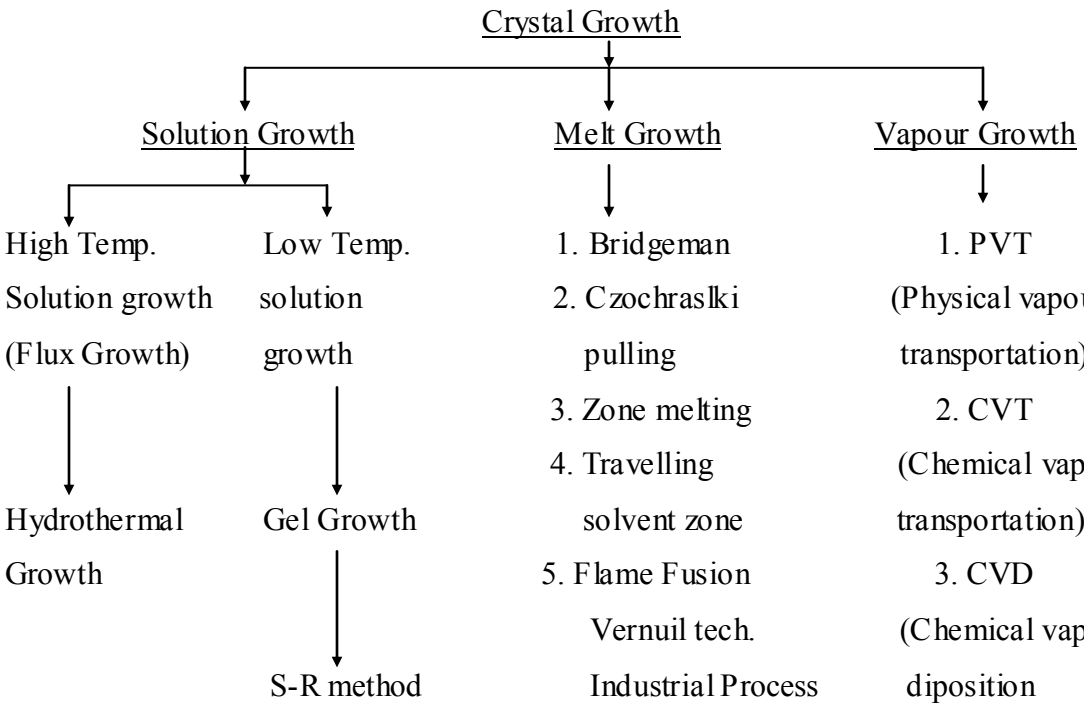

1.6 Solution Growth Technique

This is the oldest method for growing crystals and it is based on the principle that the crystals can be obtained from supersaturated solution by slow cooling or by removing some of the solvent from the solution by evaporation.

Enormous quantities of materials such as sugar, salt of inorganic and organic chemicals crystallized from solution in water, and excellent quality of ferroelectric and piezoelectric crystals such as ammonium dihydrogen phosphate (ADP), potassium dihydrogen phosphate (KDP) and triglycine sulphate TGS are commercially grown for use in electronic devices.

A supersaturated solution of a substance in a suitable solvent is prepared and cooled slowly in a thermostat whose temperature is lowered at a constant rate. A small seed crystal is suspended in the solution and the seed crystal begins to grow slowly. Seed crystal should be prepared carefully so that well-defined crystal is obtained as the seed crystal and care should be taken to avoid any damage to the surface of the crystal.

The main disadvantage of this method is the need to use a range of temperature. The use of range of temperature may vary the properties of grown crystal. This method also requires a programmed temperature – controlling device but still the method is used widely with great success for growing crystals. The factors that control the growth process are:

i. Character of the solution.
ii. Effect of additives and purity.
iii. Operating variables such as the degree of super-saturation, efficiency of agitation and temperature range and
iv. Seed crystal.

Growth of crystals from solution is mainly a diffusion-controlled process, the medium must be viscous to enable faster transference of the growth units from the bulk solution by diffusion. Hence, a solvent with less viscosity is preferable. Super-saturation is an important parameter for the solution growth process. The solubility data at various temperatures are essential to determine the level of super saturation. Hence, the solubility of the solute in the chosen solvent must be determined before starting the growth process. The solubility of the solute may be determined by dissolving the solute in the solvent maintained at a constant temperature with continuous stirring. On reaching saturation, the

equilibrium concentration of the solute may be determined gravimetrically. By repeating the above procedure for different temperature, the solubility curve can then be plotted [9].

1.6.1 Low Temperature Solution Growth

The method of the crystal growth from low-temperature aqueous solution is extremely popular in the production of many technologically important crystals. Materials having moderate to high solubility in the temperature range ambient to 100^0C at atmospheric pressure can be grown by low-temperature solution method. The mechanism of crystallization from solution is governed, in addition to other factors, by the interaction of the ions or molecules of the solute and the solvent which is based on the solubility of substances on the thermo-dynamical parameters of the process, temperature, pressure and solvent concentration [3].

The principal advantages of crystal growth from low temperature solution are the proximity to ambient temperature and, consequently. The degree of control, which can be exercised over the growth conditions. Temperatures can be readily stabilized to $\pm 0.01^0$C. As a result, super saturations can be accurately and precisely controlled. These factors, coupled with the case of efficient agitation of the growing crystal and solution, reduce fluctuations of all kinds of minimum. The proximity to ambient temperature reduces the possibility of major thermal shock to the crystal both during growth and on removal from the apparatus. The method is particularly suited to those materials, which suffer from decomposition in the melt or in the solid at high temperatures and which undergo phase transformation above the present working range. There are numerous organic and inorganic materials, which fall within these categories. It also permits the preparation of a variety of different morphology conditions.

Advantages of low temperature solution method:

i. Growth apparatus is relatively simple and cheap.
ii. Low growth temperature introduces small thermal stresses in the crystal was obtained.
iii. The crystals obtained usually have well developed faces (growth habit) which enable to investigate crystal growth process including in situ observations and capture of impurities.
iv. It is the only method for the growth of substances, which undergo decomposition before melting.

Low temperature solution growth can be sub-divided into the following methods

1. Slow cooling method
2. Slow evaporation method
3. Temperature gradient method

In recent years, an appreciable attention is given to grow crystals from solutions with faster growth rates by adopting faster cooling rates. Possibility of faster cooling rate depends mainly on the stability of the solutions, which indeed depends on meta-stable zone width of the solutions in their super saturated regions. Larger the zone width higher the stability. Solutions with narrow meta-stable zone widths very often end up with secondary nucleation, which affect the growth of main crystal significantly.

1.6.2 Slow Cooling Method

In order to grow the crystals, super saturation of the solutions can be obtained by lowering the temperature of the solutions and that will result a seed crystal to grow. If the solution is cooled very slowly, then the growing crystal takes up all the solute in excess of the equilibrium solubility. It is needed to use a wide range of temperatures. The possible range is usually small so that much of the solute remains in the solution at the end of a run. BY providing the desired rate of cooling, good quality crystal will grow on the seed. Generally, 0.01 or 0.02^0C per day cooling rate is preferred.

1.6.3 Slow Evaporation Method

A super saturation can be obtained from saturated solutions by evaporation of some of the solvent. In this case, temperature held constant and provision must be given for evaporation. As long as the evaporation starts, the growth of the seed takes up the solid. The amount of solute that can be deposited on a seed by evaporation depends on the amount of saturated solutions utilized for each seed crystal present. With a non-toxic solvent, it is permissible to allow evaporation into the atmosphere. This method can be used for that materials those have very small temperature co-efficient of solubility.

1.6.4 Temperature Gradient Method

Growing of crystals from solution is performed by maintaining a temperature difference between a region of growth and dissolution with a continuous exchange of solution between them. A saturated solution is in contact with excess solid (nutrient) and transport of materials from a hot region to a cooler region causes the growth precede. The main requirement is that the solution should have a fairly wide mata-stable range and a reasonably large positive temperature coefficient of solubility.

1.7 Purification

Organic materials, as purchased are of considerably variable quality, with purity lying in the range 95-99%. The most essential feature of growth of high optical quality crystal is the material and the solution purification [2]. Purification of the materials may be carried out in many ways:

i. Zone-refining
ii. Sublimation
iii. Re crystallization and
iv. Fractional distillation of the solvent

1.8 Recrystallization

It is essential to increase purity to a respectable level before proceeding further [4]. Considerably, re-crystallization will produce material, which is pure for crystal growth. LA was re-crystallized with distilled water. The solvent was saturated with LA at 30 ^{0}C. The solution was filtered to avoid any insoluble impurities by using heated apparatus to prevent nucleation. The solution is cooled down at room temperature, in order to obtain maximum yield. Then the grown crystals were re-crystallized further. The re-crystallization process may take place in supersaturated and saturated solutions. Re-crystallization process consists of dissolution and crystallization. Some crystals or layers of some crystals are dissolved and new crystals are precipitated from the solution. Re-crystallization of precipitates in saturated solutions takes place due to the dynamic nature of the equilibrium between the liquid and solid phases. It produces larger crystal, because small particles are dissolved and re-deposited on the surfaces of large crystals. Re-crystallization may result from the dependence of the solubility of particles on their size. According to this dependence, fine particles are dissolved because a solution is unsaturated with respect to such particles, while large crystals grow, the dissolution of small particles produces a temporary saturation with respect to large crystals.

1.9 Mechanism of Growth

In solution growth, for any material to be grown, the equilibrium concentration of the solution at different temperature must be known. Growth of crystals from solution mainly depends on the super-saturation. High super-saturation of the solution leads to spontaneous nucleation. In order to grow good crystals of perfect morphology, seeded growth is selected. The concentration of the solution must be slightly greater than its equilibrium concentration.

The influence of solvent on crystal growth can be understood by crystal-medium interface. In solution, the solute molecules will be dissolved. The solution can be maintained in the meta-stable region by maintaining the accurate temperature. A seed crystal is introduced in the solutions for the growth to proceed. On attachment of the

molecule to the crystal surface, partial desolation occurs. Solvation and desolation of solute molecules are therefore integral parts of the growth process and will to some extent, influence the kinetics and thermodynamics of crystal growth.

1.10 Solubility and Supersaturation

Solution is a homogeneous mixture of a solute in a solvent. Solute is the component, which is present in a smaller quantity. For a given solute, there may be different solvents.

An ideal solvent should

a) yield prismatic crystals
b) have significant, but no successive solubility
c) have low volatility
d) have low viscosity
e) have a good solubility gradient
f) have no corrosion of growth apparatus
g) have low vapor pressure at the growth temperature
h) have reversible solubility of the material

If the solubility is too high, as in the case of thiourea dissolving in starch and in water, it is very difficult to grow bulk single crystals. Since solution growth is related greatly to the solubility of the material, the choice of solvent is important.

Changes in super-saturation, solvent may lead to dramatic modifications by dissolving the solute in the crystal morphology. The solubility of a solute may be determined by dissolving the solute in the solvent maintained at a constant temperature with continuous stirring. The solubility data at various temperatures are essential to determine the level of super-saturation. As the growth of crystals from solution is mainly a diffusion-controlled process, the medium must be viscous to enable faster transference of the growth units from the bulk solution by diffusion. Hence a solvent with less viscosity is preferable. The degree of super-saturation of a solution can be defined in two ways. The concept of absolute super-saturation

$$\Delta C = C - C_0$$

Where C is the concentration of the dissolved substance at a given moment and C_0 is its solubility limit.

In a majority of the cases the solubility of a solute in a solvent increases with temperature, but there are a few well-known exceptions in this rule. The solubility characteristics of the solute in a given solvent have a considerable influence on the choice of a method of crystallization. A solvent, in which the solute has solubility of 10 to 60%, may be considered suitable for crystal growth. In the case of very high solubility, growth rate may be very low due to the solution. Viscosity, which renders the system diffusion controlled. Otherwise the resulting crystals may possess unwanted morphology. Similarly, solvents in which a solute is soluble also provide low growth rates due to the low solubility. In both these cases it is desired to use solution modifiers to change solubility or viscosity. However, it is not possible to predict a growth aid that will be effective in the growth of a compound from a particular solvent since the mechanism of the action of these growth aids is obscure.

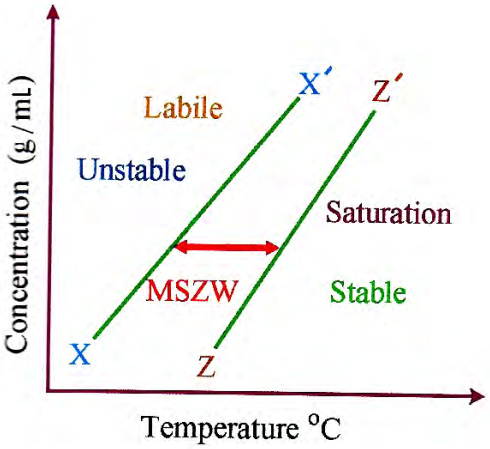

Fig.1.1Typical solubility diagram

1.11 Metastable Zone width

Metastable zone width (MSZW) is a critical parameter in the crystallization process as it reveals the nucleation behavior of the system. It is the difference between the solubility

temperature and the nucleation temperature. MSZW is a nucleation kinetic – limited parameter that is highly dependent on the process conditions. MSZW is essential parameter for the growth of large size crystal from solution, since it is the direct measure of stability of the solution in its supersaturated region. Larger the zone width, the stability is high. Solution with narrow metastable region very often end up with secondary nucleation. Many factors may influence the value of MSZW, e.g. rate of cooling, agitation, the presence of foreign particles and impurities

1.12 Nucleation Mechanism

The crystal growth process starts with the nucleation stage. Several atoms or molecules in a supersaturated vapor or liquid start forming clusters; the bulk free energy of the cluster is less than that of the vapor or liquid. Nucleation is defined as the process of generating, within a meta-stable mother phase, the initial fragments of a new and more stable phase capable of developing spontaneously into gross fragments of the stable phase. Nucleation may occur spontaneously or it may be induced artificially, are referred to as homogeneous and heterogeneous nucleation respectively. The term "primary" indicates nucleation in systems that do not contain crystalline matter viz, homogenous and heterogeneous. Nuclei that are often generated in the vicinity of crystals present in supersaturated system is referred to as secondary nucleation.

Classification of nucleation

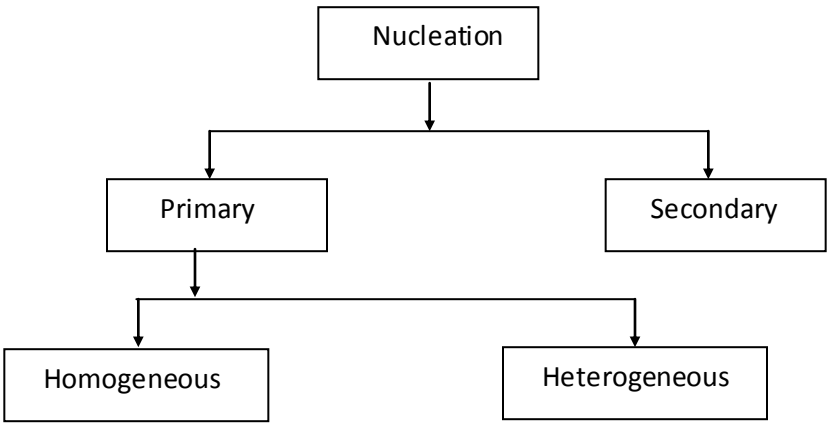

Crystallization process is initiated by the formation of embryos or nuclei with number of micro size solid particles present in the solution, termed as centers of crystallization. The mechanism of formation of such embryos is the simple collision process of a single molecule A_1 with a cluster A_{i-1} consisting of (i-1) molecules and thus giving rise to a cluster A_i; ie.,

$$A_1 + A_{i-1} = A_i$$

In a supersaturated system, when few atoms or molecules join together a change in energy takes place in the process of formation of the cluster. Driving force for crystallization is the degree of Super saturation which is given by

$$S = C - C^*$$

Where C is the actual concentration and C* is the equilibrium concentration of the solution The total Gibb"s free energy change ΔG, of the embryo between the two phases associated with this process is given as

$$\Delta G = \Delta G_s + \Delta G_v$$

Where ΔG_s is the surface free energy change and ΔG_v is the volume free energy change. For the spherical nucleus of radius, r

$$\Delta G = (4/3)\ \pi r^3\ \Delta G_v + 4\ \pi r^2$$

Where γ is the interfacial tension and ΔG_v is the free energy change per unit volume and is a negative quantity. Since the surface free energy increases with r^2 and volume free energy decreases with r^3 and the net free energy change increases with increase in size and attains a critical size after which it decreases. At critical condition, the free energy formation obeys the condition,

$$\frac{d\Delta G}{dr} = 0$$

Hence the radius of the critical nucleus is expressed as

$$r^* = \frac{-2\gamma}{\Delta G_v} \qquad \text{Where} \quad \Delta G_v = \frac{-kT\ln(S)}{V} \qquad \text{and} \quad S = \frac{C}{C^*}$$

Where V = molar volume of the crystal

k = Boltzmann‟s constant

C = actual concentration of the solution

C* = equilibrium concentration of the solution

T = Temperature of the solution in K

S = super saturation ratio

Hence, the critical free energy barrier

$$\Delta G^* = \frac{16\pi\gamma^3}{3\Delta G v^2}$$

The number of molecules in the nucleus is expressed as

$$i^* = \frac{4}{3}\pi\gamma(r^3)$$

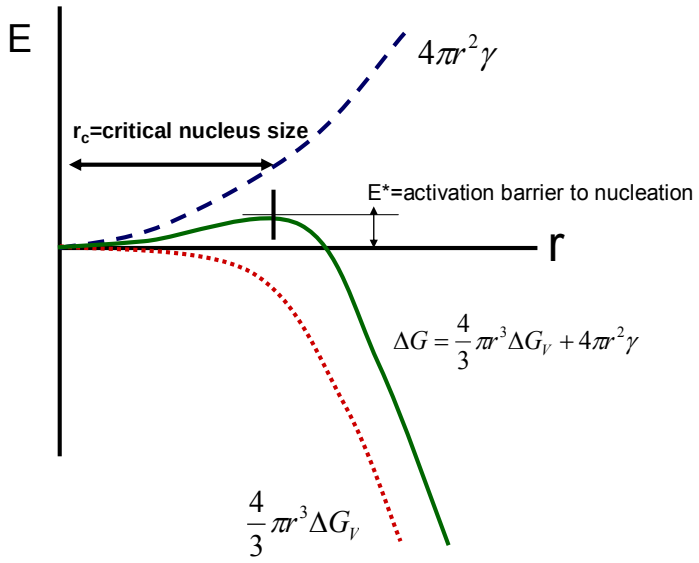

The presence of surface tension always produces an activation barrier to nucleation of condensed phases (both solids and liquids!)

Fig.1.2 Gibb's free energy diagram

The critical parameter involved in between a growing crystal and the surrounding mother liquor is the interfacial energy. Interfacial energy is a measurement of the cohesive

(excess) energy present at an interface arising from the imbalance of forces between molecules at an interface (gas/liquid, liquid/liquid, gas/solid, liquid/solid). It can be quantified as the force acting normal to the interface per unit length (force/unit length, N/m). The interfacial energy γ can be determined experimentally by conducting nucleation experiments using the saturated solution of any material. The induction period, a measure of the nucleation rate n, is determined experimentally for any solution at different super-saturations. According to the classical theory of homogeneous formation of spherical nucleus

$$\ln t_{ind} = -\ln A + \frac{16\pi\gamma^3 V^2 N_a}{3R^3T^3(\ln S)^2}$$

Where V is the molar volume of the crystal, N_A is the Avogadro‟s number, R is the gas constant and T is the temperature, A is constant, t_{ind} is induction period and S is the supersaturation (S = C/C*) where C is the actual concentration and C* is the equilibrium concentration. The function, ln A weakly depends on temperature and hence there is a linear depence between ln t_{ind} and $1/(\ln S)^2$ at constant temperature. A plot of ln t_{ind} against $1/(\ln S)^2$ is a straight line. The intercept of the straight line on the y-axis gives the value of ln A and the slope m is given by

$$m = \frac{16\pi\gamma^3 V^2 N_a}{3R^3T^3(\ln S)^2}$$

The interfacial energy can be calculated from the slope of the line as

$$\gamma^3 = \frac{3R^3T^3m}{16\pi V^2 N_A}$$

The energy of formation of a critical nucleus can be calculated as

$$\Delta G = \frac{RTm}{(LnS)^2}$$

The radius of the nucleus in equilibrium with its solution can be computed as

$$r = \frac{2\gamma V}{RTLnS}$$

1.13 Objectives of the Present Work

Modern technology is based on single crystals of nonlinear optical, semiconductor, dielectric, ferroelectric, superconductor, acousto-optic and optoelectronic materials. Hence, much attention was paid on the single crystals. As single crystals of suitable size and perfection are required for laser, optical communication, detectors, integrated circuits and data storage technology, they become a vital and fundamental part of material science and engineering.

Single crystal growth has prominent role to play in the present era of rapid technical and scientific advancement, where the application of crystals has unbounded limits. Frequency conversion is an important and popular phenomenon for extending the useful wavelength range of lasers. This has led to the production of various devices, such as harmonic generators, optical parametric oscillators, electro-optic modulators and amplifiers for high power lasers. Hence efforts were focused at the development of new and efficient frequency conversion materials. With the aim of discovering new useful materials for academic and industrial use an attempt has been made to modify ADP, KDP and KAP crystals by doping amino acid LA with different concentrations in their mother solutions.

The present investigation is aimed at:

a) Synthesizing of pure LA and LA doped ADP, KDP and KAP salts.

b) Producing optically transparent large size single crystals.

c) Analyzing these new crystals by powder XRD.

d) Studying the vibrational spectra of the molecules using FTIR analysis.

e) Studying UV-Vis spectra and thermal strengths of the materials to find their suitability in SHG applications.

f) Studying electrical conductivity and mechanical hardness of the materials for optoelectronic devices.

g) Seeing the effect of LA doping on the grown crystals.

h) Characterization the surface morphology of the crystals.

1.14 Review Works

Pure and amino acid (L-arginine and L-alanine) doped KDP crystals were grown from solution at a temperature 40^0C by employing slow evaporation of the solvent. Both pure and doped KDP crystals crystallizes in the same tetragonal crystal system and the lattice parameters calculated from the XRD pattern of the pure and doped KDP crystals show very slight changes. There is no change in the morphology of the doped crystals and also no change in the growth rate as compared to the growth rate of the pure KDP crystal [15]. Muley et al [15] reported the increase of transparency and the increase in the second harmonic generation (SHG) efficiency of pure KDP crystal by doping LA. They also reported that the thermal stability of the LA doped crystals decreases with the increasing concentration of the LA in KDP crystals.

Parikh et al [16] explained the FT-IR spectra, paper chromatography and CHN analysis which confirmed the presence of LA in KDP crystals were grown by slow solvent evaporation technique. They also reported that the SHG efficiency and the percentage optical transmission increased as the doping increased. Thermograms of pure and LA doped KDP crystals suggested that as the doping increased the crystals became thermally less stable and dehydrated faster at comparatively lower temperature. The values of kinetic and thermodynamic parameters decreased with the increase in the level of doping. The dielectric constant and the dielectric loss values of LA doped KDP crystals were lower than the pure KDP crystals. The a. c. resistivity remained almost the same in high frequency range and exhibited slight variation at low frequency for pure and doped KDP crystals.

Meena et. al [17] explained DC and AC electrical characterization of pure and L-arginine added KDP and ADP single crystals which were carried out along both a- and c-directions at various temperatures ranging from 40 to 140 ^{0}C. They found that the electrical parameters, viz. ζ_{dc}, ε_r, tanδ and ζ_{ac} increase with the increase in temperature due to the temperature dependence of the proton transport which depends mainly on the thermally generated L-defects and decrease with the increase in L-arginine concentration

in the crystals of KDP and ADP due to the reduction of L-defects caused mainly by the creation of additional hydrogen bonds by the impurity which obstruct the movement of proton.

Pure and L-arginine doped KDP crystals were grown by slow evaporation technique and calculated the values of kinetic and thermodynamic parameters by Parikh and Parekh [18]. They also found that the second harmonic signal strength and the second harmonic generation efficiency were increased with doping concentration.

Dhanaraj et. al [19] studied the effect of amino acid additives on crystal growth parameters and also explained the microhardness decreases with the increase of doping concentration.

Ananda Kumari et. al [20] made good quality large size optically transparent ADP crystals and ADP crystals with nitric tri acetic acid and EDTA by slow evaporation technique. EDAX data has confirmed the presence of impurities in the crystal lattice. ADP crystals with nitric tri acetic acid and EDTA have shown appreciable increase in SHG efficiency as compared to pure ADP crystals.

Anne et. al [21] explained d.c. electrical conductivities along both the a- and c- directions at various temperatures ranging from 40 to 150 ^{0}C of pure and impurity (urea and thiourea) added ADP single crystals. They said that the conduction in ADP is protonic and mainly due to the anions and not the cations.

Geetha et. al [22] made good quality single crystals of pure and doped KAP single crystals by slow cooling method. The grown crystals with various dopants have similar morphology to the pure one. The powder X-ray diffraction analysis reveals the stable lattice on doping in KAP. The FTIR analysis confirm the substitution of potassium by the dopants rather than the hydrogen in the KAP crystals. The SHG emission was confirmed for all the doped KAP crystals.

Krishnan et. al [23] made good quality single crystals of potassium acid phthalate (KAP) by slow evaporation method. From the X-ray diffraction, it was confirmed that the crystal belongs to orthorhombic structure with space group $Pca2_1$. FTIR analysis was carried out

to confirm the presence of functional groups of the grown crystals. the optical transmittance of the crystal confirms the transparency of the crystal. By tailoring the absorption coefficient and tuning the band gap of the material, one can achieve the desired material which is suitable for the fabrication of various optoelectronic devices.

Single crystals of KAP, amino acid doped KAP such as DLAKAP and METKAP have been grown from aqueous solution by slow cooling method. The incorporation of dopants was confirmed by powder XRD analysis and FTIR analysis. The maximum temperature for NLO applications has been found by thermal analysis. METKAP has shown improved optical transmittance compared to KAP crystals. All the crystals have their cut off below 250 nm, which satisfies the criteria for SHG. The Kurtz and Perry powder technique confirms SHG in the pure as well as doped crystals. Etch patterns observed on the {010} faces of KAP, DLAKAP and METKAP crystals reveal that the surfaces possess high and low growth steps. Flat bottomed etch pits were also observed. The frequency response of pure and amino acid doped KAP single crystals was observed and the behavior is attributed to the piezoelectric nature of the crystal. The mechanical stability of the crystals has been studied using Vickers hardness testing and the hardness numbers for the doped crystals are reported in [24].

1.15 Brief Outline of the Work Presented in the Thesis

The thesis is divided into seven sections. The first chapter is an introductory section on crystal growth and nonlinear optics. The second chapter discussed about the different physical properties of pure LA, pure and LA doped ADP, KDP and KAP crystals. This chapter also gives an account of the various characterization techniques employed to evaluate the prospects of these materials for NLO applications. The third chapter gives an account of the growth of pure LA and its structural, optical, mechanical, thermal and electrical characterization. In the fourth chapter detailed aspects of similar investigations of pure and LA doped ADP crystals. Similar investigations for pure and doped KDP crystal explained in chapter five. The detail of the growth of KAP single crystals by slow evaporation technique is included in chapter six. The seventh chapter gives a summary of the important outcomes of the present investigations. It also gives a comparative

assessment on the prospects of the four single crystals investigated in the present work, pure LA, pure and doped ADP, KDP and KAP, for possible non linear optical applications. The scope for future investigations on these materials is also highlighted in this chapter.

In the present study we have employed the characterization tools such as powder XRD, EDX, FTIR, UV-Vis-NIR spectroscopy, Vicker‟s microhardness analysis, TGA/DTA, Electrical, dielectrics and chemical etching studies to reveal the growth mechanism and to determine dislocation density.

1.16 References

[1] Boomadevi, S., Dhanasekaran, R. and Ramasamy, P., Cryst. Res. Technol. **37**,p.159, 2002.

[2] Bloembergen, N., "Non Linear Optics", Benjamin, New York, 1965.

[3] Catesby, C. G. C.," The crystals structure of Urea Ammonium Bromide", Acta Cryst. Vol. **18**, p.392-398, 1972.

[4] Chernov A. A.,"Modern Crystallography-III", Crystal Growth, Springer-Verlang, Solid State series **36**, New York, 1984.

[5] Chemla, D. S., and Zyss, J., "Nonlinear Optical Properties of Organic Molecules and Crystals", Academic Press, Boston, 1987.

[6] Hann, R. A. and Bloor, D.,"The Growth, Perfection and properties of crystals; Organic materials for non-linear optics", Special Publication No. **69**, Oxford, Edited, p.71-82, 1989.

[7] Hartman, P.,"Crystal growth; an introduction, Ed. Hartman, P., North-Holland Publishing Company, Amsterdam, 1973.

[8] Lyons, M. H.,Ed. "Materials for Non Linear and Electro Optics", Inst. of Physics Conf. Series, p.103, 1989.

[9] Miers, H. A. and Issac, F.,"The spontaneous crystallizations", Proc. Roy. Spec., Vol. **A79**, p.322-325, 1987.

[10] Ramasamy, P., Subramanium, C. and Dhanasekaran, R., "Proceedings of UGC summer school on crystal growth and characterization of Advanced Materials for solid state Applications", Anna University, Madras, 1986.

[11] Raskovich, L. N. and Kronsky, N. V., J. Cryst. Growth, **182**, p.434, 1997.

[12] Santhana Raghavan, P. and Ramasamy, P.,"Crystal Growth Processes and Methods", KRU Publications, Chennai, India, 2000.

[13] Zyss, J., "Nonlinear Organic Materials for Integrated Optics: A review", J. Molec. Electronics, Vol. **1**, p.25, 1985.

[14] Halfpenny, P. J., Sherwood, J. N. and Simpson, G. S., " The Growth and Perfection of Organic Crystals", International Summer School on Growth and Characterization of Crystals, Lecture notes and Abstracts of Contributions by Participants, Cracow-Krynica, Poland. 4-14, p.1, 1994.

[15] Muley, G. G., Rode, M. N. and Pawar, B. H., "FT-IR, Thermal and NLO Studies on Amino Acid (L-arginine and L-alanine) Doped KDP Crystals", ACTA PHYSICA POLONICA A, Vol. **116**, No. 6, p. 1033-1038, 2009.

[16] Parikh, K. D., Dave, D. J., Parekh, B. B. and Joshi, M. J., "Growth and characterization of L-alanine doped KDP crystals", Cryst. Res. Technol. **45**, No. 6, p. 603-610, 2010.

[17] Meena, M. and Mahadevan, C. K., "Growth and electrical characterization of L-arginine added KDP and ADP single crystals", Cryst. Res. Technol. **43**, No. 2, p. 166-172, 2008.

[18] Parikh, K. D., Dave, D. J., Parekh, B. B. and Joshi, "Thermal, FT-IR and SHG efficiency studies of L-arginine doped KDP crystals", Bull. Mater. Sci., Vol. **30**, No. 2, p. 105-112, 2007.

[19] Dhanaraj, P. V., Bhagavannarayana, G. and Rajesh, N. P., "Effect of amino acid additives on crystal growth parameters and properties of ammonium dihydrogen orthophosphate crystals", Materials Chemistry and Physics, Vol. **112**, ISSUE 2, p. 490-495, 2008.

[20] Ananda Kumari, R., "Growth and characterization of NLO crystal", Indian Journal of Pure & Applied Physics, Vol. **47**, p. 369-371, 2009.

[21] Anne, Assencia, A and Mahadevan, C, "D.C. electrical conductivity measurements on ADP single crystals added with simple organic compounds", Bull. Mater. Sci., Vol. **28**, No. 5, p.415-418, 2005.

[22] Geetha, S. K., Perumal, R., Moorthy Babu, S. and Anbarasan, P. M., "Habit modification and improvement in properties of potassium hydrogen phthalate (KAP) crystals doped with metal ions", Cryst. Res. Technol. **41**, No. 3,p. 221-224, 2006.

[23] Krishnan, S., Justin Raj, C., Dinakaran, S. and Jerome Das, S., "Investigation of optical band gap in potassium acid phthalate single crystal", Cryst. Res. Technol. **43**. N0. 6, p. 670-673, 2008.

[24] Uthayarani, K., Sankar, R. and Shashidharan Nair, C. K., "Growth, spectral and thermal properties of KAP single crystals in the presence of DL-Alanine and L-Methionine amino acid dopants", Cryst. Res. Technol. **43**, No. 7, p. 733-739, 2008.

CHAPTER 2

MATERIALS AND METHODS OF CHARACTERIZATION

CHAPTER 2

MATERIALS AND METHODS OF CHARACTERIZATION

2.1 Introduction

The mechanism of crystallization from aqueous solutions is governed by the interaction of the ions or molecules of the solute and the solvent. In solutions, the growth is due to the diffusion of the solute to the surface separating the solid and liquid phases. The essential required for crystal growth is the creation of super saturation. In the present study, super saturation will be achieved by the slow cooling of the solution.

2.2 Materials Selected for Growing Crystals

Analar grade KAP, KDP, ADP with 100% (e-Merck) were used in the present study. LA with purity 99% (SIGMA, USA) was used as an additive in the present study.

2.2.1 Some Physical Parameters of Pure LA

Compound: L-alanine (Amino Acid)
Molecular formula: CH_3CHNH_2-COOH
Molecular weight: 89.09 g/mol
Crystal system: Orthorhombic
Density: 1.37 g/cc
Color: Colorless
Cell dimension: a= 6.008 Å, b= 12.317 Å and c= 5.804 Å

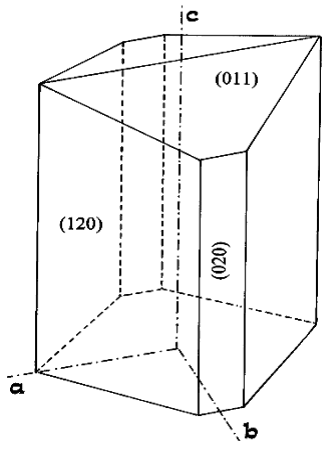

Fig. 2.1 The morphology of L-alanine crystal

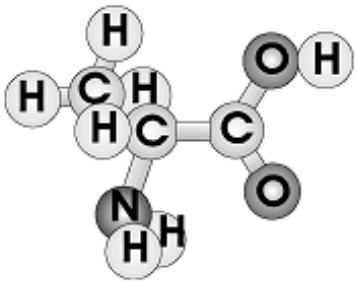

*Fig. 2.2 Molecular structure of L-*alanine

Fig. 2.3 Hydrogen bonding in crystalline L-alanine

2.2.2 Influence of L-alanine as Impurities

Amino acids such as LA has special features such as

- molecular chirality, which forces the molecule to crystallize in a non centrosymmetric space group, which is the essential criterion for SHG material.
- wide transparency ranges in the visible and UV spectral regions.
- zwitterionic nature of the molecule ($^{+}NH_3 – C_2H_4 – COO^{-}$), which favors the way for possessing high electro optic parameters and good mechanical and thermal stability of the crystals

2.2.3 Some Physical Parameters of Pure ADP

Compound: ADP

Molecular formula: $NH_4H_2PO_4$

Molecular Weight: 115.03 g/mol

Crystal system: Tetragonal

Density: 1.799 g/cc

Color: Colorless

Cell dimension: a = b = 7.473 Å, c = 7.457 Å

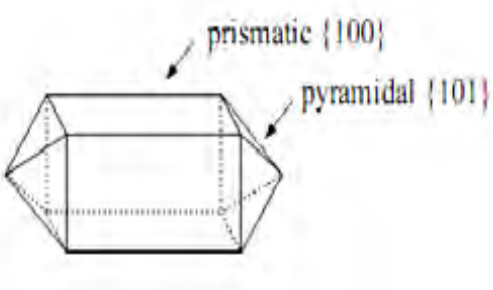

Fig. 2.4 Morphology of pure ADP crystal

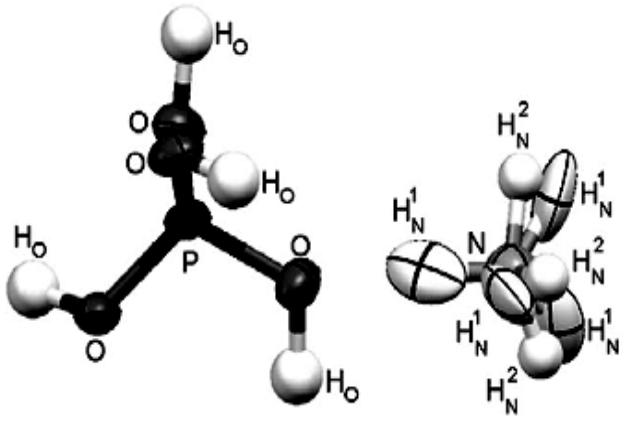

Fig. 2.5 Molecular structure of pure ADP crystal

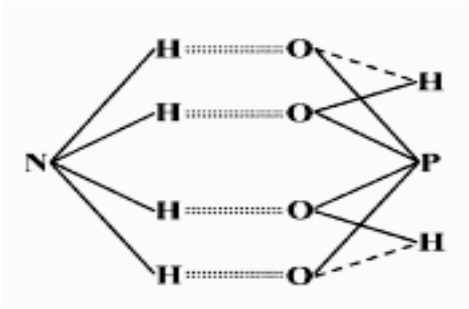

Fig. 2.6 Bond graph of ADP molecule. The dotted lines represent hydrogen bonds between NH_4^+ and $H_2PO_4^-$ groups, while the hydrogen bonds between $H_2PO_4^-$ groups are shown as the dashed lines, other stronger chemical bonds are shown by the solid lines

2.2.4 Some Physical Parameters of Pure KDP

Compound: KDP

Molecular formula: KH_2PO_4

Molecular weight: 136.09 g/mol

Crystal system: Tetragonal

Density: 2.344 g/cc

Color: Colorless

Cell dimension: a = b = 7.410Å, c= 6.982Å

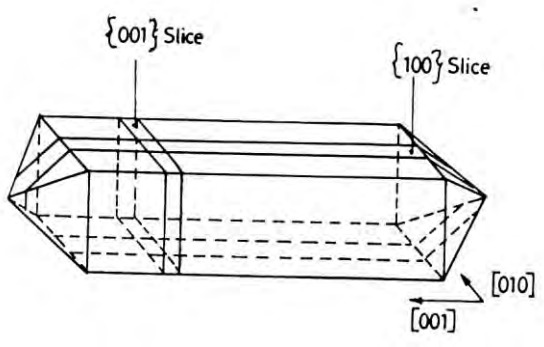

Fig. 2.7 Morphology of KDP crystal

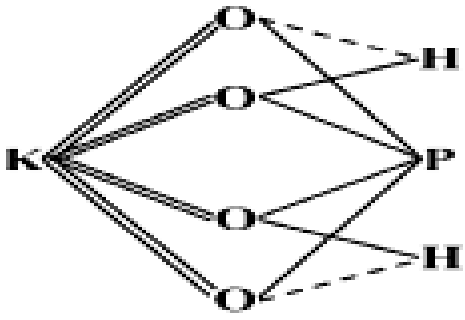

Fig. 2.8 Bond graph of KDP molecule. The dotted lines represent hydrogen bonds between K^+ and $H_2PO_4^-$ groups, while the hydrogen bonds between $H_2PO_4^-$ groups are shown as the dashed lines, other stronger chemical bonds are shown by the solid lines

2.2.5 Some Physical Parameters of Pure KAP

Compound: KAP

Molecular formula: $C_8H_5KO_4$

Molecular weight: 204.23 g/mol

Crystal system: Orthorhombic

Density: 1.64 g/cc

Color: Colorless

Cell dimension: a = 9.749Å, b = 12.905Å and c = 6.647Å

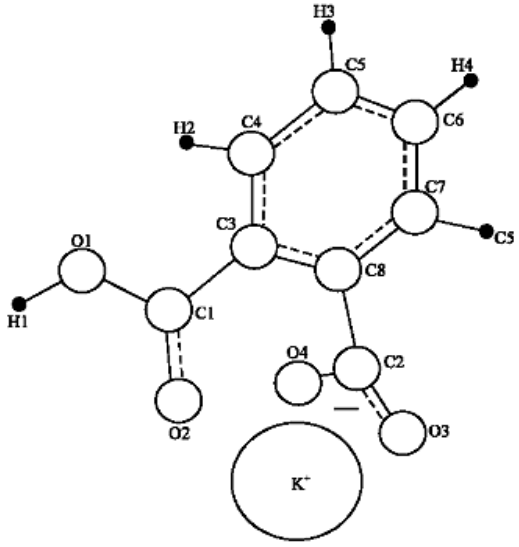

Fig. 2.9 Molecular structure of KAP crystal

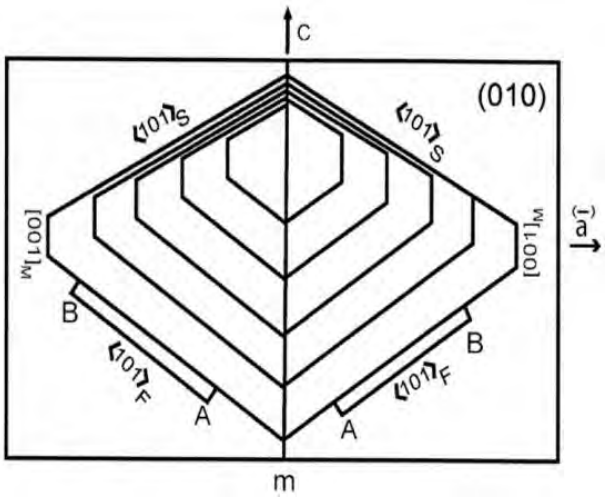

Fig.2.10 Schematic drawing of the spiral morphology on KAP (010); indication of step velocity F = fast, M = medium, S = slow

2.3 Methods of Characterization

2.3.1 Fourier Transform Infrared Spectroscopy (FTIR)

FTIR is the preferred method of IR spectroscopy. In this spectroscopy, IR radiation is passed through a sample. Some of the infrared radiation is absorbed by the sample and some of it passed through (transmitted) the sample. IR radiation refers broadly to that part of the electromagnetic spectrum between the visible and microwave regions. An infrared spectrum represents a fingerprint of a sample with absorption peaks which correspond to the frequencies of vibrations between the bonds of the atoms making up the material. The frequency or wavelength of absorption depends on the relative masses of the atoms, the force constants of the bonds, and the geometry of the atoms. Because each different material is a unique combination of atoms, no two compounds produce the exact same IR spectrum. Therefore, IR spectroscopy can result in a positive identification (qualitative analysis) of every different kind of material. In addition, the size of the peaks in the spectrum is a direct indication of the amount of material present. This makes IR spectroscopy useful for several types of analysis.

A list of information provides from the FTIR spectrum given below:

1. It can identify unknown materials
2. It can determine the quality or consistency of a sample
3. It can determine the amount of components in a mixture

In the present work Potassium Bromide (KBr) pellets of LA, ADP, KDP, KAP and different concentration of LA doped ADP, KDP and KAP were prepared by mixing 1mg of dry finely powder of these crystals with 300mg of KBr. The mixture was finally milled in a crucible for two minutes and then pressed into a pellet of 13mm dia under the 13440 lbs. (PSI) in an evaquable die. The resulting pellet was very thin. Since KBr is hygroscopic, the pellet was kept in a vacuum dessicator to avoid any moisture absorption. The FTIR spectra of the above crystals were recorded by KBr pellet technique using a Shimadzu FTIR – 8900 spectrophotometer in the wave number range 400-4000 cm^{-1}.

From the FTIR spectrum we can get more information about the structure of a crystal. In this technique almost all functional groups in a molecule absorb characteristically within a definite range of frequency. The absorption of IR radiation causes the various bands in a molecule to stretch and bend with respect to one another.

2.3.2 Energy Dispersive X-ray Analysis

It is a technique used for identifying the elemental composition of the specimen, or an area of interest thereof. The EDX analysis system works as an integrated feature of a scanning electron microscope (SEM), and can not operate on its own without the latter.

During EDX Analysis, the specimen is bombarded with an electron beam inside the scanning electron microscope. The bombarding electrons collide with the specimen atoms' own electrons, knocking some of them off in the process. A position vacated by an ejected inner shell electron is eventually occupied by a higher-energy electron from an outer shell. To be able to do so, however, the transferring outer electron must give up some of its energy by emitting an X-ray.

The amount of energy released by the transferring electron depends on which shell it is transferring from, as well as which shell it is transferring to. Furthermore, the atom of every element releases X-rays with unique amounts of energy during the transferring process. Thus, by measuring the amounts of energy present in the X-rays being released by a specimen during electron beam bombardment, the identity of the atom from which the X-ray was emitted can be established.

The output of an EDX analysis is an EDX spectrum. The EDX spectrum is just a plot of how frequently an X-ray is received for each energy level. An EDX spectrum normally displays peaks corresponding to the energy levels for which the most X-rays had been received. Each of these peaks are unique to an atom, and therefore corresponds to a single element. The higher a peak in a spectrum, the more concentrated the element is in the specimen.

An EDX spectrum plot not only identifies the element corresponding to each of its peaks, but the type of X-ray to which it corresponds as well. For example, a peak corresponding to the amount of energy possessed by X-rays emitted by an electron in the L-shell going down to the K-shell is identified as a K-Alpha peak. The peak corresponding to X-rays emitted by M-shell electrons going to the K-shell is identified as a K-Beta peak.

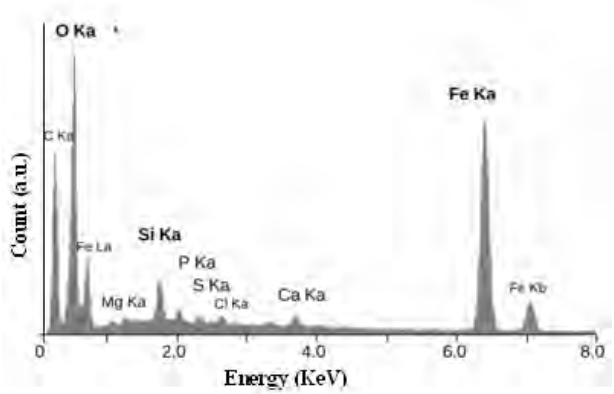

Fig.2.11 EDX spectrum of the mineral crust of Rimicaris exoculata

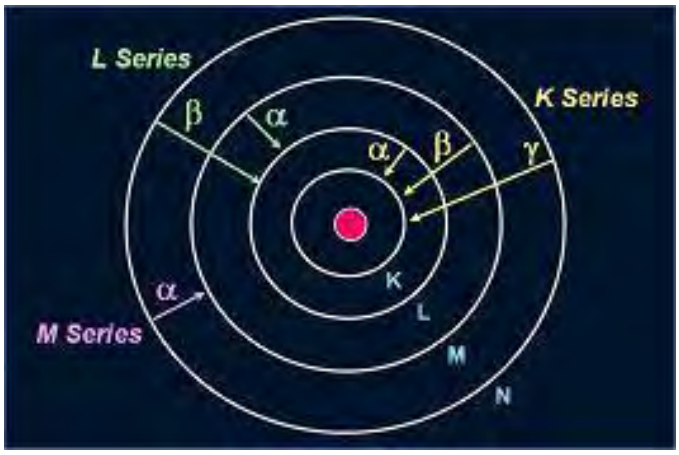

Fig.2.12 Elements in an EDX spectrum are identified based on the energy content of the X-rays emitted by their electrons as these electrons transfer from a higher-energy shell to a lower-energy one

2.3.3 Powder X-ray Diffraction

From XRD pattern the lattice parameters of a crystal and the dimension of the unit cell can be calculated. And also the shape of the crystal can find out. For known crystal shape we can find out the lattice parameters by using the Bragg‟s law, the peak positions can be calculated theoretically using this formula

$$\theta = arc\ sin\ (\lambda/2d)$$

where λ is the wavelength of the x-ray, and $d = (k\lambda/2sin\theta)$ [Scherrer equation]. After that using the Crystallographic formulae $1/d^2 = 1/a^2\ (h^2+k^2+l^2)$ for interplanar spacing.

For unknown crystal shape we have to use JCPDS (Joint Committee for Power Diffraction Standards) (1969) data which is replaced by ICDD (International Centre for Diffraction Data) (1978). In this case we have to find first the spacing (d) of the peak from the XRD pattern by using Scherrer equation and the ratio (I/I_1), where I is the intensity of the peak and I_1 is the relative intensity. Find out the values of hkl from that data by using those two values.

2.3.4 UV – Visible Spectroscopy

Ultraviolet (UV) spectroscopy is a method of determining which wavelengths (colors) of visible light a sample absorbs or emits. It is useful to characterize the absorption, transmission, and reflectivity of a variety of technologically important materials. This application usually requires recording at least a portion of the spectrum for characterization of the optical or electronic properties of materials. In transmittance spectroscopy, different wavelengths of monochromatic light are shot at a sample, and the wavelengths that do not interact with the sample are measured by a detector on the other side of the sample. In absorbance spectroscopy, the light that is absorbed (that is to say, the light that does interact with the sample) is measured using the same setup. For most molecules, absorption wavelengths corresponding to transitions between the ground state and any vibrational level of the first excited state fall in the range of ultraviolet and visible light. Low-energy transitions are also possible between vibrational levels within a single electronic level. These transitions produce radiation in the infrared range. Figure 2.13 illustrates the relationship between specific energy transitions in the energy level diagram (upper graph) and the absorbance spectrum (lower graph). Transmission Spectroscopy is highly interrelated to Absorption Spectroscopy. This technique can be used for solid, liquid, and gas sampling. Here, light is passed through the sample and compared to light that has not. The output depends on the path length or sample thickness, the absorption coefficient of the sample, the reflectivity of the sample, the angle of incidence, the polarization of the incident radiation, and for particulate matter, on the particle size and orientation. In the Beer-Lambert Law: $A = -\log_{10}(I_T/I_o)$
Where the term I_T/I_o is called transmittance.

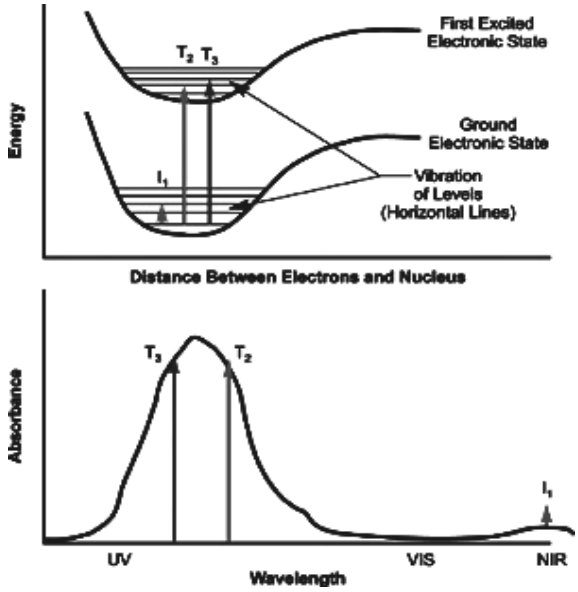

Fig. 2.13 Illustrates the relationship between specific energy transitions in the energylevel diagram (upper graph) and the absorbance spectrum (lower graph)

Where I_T is the monochromatic radiant power transmitted by the absorbing medium. I_o is the monochromatic radiant power incident on the medium. This form of spectroscopy has a setup similar to the one used for Absorption. The dependence of optical absorption coefficient with the photon energy helps to study the band structure and the type of transition of electrons. The optical absorption coefficient (α) can be calculated from the transmittance using the following relation

$$\alpha = [2.3026 \log (1/T)]/d$$

Where T is the transmittance and d is the thickness of the sample. For a direct band gap material, the absorption coefficient α is related to light frequency according to the following formula.

$$\alpha h\nu = A(h\nu - E_g)^{1/2}$$

Where A is a constant, Eg is the optical band gap energy, h is the Plank‟s constant and v is the frequency of the incident photons. The band gap energy of the sample can be estimated by plotting $(\alpha h\nu)^2$ versus hν and by extrapolating the linear portion near the

onset of absorption edge to the energy axis. The extinction coefficient, *K* can be obtained from the following relation.

$$K = \frac{\alpha\lambda}{4\pi}$$

Where λ is the wavelength. The refractive index (n) can be determined from the reflectance data using, *n = [-(R+1)±2√R] /(R-1).* The real ε_r and imaginary ε_i parts of the dielectric constant can be determined using the formula $\varepsilon_r = n^2 - k^2$ and $\varepsilon_i = 2nk$.

In the present work the optical properties of LA and LA doped ADP, KAP and KDP crystals were studied by the transmission spectrum using Shimadzu UV-1601 visible spectrometer. In this experiment the transparent crystal with 2mm thickness samples were used and mounted in a standard manner so that equal area of samples was exposed to the radiation. The optical constants were calculated from transmission spectrum. Dielectric properties of as grown crystals also estimated by using the values of optical constants.

For optical application, especially for SHG, the material considered must be transparent in the wavelength region of interest. We can measure this property from the optical transmission studies of UV spectrum. Nonlinear optical single crystals are used in the area of fibre optic communication, optical frequency conversion, optical data storage etc.

2.3.5 Thermal Analysis

2.3.5.1 Thermogravimetric (TG) and Differential Thermal Analysis (DTA)

TGA is a thermal analysis technique which measures the weight change in a material as a function of temperature and time, in a controlled environment. This can be very useful to investigate the thermal stability of a material, or to investigate its behavior in different atmospheres (e.g. inert or oxidizing). It is suitable for use with all types of solid materials, including organic or inorganic materials.

TGA is commonly employed in research and testing to determine characteristics of materials such as polymers, to determine degradation temperatures, absorbed moisture

content of materials, the level of inorganic and organic components in materials, decomposition points of explosives, and solvent residues. It is also often used to estimate the corrosion kinetics in high temperature oxidation.

DTA is a calorimetric technique, recording the temperature and heat flow associated with thermal transitions in a material. This enables phase transitions to be determined (e.g. melting point, glass transition temperature, crystallization etc.).

Simultaneous TGA-DTA/DSC measures both heat flow and weight changes (TGA) in a material as a function of temperature or time in a controlled atmosphere. Simultaneous measurement of these two material properties not only improves productivity but also simplifies interpretation of the results. The complementary information obtained allows differentiation between endothermic and exothermic events with no associated weight loss (e.g., melting and crystallization) and those that involve a weight loss (e.g., degradation).

Equipment

The analyzer usually consists of a high-precision balance with a pan (generally platinum) loaded with the sample. A different process using a quartz crystal microbalance has been devised for measuring smaller samples on the order of a microgram (versus milligram with conventional TGA)[1]. The sample is placed in a small electrically heated oven with a thermocouple to accurately measure the temperature. The atmosphere may be purged with an inert gas to prevent oxidation or other undesired reactions. A computer is used to control the instrument.

Methodology

Analysis is carried out by raising the temperature of the sample gradually and plotting weight (percentage) against temperature. The temperature in many testing methods routinely reaches 1000°C or greater, but the oven is so greatly insulated that an operator would not be aware of any change in temperature even if standing directly in front of the device. After the data are obtained, curve smoothing and other operations may be done such as to find the exact points of inflection.

2.3.6 Vicker's Microhardness

The mechanical properties of crystalline and non-crystalline substances are closely related with their other physical and electrical properties, and determine the performance of devices prepared from the solids. Consequently, there is a constant interest in assessing the mechanical properties of solids. Hardness testing, which involves the production of indentations in small areas on the surface by pressing a hard indenter of specified geometry into the solid, is frequently used to assess the mechanical properties. Since the deformed region beneath and around an indentation is confined to a small volume of the solid, the technique is essentially non-destructive in contrast to destructive experimental techniques involving compression, extension or bending of bulk samples for the determination of the mechanical properties introducing mechanical deformation in the entire bulk. The hardness H of a solid is defined as its resistance to local plastic/permanent deformation. The simplest way to obtain it is to press a hard indenter of known geometry and to divide the applied load P by the area A of the indentation produced, i.e. $H = P/A$

Hardness studies will be done by using Vicker"s hardness formula, $H = 1.8544 \times P/d^2$ kg/mm^2 where P is the applied load in kg and d is the mean diagonal length of the sample in millimeters.

2.3.7 DC Electrical Conductivity

The DC electrical conductivity measurements were carried out to an accuracy of ±4% using the conventional two-probe (parallel plate capacitor) technique at various temperatures ranging from 35 to 140^0C along c- direction. The resistance of the crystal was measured using a million magohmmeter. Temperature was controlled to an accuracy of ±1 K. Crystals with high transparency and large surface defect-free 2 mm thickness were selected and used for DC electrical measurement. The dimensions of the crystals were measured using a travelling microscope. The DC conductivity ζ_{dc} of the crystals was calculated using the relation; $\zeta_{dc} = d/(RA)$; Where R is the measured resistance, d is the thickness of the sample and A is the area of the face in contact with the electrode.

2.3.8 AC Electrical Conductivity and Dielectric Properties

Dielectric constant can be measured from the AC experiment. The increase in dielectric constant at low frequency is attributed to the space charge polarization. In normal dielectric behavior, the dielectric constant decreases with increasing frequency reaching a constant value, depending on the fact that beyond certain frequency of the electric field, the dipole does not follow the alternating field. Materials with high dielectric constant values are good candidates for heating devices and low dielectric values are good for optical devices. Dielectric materials are used in the fabrication of capacitors, thin film transistors, resistors, insulators, tunneling devices, etc. Dielectrics have the strange property of making space seem bigger or smaller than it looks. The dielectric constant value tells us how much smaller or bigger the space gets. It shows itself in two ways. First, when we put some dielectric between two electric charges it reduces the force acting between them, just as if we'd moved them apart. Secondly, the dielectric constant of a material affects how electromagnetic signals (light, radio waves, millimeter-waves, etc.) move through the material. A high value of dielectric constant makes the distance inside the material look bigger. This means that light travels more slowly. It also „scrunches up" the waves to behave as if the signal had a shorter wavelength. For electromagnetic waves, just like the forces between charges, the dielectric warps the space to make it look a different size.

How effective a dielectric is at allowing a capacitor to store more charges depends on the material the dielectric is made. Every material has a dielectric constant ε . This is the ratio of the field without the dielectric (E_o) to the net field (E) with the dielectric: $\varepsilon = E_o/E$

2.3.9 Crystal Dissolution and Chemical Etching

When a crystal is placed in an etching solution, dissolution does not start instantaneously. In fact, in a small fraction of time the so-called double layer develops at the interface as a consequence of the difference in chemical potential of the ions in the crystal and in the

solution. The dissolution rate of a crystal is affected by both internal and external factors. The internal factors are connected with the chemical nature, type of bonding, elements, etc., of the crystal, with the presence and chemical nature of impurities incorporated into the crystal lattice, with the crystallographic orientation of the surface, and with cracks and lattice imperfections such as dislocations and point defects. External factors are the nature of the solvent, the composition of the solvent, its temperature, the stirring of the solvent, and the addition of impurities to the solvent. In some cases, especially for metals and semiconductors, the time of etching also influences the dissolution rate. The heterogeneous nature of the reactivity of the crystal surface has been known for a long time. The existence of a relation between the heterogeneities and the dislocations of the crystals was first suggested by Read and Shockley [11].

Selective etching (dissolution) of a surface has proved to be one of the most powerful methods for mapping and characterizing growth defects. The stress field generated by dislocations facilitates easy dissolution around these sites. Such dislocation etch pits have characteristic shapes, and this gives information about the kind, configuration and inclinations of the dislocations. Etch pits reveal the emergence of dislocations at the surface under examination and thus give a direct measure of dislocation density in the plane of examination.

When a crystal face is exposed to a solvent, dissolution begins by the nucleation of unit pits on one molecular depth, which then grows in size by the retreating steps across the crystal surface. Dissolution takes place under the conditions of low under-saturation by the retreat of surface steps, which have kinks at the active sites. The geometry of etch pits is determined by the relative rates of removal of atoms along different directions. The dislocations can be either nucleated during growth (grown-in), or generated after growth (post-growth). The post growth dislocations may result either from stress induced plastic deformation or from vacancy condensation. In mane cases these categories can be distinguished on the basis of their typical geometry and distribution. External factors such as temperature, stirring and added impurities affect this removal rate and thus leads to a change in geometry of etch pits. Since the geometrical variation of etch pits strongly

depends on the arrangement of ions or atoms which comprise the crystal faces, the shapes of etch pits also differ for various crystal faces. The shapes of etch pits can also be varied by altering the concentration of the solvent.

The necessary condition for the formation of visible etch-pits is the proper resolution of three dissolution rates. The first one is the normal rate V_n along the dislocation line and is directed normal to the surface. The second is the tangential or lateral etch rate V_t that describes the rate of spreading up of the elementary steps along the surface. The third one is the rate of dissolution of the surface V_P in areas free from dislocations. This rate is also directed perpendicular to the surface.

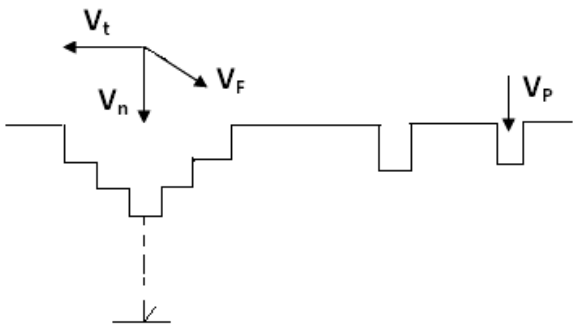

Fig. 2.14 The different etch rates involved in the formation of an etch pit at a dislocation site.

The absolute values of these rates for a crystal are governed by the nature and composition of the etchant as well as by the conditions like temperature and stirring. Impurities segregated along the dislocation lines also affect the values of V_n and V_t. One of the important conditions for the formation of etch-pits is that the rate of dissolution along the surface (V_t) must not greatly exceed that perpendicular to the surface (V_n). The optimum ratio V_n/V_t is found to be ~0.1.

Selective etching (dissolution) of a surface has proved to be one of the most powerful methods for mapping and characterizing growth defects. The necessary condition for the formation of visible etch-pits is the proper resolution of three dissolution rates.

1. The first one is the normal rate V_n along the dislocation line and is directed normal to the surface.
2. The second is the tangential or lateral etch rate V_t that describes the rate of spreading up of the elementary steps along the surface.
3. The third one is the rate of dissolution of the surface V_P in areas free from dislocations. This rate is also directed perpendicular to the surface.

In the present study chemical etching was carried out using double distilled water which was used as solvent for the crystal growth experiments. Transparent crystal free from inclusions and cracks were selected for this study. Crystal surface was first dipped in water for ten seconds at room temperature and then dried with filter paper, the surface was immediately examined for their microstructure by using an optical microscope (SWIFT) in the reflection mode with „100 X" magnification.

2.4 References

[1] Mansfield, E.; Kar, A.; Quinn, T. P.; Hooker, S. A., "Quartz Crystal Microbalances for Microscale Thermogravimetric Analysis", 2010.

[2] Tabor, D. in: Microindentation Techniques in Materials Science and Engineering, Blau,P. J. and B. R. Lawn (Eds.), (ASTM, Philadelphia), 129, 1985.

[3] Sangwal, K., "Etching of Crystals",Theory, Experiment and Application;.North-Holland: Amsterdam, 1987.

[4] Sangwal, K., Szurgut,M., Karniewiez, J. and W. Kolasinski, "On the Selective Etching of KDP Crystals", J. Crystal Growth, **58**, p.261-266, 1982.

[5] Van Enckevort, W. J. P. and W. H. Van Der Linden, "On the Relation Between Etch Pits or Growth Hillocks and Dislocations on the (111) Faces of Potassium Aluminum Alum", J. Crystal Growth, **47**, p. 196-202, 1979.

[6] Rosencher, E., and Vinter, B., "Optoelectronics", Cambridge University Press, 2002.

[7] Pankove, J. I.,"Optical Processes in Semiconductors", Dover Publications, New York, 1971.

[9] Goldstein, J. I., "Scanning electron microscopy and X-ray microanalysis", Vol.**1**, Springer, p.1- 689, 2003.

[10] Palik, E. D.,"Handbook of Optical Constants of Solids II (Academic Press, San Diego) (now Elsevier), 1991.

[11] Read, W. T. and Shockley, W., "Dislocation models of crystal grain boundaries", Physical Review, Vol. **78**, No. 3, pp. 275-289, 1950.

CHAPTER 3

GROWTH AND CHARACTERIZATION OF AMINO ACID (L-ALANINE) CRYSTAL

CHAPTER 3

GROWTH AND CHARACTERIZATION OF AMINO ACID (L-ALANINE) CRYSTAL

3.1 Introduction

The first growing development of optical fiber communication systems has stimulated the search for highly nonlinear materials capable of fast and efficient processing of optical signals. Nonlinear crystals have proven to be interesting candidates for number of applications like second harmonic generation, frequency mixing, electro optic modulation, optical parametric oscillation, etc. [1]. Organic crystals are being recognized as the materials of the future for their molecular structure and higher nonlinear properties. The development of highly efficient nonlinear crystal for UV-Vis region is extremely important for both laser spectroscopy and laser processing. In the last decade, organic NLO with aromatic rings have given much attention because of their high nonlinearity, fast response and tailor made flexibility. LA is an efficient organic NLO compound under the amino acid category. LA was first crystallized by Bernal [2]. Simpson et. al [3] and Destro et. al [4] were studied the crystal structure at room temperature and lower temperatures. In their attempts, very small crystals were grown, which were unsuitable for optical investigations. Large crystals of dimensions (3 cm^3) with promising NLO property were reported by Misoguti et. al [5]. The pure LA crystals grown from aqueous solution was reported by Vijayan et. al [6], and found higher damage threshold than KDP. Nucleation thermodynamical properties of pure LA were reported by Raghavalu Thenneti et. al [7]. Pure and lithium doped LA crystals have been grown by slow evaporation technique at 32 ^0C by Suresh Kumar et. al [8]. He found that the optical transmittance, thermal stability, SHG and hardness of LA crystals have been improved by lithium dopant. Many optically active amino acids show high efficient optical SHG and are promising candidates for coherent blue-green laser generation and frequency doubling applications. More over; amino acids such as LA, L-histidine and L-threonine have special features such as (i) molecular chirality, which forces the molecule to crystallize in a non centrosymmetric space group, an essential criterion for SHG material. (ii) wide

transparency ranges in the visible and UV spectral regions. (iii) zwitterionic nature of the molecule ($^{+}NH_3$ $-C_2H_4$ $-$ COO^{-}), which favors for possessing high electro optic parameters and good mechanical and thermal stability of the crystals. In this paper, we report the growth and characterization of LA single crystal. The solubility of LA was estimated at different temperatures using double distilled water. The grown crystals were characterized by various methods.

3.2 Experiment

3.2.1 Determination of Solubility of L-alanine

The solubility of pure L-alanine crystals in double distilled water was determined in the temperature range 30 – 45 ^{0}C insteps of 5 ^{0}C using a constant temperature bath of accuracy ± 0.01 ^{0}C. The variation of solubility (g/100 mL H_2O) with temperature is shown in fig.3.1. The results indicate that there is a positive slope of solubility of LA crystal.

3.2.2 Metastable Zone Width Measurement

Metastable zone width is an essential parameter for the growth of large size crystals from solution since it is the direct measure of the stability of the solution in its supersaturated region. The width of the metastable zone of the solution in their saturated state was determined by the nucleation method. Crystal can be grown only from supersaturated solution. The region of supersaturated solutions can be divided into two sub-regions: Metastable (stable) and labile (unstable) zones. Nucleation will occur spontaneously in the labile zone. Metastable zone refers to the level of supersaturation where spontaneous nucleation can not occur and a seed crystal is essential to facilitate growth. 100 ml of LA solution saturated at 30 ^{0}C was prepared in accordance with the solubility diagram. The solution was stirred at 300 rmp using a DC motor for about 6 hours for homogenization and then filtered using a micro filter paper (10 µm). The saturated solution in a beaker kept in a constant temperature bath with cryostat facility with an accuracy of ± 0.01 ^{0}C. The temperature of the bath was reduced at the rate of 4 ^{0}C per

hour while stirring the solution continuously. The temperature at which the first speck of the particle appeared was recorded. The difference between the saturated temperature and the temperature at which the first visible speck formed given the metastable zone width. The experiment was repeated for solutions saturated at 30, 35, 40 and 45 ^{0}C. The obtained solubility and nucleation curve for LA is shown in fig. 3.1. In general, the metastable zone width decreases with increasing temperature. In the case of LA the metastable zone width first decreases and then increases with increasing temperature. It happened due to high solubility and the LA solution is more viscous at higher temperature.

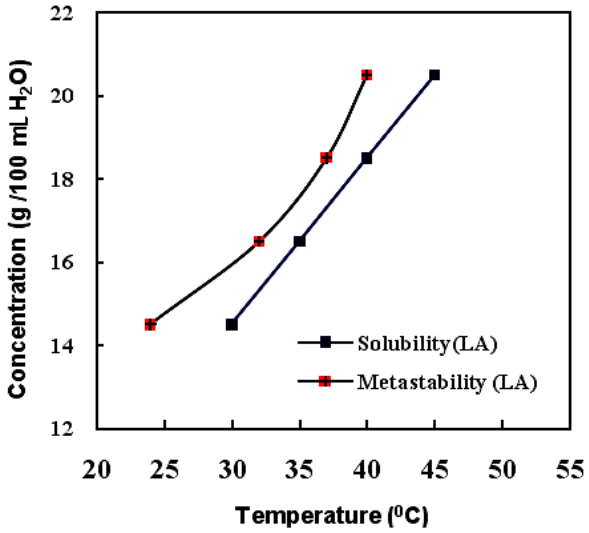

Fig.3.1 Metastable zone width of pure LA

3.2.3 Growth of Pure LA Crystals

The crystallized salts of LA (AR grade chemical from Sigma) were used in the present crystal growth experiment. This material was further purified by repeated crystallization process, and the crystallized material was used for crystal growth. The concentrated solution at 30 ^{0}C was prepared for crystal growth with the help of the solubility diagram. After obtaining the saturation, the prepared solution was filtered using micro filter paper (10 µm) and the solution was optimally closed using a perforated thin polyethylene sheet and placed in a constant temperature bath for seed growth. A suitable good quality seed crystal was selected from the supersaturated solution and hung inside the mother solution

and kept it in a constant temperature bath with an accuracy ± $.01^0$ C. A colorless bulk crystal with dimensions 17 x 5 x 3 mm^3 was harvested after 30 days by the solvent evaporation process at room temperature, shown in Fig. 3.2.

Fig. 3.2 Solution grown LA crystal

3.3 Characterization of Pure LA Crystals

The grown crystals were subjected to spectral analysis for the investigation of structural and optical properties. In order to confirm the presence of elements into LA crystals was subjected to EDX. EDX pattern was recorded using JEOL-6360 Scanning Electron Microscope. XRD pattern was recorded using a Philips X pert PRO X-ray diffractometer with CuK_α (λ = 1.5418 Å) radiation for structural analysis. In order to confirm the presence of functional groups in the crystal lattice, FTIR spectrum was recorded by KBr pellet technique using a Shimadzu FTIR – 8900 spectrophotometer in the wave number range 400-4000 cm^{-1}. The optical properties of the grown crystal were studied by the transmission spectrum using Shimadzu UV-1601 visible spectrometer in the wavelength region from 200 to 1100 nm. Crystals with high transparency and defect-free with the dimensions of 8 mm x 6 mm x 2 mm were cut into a rectangular size and surfaces were coated with silver paint to give good electrical contact between the electrodes were selected for the electrical conductivity measurements. The DC electrical conductivity measurements were carried out along the unique axis (c-) using the conventional two-probe technique using a million ohmmeter at various temperatures ranging from 35 to

140 ^{0}C. The field is applied to perpendicular to c- axis. The DC electrical conductivity (ζ) of the crystal was calculated using the relation ζ = d/(RA), where R is the measured resistance, d is the thickness of the sample crystal and A is the area of the face of the crystal in contact with the electrode. Thermal analysis was conducted on pure LA crystal using simultaneous TG, DTA and DTG using thermal analyzer (model no.TG/DTA-6300) from 40 to 600 ^{0}C at heating rate of 15 ^{0}C/min in nitrogen atmosphere. The Vickers microhardness number (VHN) of pure LA crystal was studied using Shimadzu HMV-2T (Vickers Microhardness tester). The surface morphology of pure LA on the (001) plane in the water was studied by optical microscope.

3.4 Results and Discussion

3.4.1 Fourier Transform Infrared Spectroscopy

FTIR spectrum of LA crystal recorded in the range 400-4000 cm^{-1} is shown in the fig. 3.3. The broad envelope between 2400 and 3400 cm^{-1} is due to overlapping of peaks by N-H of NH_3 and C-H stretching modes. The broading is due to hydrogen bonding interaction of N-H groups. The C = O stretching mode at 1600 cm^{-1} is also broadened. The bending modes of CH_3 are positioned at 1355.9 and 1450.4 cm^{-1}. The presence of torsional oscillation of NH^+_3 is evident from the peak at 538.1 cm^{-1}. The peak at 1112.9 cm^{-1} is due to –C-O (with a vertical double bond of oxygen on C) stretch. The peaks at 1502.4 and 1413.7 cm^{-1} could be assigned to asymmetric and symmetric modes of carboxylate anion. The overtone band at 2111.9 cm-^{1} is due to the contribution of the symmetrical NH_3^+ bending and the torsional oscillation of the NH^+_3 group.

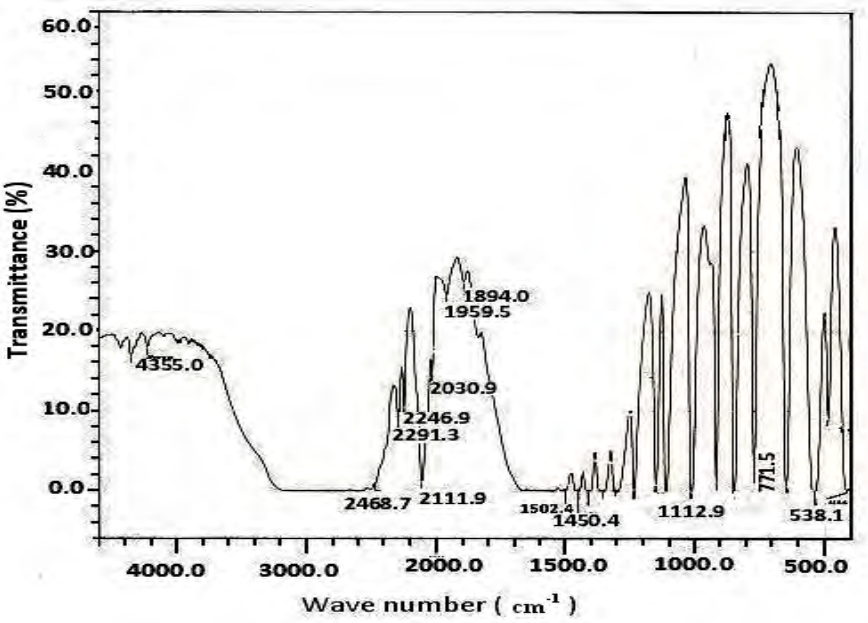

Fig. 3.3 FTIR spectrum of pure LA crystal

Table 3.1 Vibrational frequencies obtained for pure LA crystal through FTIR studies

Calculated Frequencies (cm^{-1})	Observed IR frequencies (cm^{-1})	Assignments
(Literature data)	Pure L-alanine	
3400-3250	3260	N-H stretching
3300-2500	2600	O-H stretching
3100-2210	2469	C-H stretching
2260-2100	2112	Torsional vibration of NH_3^+
1650-1580	1600	Asymmetric stretching of CO_2^-
1550-1475	1502	Symmetric bending of NH_3^+
1500-1400	1450	Degenerative deformation of CH_3
1500-1400	1414	Symmetric stretching of CO_2
1370-1350	1356	C-H deformation in CH_3
1320-1000	1113	C-O stretching, $NH_{3\ rocking}$
1000-650	850	O-H out-of-plane deformation
1000-650	771	CH_2rocking
700-610	648	O-C=O in plane deformation
690-515	538	Torsional vibration of NH_3^+

3.4.2 Energy Dispersive X-ray Spectroscopy

In order to confirm the presence of the elements of pure LA in the crystal was subjected to EDX. The EDX spectrum of pure LA is shown in the fig.3.4. Atomic percent confirmed the presence of all elements in the LA crystal.

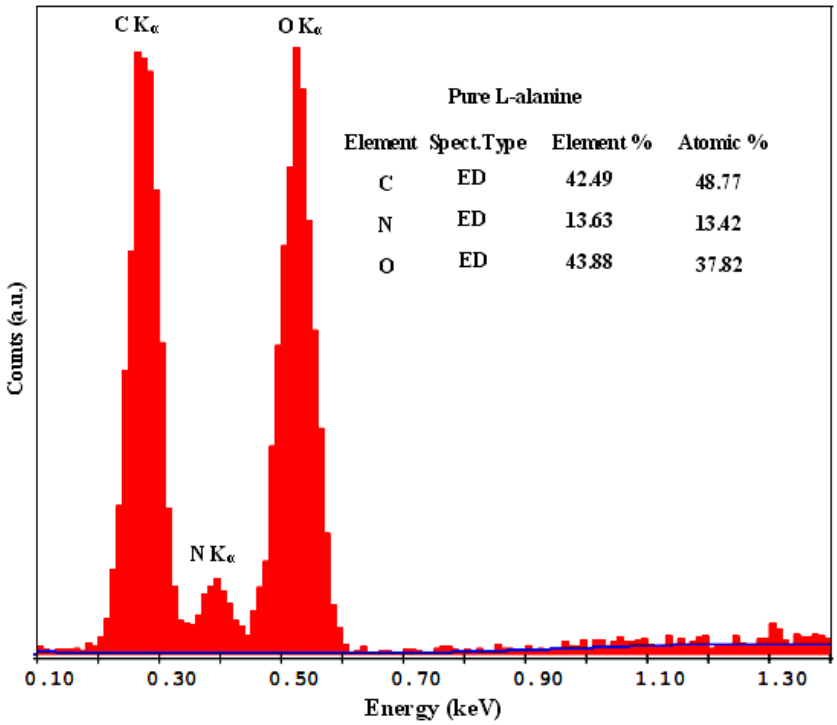

Fig. 3.4 EDX spectrum of pure LA crystal

3.4.3 X-ray Diffraction Analysis

The well grinded powder of as grown LA crystal was used to identify the crystal phase and structure. The XRD spectrum is shown in fig. 3.5. Well defined Bragg peaks are obtained at specific 2θ angles indicating that crystals are ordered (fig. 3.5).The narrow and strongest peak along the (120) direction confirms the crystalline nature of the grown crystals. The d spacing and hkl values for prominent peaks in the spectrum were identified and compared with ICDD (International Centre for Diffraction Data) data. It was confirmed that the crystal belongs to the orthorhombic crystal system with the lattice

parameters a = 6.008 Å, b = 12.317 Å, c = 5.804 Å and volume of the cell is v = 429.53 $(Å)^3$. The obtained lattice parameter values are in good agreement with the reported literature values [5].

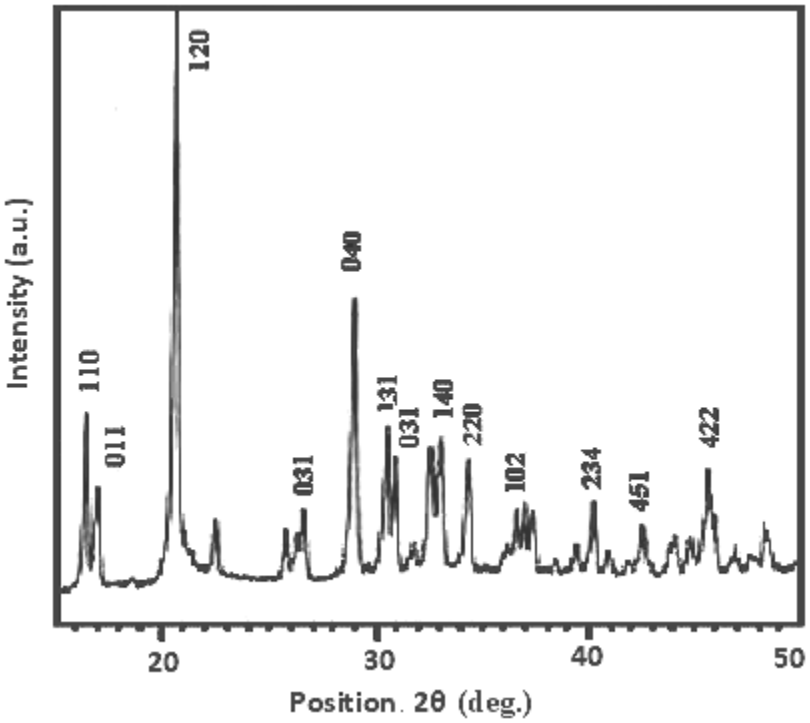

Fig. 3.5 XRD spectrum of pure LA crystal

Lattice parameters calculation for LA (Orthorhombic) crystal system and tabulated in the table 3.2

$$a \neq b \neq c \qquad \alpha = \beta = \gamma = 90^{\circ}$$

$$\frac{1}{d_{hkl}} = \sqrt{\frac{h^2}{a^2} + \frac{k^2}{b^2} + \frac{l^2}{c^2}}$$

Table 3.2 Powder XRD data of pure LA crystal

Lattice parameters	Calculated values	Reference [6]	Reference [8]
a(Å)	6.028 (Å)	6.032 (Å)	6.041 (Å)
b(Å)	12.317 (Å)	12.343 (Å)	12.356 (Å)
c(Å)	5.804 (Å)	5.784 (Å)	5.778 (Å)
Volume $(Å)^3$	430.929 $(Å)^3$	430.636 $(Å)^3$	431.284 $(Å)^3$
Crystal system	Orthorhombic	Orthorhombic	Orthorhombic

3.4.4 Optical Transmission Analysis

The UV-Vis NIR optical transmission and absorption spectra of pure LA crystal are shown in fig. 3.5 and fig. 3.6. It is clear from the figure that the as grown LA crystal has the sufficient transmission in the entire visible and near IR region. Which is the most desirable property of materials possessing NLO activity? There was a strong absorption at 290 nm. Absorption in the near ultraviolet region arises from electronic transitions associated within the sample.

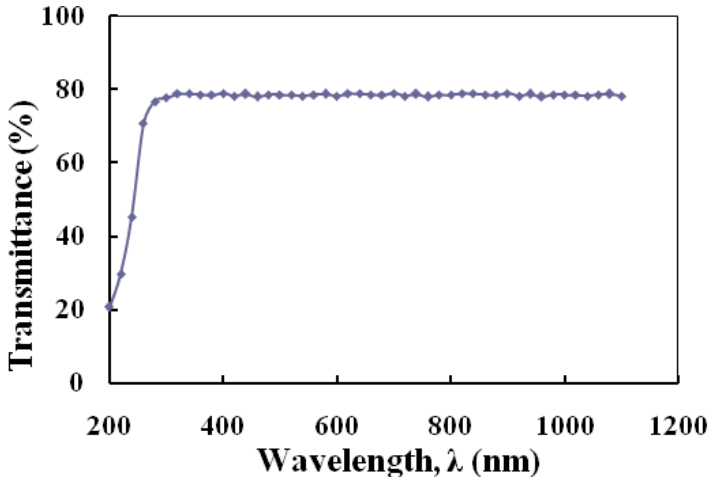

Fig. 3.6 Transmission spectrum of pure LA crystal

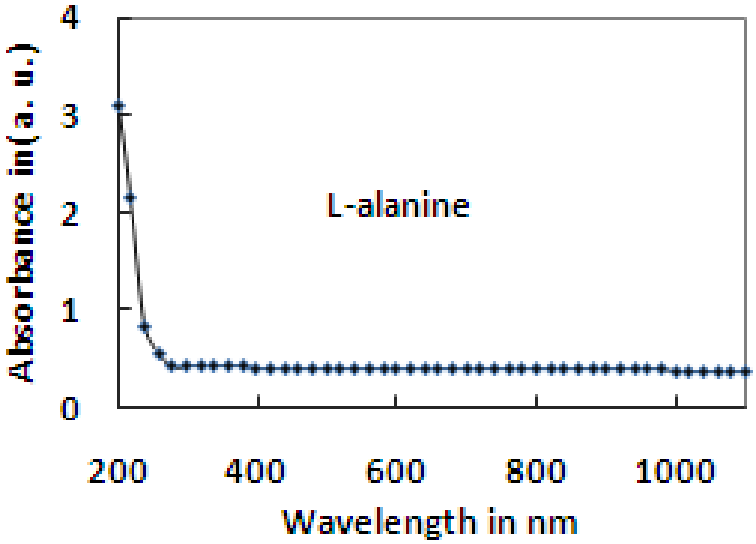

Fig. 3.7 Absorption spectrum of pure LA crystal

3.4.5 Optical Parameters Calculation

The dependence of optical absorption coefficient with the photon energy helps to study the band structure and the type of transition of electrons. The optical absorption coefficient (α) calculated from the transmittance using the following relation

$$\alpha = [2.3026 \log (1/T)]/d$$

where T is the transmittance and d is the thickness of the sample. For a direct band gap material, the absorption coefficient α is related to light frequency according to the following formula.

$$\alpha h\nu = A(h\nu - E_g)^{1/2}$$

Where A is a constant, Eg is the optical band gap energy, h is the Planck's constant and ν is the frequency of the incident photons. The band gap energy of the sample can be estimated by plotting $(\alpha h\nu)^2$ versus hν and by extrapolating the linear portion near the onset of absorption edge to the energy axis. The band gap energy was found to be 2.75 eV. The extinction coefficient, *K* calculated from the following relation.

$$K = \frac{\alpha\lambda}{4\pi}$$

where λ is the wavelength. The reflectance in terms of absorption coefficient can be written as

$$R = 1 \pm [1 - exp(-\alpha t) + exp(\alpha t)]^{1/2} / 1 + exp(-\alpha t)$$

The refractive index (n) calculated from the reflectance data using, n = [-(R+1)±2√R] /(R-1). The real ε_r and imaginary ε_i parts of the dielectric constant calculated by using the relations $\varepsilon_r = n^2 - k^2$ and $\varepsilon_i = 2nk$.

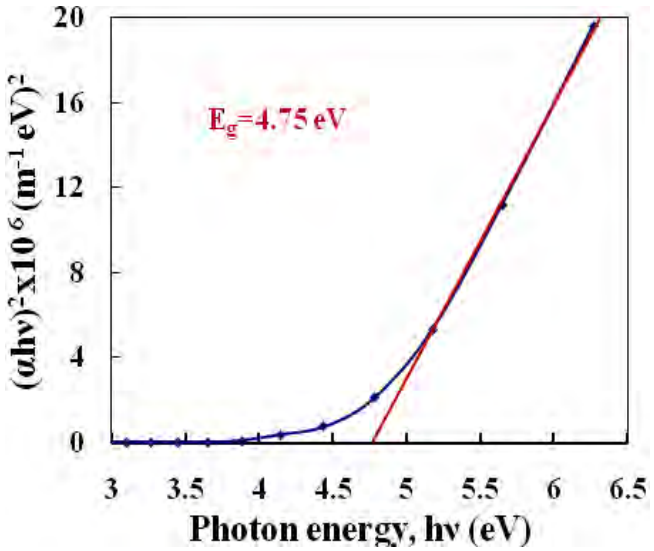

Fig. 3.8 Photon energy vs $(\alpha hv)^2$ of pure LA crystal

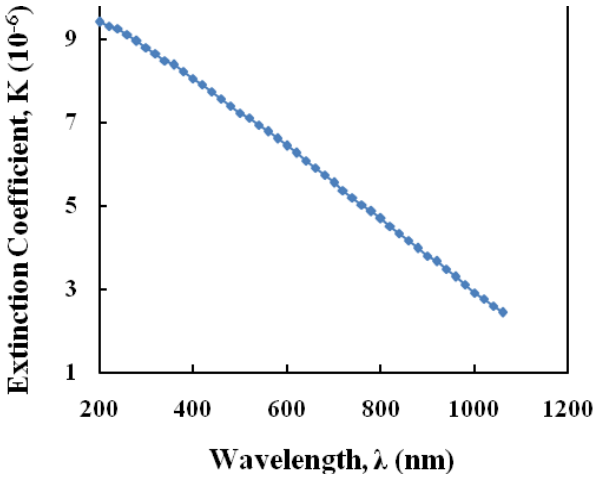

Fig. 3.9 Wavelength vs extinction coefficient, K

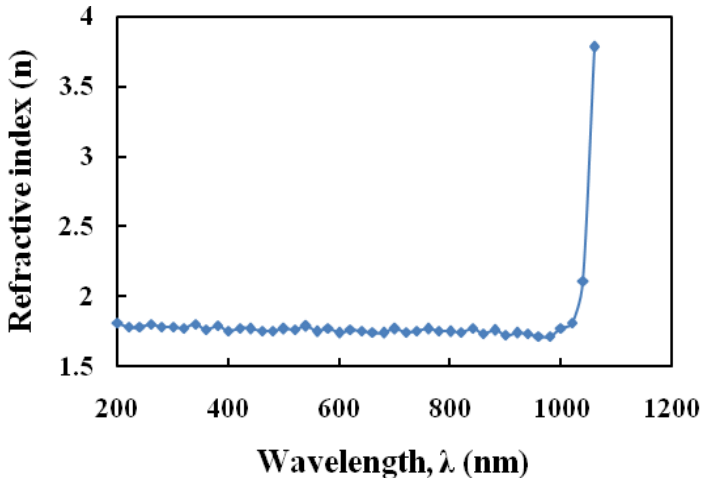

Fig. 3.10 Photon energy vs refractive index

3.4.6 Dielectric Studies

The study of dielectric constant of a material gives an outline about the nature of atoms, ions and their bonding in the material. The dielectric constant (ε_r) and dielectric loss ($\tan\delta$) depend on frequency of applied field. Fig. 3.11 shows the variation of dielectric constant with photon energy. The value of dielectric constant decreases as the frequency increases and it becomes independent of frequency at higher frequency region. The high value of dielectric constant in the low frequency region may be due to the contributions of electronic, ionic, dipolar, and space charge polarizations [12]. The electronic exchange of the number of ions in the crystal gives local displacement of electron in the direction of the applied field, which in turn give rise to polarization. Continuous and gradual decrease in dielectric constant suggests that pure LA crystal like any normal dielectric may possess domains of different size and varying relaxation times. It is evident that the lower value of dielectric constant is a suitable parameter for the enhancement of SHG coefficient [13]. Fig. 3.12 shows the variation of dielectric loss with photon energy of applied field at room temperature. The behavior of variation is similar to that of dielectric constant with frequency. This is the normal behavior observed earlier [8,14]. The dielectric loss is a measure of the energy absorbed by dielectric. Usually the dielectric has a resistance R and reactance $1/\omega C$. Which are related to the phase angle $\tan\delta = 1/\omega CR$,

where C is a capacitance. So the low dielectric loss at high frequency reveals the superior optical quality of the crystals with lesser defects, and this parameter is of vital importance for various NLO applications.

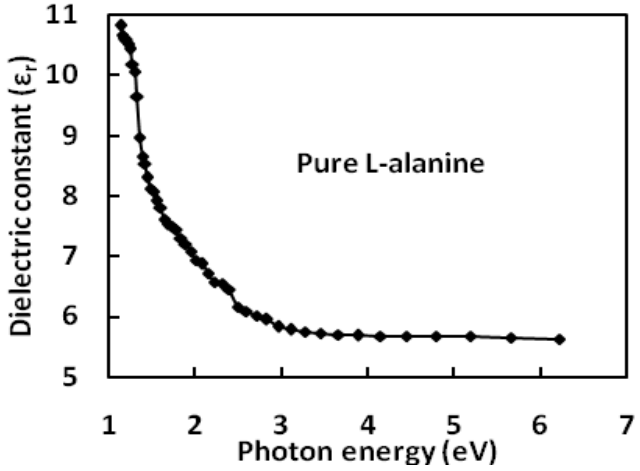

Fig. 3.11 Photon energy vs dielectric constant

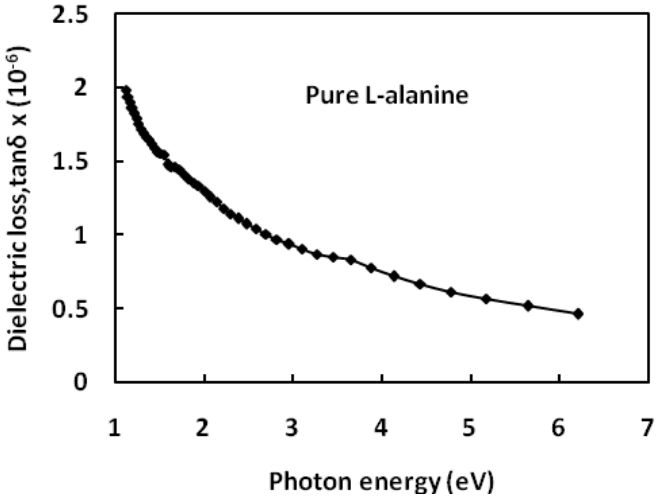

Fig. 3.12 Photon energy vs Dielectric loss (tanδ)

3.4.7 Thermal Analysis

The thermal stability of LA crystal is studied from the simultaneous TGA, DTA and DTG curves and is shown in the fig. 3.13. In the figure the DTA curve shows an endothermic peak at 272 ^{0}C for the pure LA crystal. The endothermic peak corresponds to the decomposition of the crystal. The TGA curve exhibited negligible weight loss in the region 40 ^{0}C to 200 ^{0}C as shown in the fig. 9. The decomposition begins at 146.1^{0}C and terminates at 281.9 ^{0}C. The weight loss observed from TGA graph for pure LA in the temperature range 146.1 ^{0}C to 281.9 ^{0}C is 97.0%. The use of thermogravimetry data to evaluate the kinetic parameters of solid state reaction involving weight loss has been investigated by many workers [9-10]. Very often the pyrolysis occurs through a many-stepped mechanism. The shape of the curve is determined by the kinetic parameters of pyrolysis such as order of reaction, frequency factor and energy of activation. The kinetic parameters of dehydration process of LA crystal were evaluated by using the Coates and Redfern [9] relation, which is as follows

$$Log_{10}[\{1-(1-\alpha)^{1-n}\}/\{T^2(1-n)\}] = \{log_{10}[AR/aE][1-2RT/E]\} - \{E/2.3RT\}$$

Where $\alpha = (W_0-W)/(W_0-W_f)$, W_0 is the initial weight, W is the weight at time t, W_f is the final weight, n is the order of the reaction, A is the frequency factor, E is the activation energy of the reaction, R is a gas constant and a is the heating rate in deg.C.min^{-1}.

To determine the value of activation energy and order of reaction, a plot of $log_{10}[\{1-(1-\alpha)^{1-n}\}/\{T^2(1-n)\}]$ vs 1/T is drawn for different values of n. The best linear fit gives the correct value of n. The value of activation energy can be calculated from the slope of a linear plot. The value of frequency factor can be obtained from the equation. This equation is applied for all values of n, except n = 1. For n = 1, a modified equation has been proposed [9] which is as follows

$$-log_{10}[-log(1-\alpha)^{1-n}/T^2] = [log_{10}\{AR/aE\}\{1-2RT/E\}] - [E/2.3RT],$$

Fig.3.16. Shows the linear plot for Coates and Redfern relation for LA crystal for dehydration process. Table 3.2 compiles the values of activation energy, frequency factor and order of reaction. Hence the high value of activation energy for LA crystal indicates stable nature. This can be verified from thermogram also.

Thermodynamic parameters have been evaluated for the dehydration process of L-alanine crystal by following expressions [11]. The standard entropy of activation $\Delta^{\#}S^0$ can be calculated by the relation,

$$\Delta^{\#}S^0 = 2.303 \, x \, R \, x \, log_{10} [Ah/kT_m]$$

Where, k = Boltzmann constant, h = Plank"s constant, T_m = Temperature, A = Frequency factor. The standard entropy of activation $\Delta^{\#}H^0$ can be calculated by using the following relation,

$$\Delta^{\#}H^0 = E\text{-}2RT$$

The standard Gibbs energy of activation $\Delta^{\#}G^0$ is possible to estimate from the equation

$$\Delta^{\#}G^0 = \Delta^{\#}H^0 - T\Delta^{\#}S^0$$

The estimated thermodynamic parameters are given in table 3.3.

Table 3.3 Kinetic and thermodynamic parameters of dehydration of pure L-alanine crystal.

Sample	Order of Reaction n	Activation energy kJ mol^{-1}	Frequency factor A	Standard Entropy kJ mol^{-1}	Standard Enthalpy kJ mol^{-1}	Standard Gibbs free energy kJ mol^{-1}
Pure LA	½	81.46	2.58 x 10^{10}	146.62	90.93	7.51

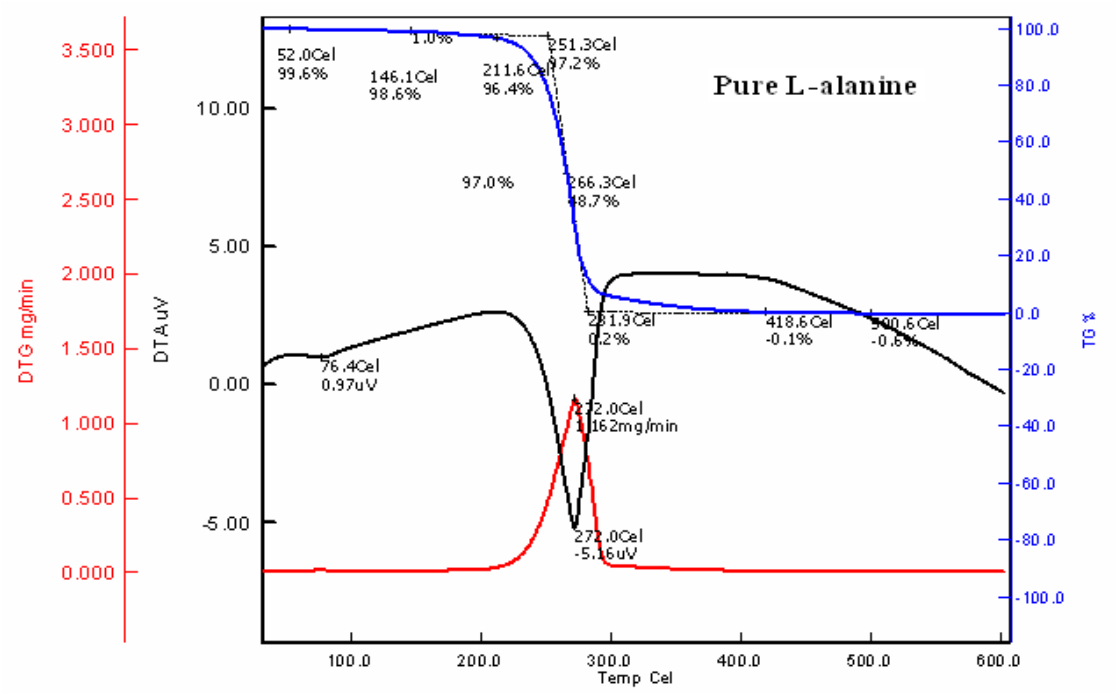

Fig. 3.13 Simultaneous graphs of TGA, DTA and DTG for pure LA crystal

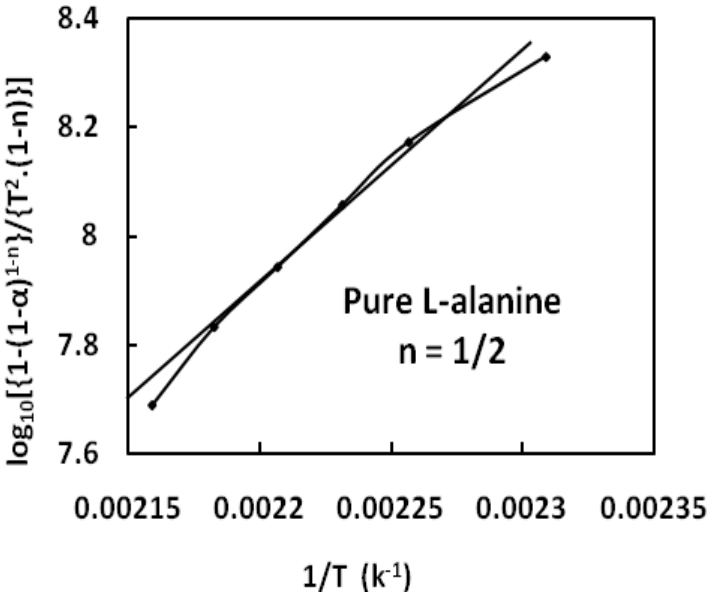

Fig. 3.14 Coates and Redfern relation for pure LA crystal

3.4.8 DC Electrical Conductivity

A graph of DC conductivity vs. temperature of pure LA crystal is plotted in fig. 3.15. It is found that conductivity increases exponentially with temperature. Conductivity is found in the order of 10^{-6} mho/m. At low temperature region, conductivity is expected due to the presence of weakly attached impurities and vacancies in the crystal lattice. At high temperature region, the attached water molecule is lost and fracture is developed and conductivity is cause mainly for intrinsic defects.

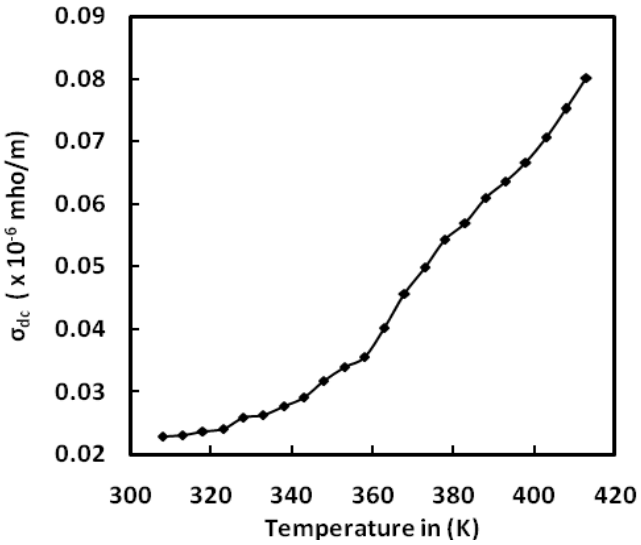

Fig. 3.15 Temperature vs DC electrical conductivity of pure LA crystal

3.4.9 Vicker's Microhardness Analysis

Microhardness studies are carried out using (120) face of the grown LA crystal. Vickers hardness measurement of LA are taken by varying applied loads for indentation time of 7 secs. For each load several trials of indentations are carried out. Vicker"s diamond pyramidal number, H_v was calculated from the following equation: $H_v = [(1.8544P)/d^2]$ kg/mm^2, where P is the applied load in kg and d is the diagonal length of indentation in mm. For load ranging from 5 to 100 g, the micro hardness value of L-alanine crystal is shown in the fig. 3.16. The microhardness (H_v) increases with load and above 30g loads, cracks started developing around the indentation mark. These

cracks happened due to generated dislocations on the surface. Usually the hardness and strength critically depend on the ease with which dislocations move.

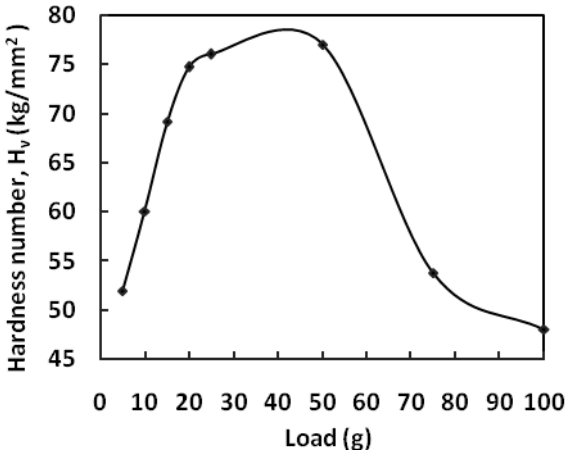

Fig. 3.16 Load vs hardness number of pure LA crystal

3.4.10 Etching Studies

The chemical etching studies were carried out on the as grown crystal of LA to study the distribution of structural defects in the grown crystal. The surface of a transparent and scratch free sample was polished with a wet filter paper, then etched in the etching solution (water) at room temperature for 10 s. Then soaked with a filter paper and examined under an optical microscope in reflection. Fig. 3.17 Illustrates the typical etch pattern observed on the (001) plane of the LA crystal. Rectangular etch pits elongated along the (001) direction were observed. These etch-pits are formed due to dislocations which are formed during the period of crystal grow [4]. The generation of dislocations is strongly correlated with the formation of inclusions in the crystals. Depending on the shape of the seed crystal, inclusions may also arise. The reason for bulk of the inclusions getting trapped could be due to fluctuations in supersaturation close to the crystal or due to transition from dissolution to growth. A number of parameters such as variation in supersaturation during the growth, non-uniform growth rate, etc., are responsible for the formation of inclusions.

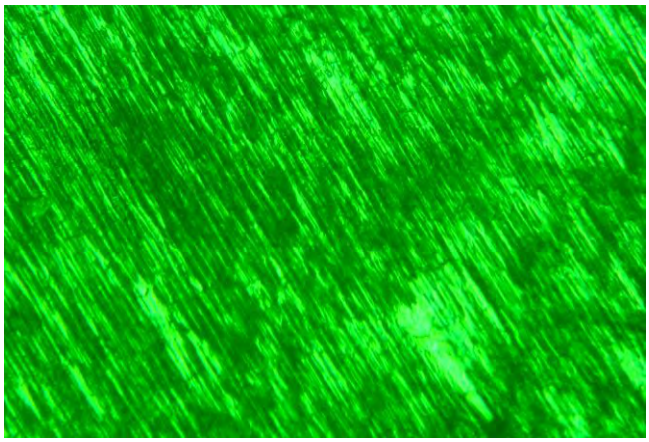

Fig. 3.17 Etch-pit pattern of pure LA crystal on the (001) plane

3.5 Conclusions

Large size LA crystal was successfully grown using the slow evaporation technique at room temperature. The grown crystals have been subjected to various characterization studies. The presence of all elements in the LA crystal confirmed by EDX. Surface morphology of pure LA crystal studied by etching. The XRD confirmed the orthorhombic structure of the crystal. Various functional groups have been identified by the FTIR spectral analysis. It is evident that the hydrogen bonding due to NH^{+}_{3} and COO^{-} is the additional major force in the crystal lattice of LA. The percentage of optical transmission is high in the visible region. TGA/DTA of pure LA crystal suggested that the LA provides better thermal stability. The high values of activation energy and standard entropy of activation suggested the stable condition of LA crystal. DC electrical conductivity increases with the temperature range of 35-140 ^{0}C. Mechanical behavior of grown crystal was studied on (120) plane using microhardness measurement and the hardness values are found to increased initially after that it decreased. So wide optical transmittance window and moderate mechanical property of LA crystal indicate that this material is an excellent candidate for SHG and optoelectronic vice applications.

3.6 References

[1] Chemla, D. S. and Zyss, J., "Nonlinear Optical properties of Organic molecules and Crystals", Academic Press, INC., p.297, 1987.

[2] Bernal, J. D., "The crystal structure of the natural amino acids and related compound",Zeitschrift fuer Kristallographie, Kristallphysik, Kristallchemie, Vol.**78**, p.363-369, 1931.

[3] Simpson J. H. and Marsh, E. R, "Micro-transitions or breathers in L-alanine", Acta. Cryst.,Vol.**8**, 550, 1996.

[4] Destro, R., Marsh, E. R and Bianchi, R., "A low-temperature (23K) study of L-alanine", J Phys. Chem., Vol. **92** (4), p.966-973, 1988.

[5] Misoguti, L.,Varela,T. A., Nunes,D. F., Bagnato, S. V., Melo, F. E. A. , Mendes Filho, J. and Zilio, S. C., "Optical properties of L-alanine organic crystals", Opt. Mater. Vol. **6**, p.147-152, 1996.

[6] Vijayan, N., Rajasekaran, S., Bhagavannarayana, G., Ramesh Babu, R., Gopalakrishnan, R., Palanichamy, M. and Ramasamy, P., "Growth and characterization of nonlinear optical amino acid single crystal: L-alanine," Crystal Growth & Design, Vol. **6**, No. 11, p.2441-2445, 2006.

[7] Raghavalu Thenneti, Ramesh Kumar, G., Raj Gokul, S., Mathivanan, V. and R. Mohan," Nucleation thermodynamical studies on nonlinear optical L-alanine single crystals", Journal of crystal Growth, Vol.**307**, Issue-1, p.112-115, 2007.

[8] Suresh Kumar, B., Sudarsana Kumar, R. M. and Rajendra Babu, K., "Growth and Characterization of pure and lithium doped L-alanine single crystals for NLO devices", Cryst. Res. Technol. Vol. **43**, No. 7, p.745-750, 2008.

[9] Coates W. A. and Redfern, J. P.," Kinetic parameters from thermogravimetric Data",Nature **201**, p.68-69, 1964.

[10] Joshi, S. V. and Joshi, M. J., "FTIR spectroscopic, thermal and growth morphological studies of calcium hydrogen phosphate dehydrate crystals", Cryst. Res. Technol. **38**, p.817, 2003.

[11] Laidler, J. K.,Chemical kinetics (New York: Harper and Row), 1987.

[13] Shahil Kirupavathy, S., Stella Mary, S., Srinivasan, P., Vijayan, N., Bhagavannarayana, G., Gopalakrishnan, R., "Investigations on the growth and characterization studies of cadmium thiourea acetate (CTA) single crystals",Journal of Crystal Growth, Vol. **306,** Issue 1, p. 102-110 ,2007.

[14] Miller, C.,"Optical second harmonic generation in piezo- electric crystals," Awl. Phys. Lett., Vol**. 5**, p. 17, 1964.

CHAPTER 4

GROWTH AND CHARACTERIZATION OF L-ALANINE DOPED AMMONIUM DIHYDROGEN PHOSPHATE (ADP) CRYSTALS

CHAPTER 4

GROWTH AND CHARACTERIZATION OF L-ALANINE DOPED AMMONIUM DIHYDROGEN PHOSPHATE (ADP) CRYSTALS

4.1 Introduction

Ammonium dihydrogen phosphate ($NH_4H_2PO_4$) is an inorganic, piezoelectric, antiferro-electric (due to hydrogen bonds) and nonlinear optical material. It is well known for its varied uses as electro-optic modulator, harmonic generators and parametric generators [1]. In the last decade the numerous applications of the NLO crystals investigated in the vast field of science and technology. But recent interest is focused on the development in the properties of the known crystals and the new semi organic (NLO) materials. Semi organic materials posses the advantage of both organic and inorganic materials in terms of high thermal and mechanical stability as well as broad optical frequency range, higher SHG and high damage threshold [2-3].

Amino acid family crystals are playing an important role in the field of non-linear optical organic molecular crystal. Among them LA, with chemical formula (CH_3 CH NH_2 COOH) is the smallest, naturally occurring chiral amino acid with a non-reactive hydrophobic methyl group (-CH3) as a side chain. LA has the zwitterionic form ($+NH_3$-C_2H_4-COO-) both in crystal and in aqueous solution over a wide range of pH, which favors crystal hardness for device application [9]. It belongs to the orthorhombic crystal system and the unit cell parameters are; a = 6.320 Å, b = 12.343 Å, c = 5.784 Å, $\alpha = \beta = \gamma = 90^0$. Recently, several new complexes incorporating the amino acid LA have been crystallized and their structural, optical and thermal properties have also been investigated [4-7]. The growth of pure LA crystals was reported [8] and found higher damage threshold than KDP.

Many reasonable studies have been carried out on pure ADP crystals [9-10]. The effect of additives as amino acid on growth, habit modification and different structures of ADP crystals have been studied [11-12]. It was also reported that the addition of some of the

amino acids as dopant enhances the NLO and piezoelectric properties of inorganic materials [12-13]. So LA doped inorganic material ADP will be of special interest as a fundamental building block to develop many complex crystals with improved NLO properties.

In this research works the effect of LA as impurity was studied (concentration ranging was from 3000 – 10000 ppm, i.e, 0.3 – 1.0 mol% and added them separately in the ADP saturated mother solution at 30^0C which were used for the growth of crystals by slow evaporation method at room temperature). The grown crystals were characterized by FTIR, EDX, Optical transmission, XRD, Thermal properties, Vicker‟s microhardness, D.C. electrical conductivity, Etching and compared all these results with pure ADP crystal.

4.2 Experiment

4.2.1 Determination of Solubility of Pure and LA Doped ADP

The solubility of pure ADP and LA doped ADP in double distilled water was determined in the temperature range 30-50 ^{0}C insteps of 5 ^{0}C using a constant temperature bath of accuracy $\pm 0.01^0$C. 500 mL of the saturated solution of pure ADP salt was prepared gravimetrically at 30 ^{0}C. This solution was stirred well for six hours constantly using magnetic stirrer and then filtered using Whatmann filter paper. This solution was taken in five different beakers of 100 mL and LA was added to each four beaker as 0.3 mol%, 0.5 mol%, 0.7 mol% and 1 mol%. After making supersaturated solution of ADP, the 5 mL of the solution was pipetted out and poured into a 10 mL beaker of known weight. The solvent was completely evaporated by warming the solution at 50 ^{0}C. The amount of the salt present in 5 mL of the solution was measured by subtracting the empty beaker‟s weight. From this the amount of the salt present in 100 mL of the solution was found out. In the same way, the amount of the salt dissolved in 100 mL at 35, 40, 45 and 50 ^{0}C was determined. Fig. 4.1 shows the solubility curves of pure and doped ADP salt. It is observed from the solubility graph that the solubility of pure and doped ADP in water increases as the temperature increases and decreases with doping concentration increase.

From this solubility data it can state that the ADP material has positive temperature coefficient.

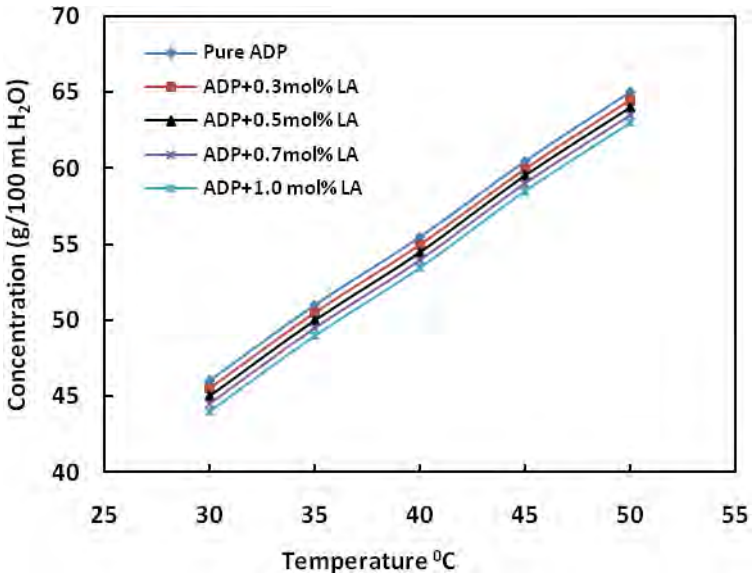

Fig. 4.1 Solubility curves of pure and LA doped ADP salt

4.2.2 Growth of Pure and LA Doped ADP Crystals

The pure ADP and LA (AR grade chemical from SIGMA) doped ADP crystals were grown using a good quality seed crystal at room temperature by solvent evaporation method. For the preparation of seed crystals, saturated solution of ADP was prepared first and then kept in a petri dish covered with a perforated polyethylene and allowed to grow seed crystals within 4-5 days. The pH of the different concentration of LA solution was ranged from 3.57 to 4.12. The purity of the crystals was improved by successive recrystallization process. The growth period takes 25-30 days for bigger size. The grown crystals were found color-less and transparent. Figure 4.2 shows the photographs of pure and doped ADP crystals.

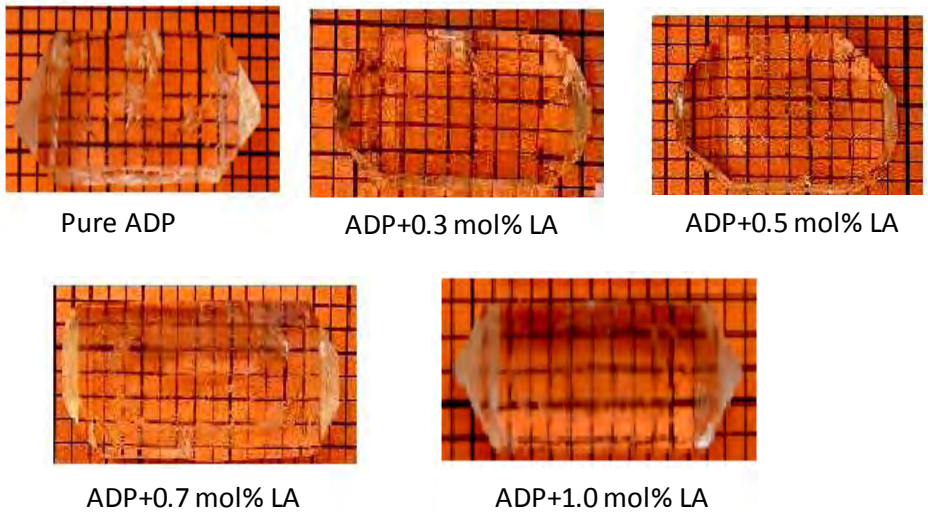

Fig. 4.2 Photographs of pure and LA doped ADP crystals

4.3 Characterization of Pure and LA Doped ADP Crystals

The grown pure and LA doped ADP crystals were subjected to investigation of structural, optical, thermal, mechanical, electrical properties. In order to confirm the presence of functional groups in the crystal lattice, FTIR spectrum was recorded by KBr pellet technique using a Shimadzu FTIR -8900 spectrometer in the wave number range 400-4000 cm^{-1}. In order to confirm the presence of the elements of LA into ADP crystals were subjected to EDX. EDX spectrums were recorded using JEOL-6360 Scanning Electron Microscope. Powder XRD pattern was recorded using a Philips X pert PRO X-ray diffractometer with CuK_{α} (λ = 1.5418 Å) radiation. The lattice parameters were calculated for pure and doped (0.3, 0.5, 0.7 and 1.0 mole% LA) ADP crystals using XRD data. The optical properties of the grown crystal were studied by the transmission spectra using Shimadzu UV-1601 visible spectrometer in the wavelength region from 200 to 1100 nm. Crystals with high transparency and large defect-free with the dimensions of 8 mm x 6 mm x 2 mm were cut into a rectangular size and surfaces were coated with silver paint to give good electrical contact between the electrodes; were selected for the electrical conductivity measurements. The DC electrical conductivity measurements were carried out along the unique axis (c-) using the conventional two-

probe technique using a million ohmmeter at various temperatures ranging from 35 to 140 ^{0}C. The field is applied to perpendicular to c- axis. The dimensions of the crystals were measured using a travelling microscope. The conductivity (ζ) of the crystal was calculated using the relation $\zeta = d/(RA)$, where R is the measured resistance, d is the thickness of the sample crystal and A is the area of the face of the crystal in contact with the electrode. Vicker‟s microhardness number of pure and doped crystals was studied using the HMV-2T, Shimadzu, Japan. Thermal analysis was conducted on pure and doped crystals using simultaneous thermogravimetric (TG), differential thermal analysis (DTA) and differential thermal gradient (DTG) using thermal analyzer (model no.TG/DTA- 6300) from 40 ^{0}C to 800 ^{0}C at heating rate of 15 ^{0}C/min in nitrogen atmosphere. Surface morphology of pure and doped crystals was studied by optical microscope SWIFT in the reflection mode with „100 X‟ magnification.

4.4 Results and Discussion

4.4.1 Fourier Transform Infrared Spectroscopy

The FTIR spectra of pure and LA doped ADP crystals are shown in Fig. 4.3 and their assignments in table 4.1. In the FTIR spectrum of pure ADP the O-H stretching vibration of water happened at 3100 cm^{-1}, P-O-H stretching at 1100 cm^{-1}, N-H stretching of ammonia at 2850 cm^{-1} and the PO_4 vibrations give their peaks at 545.8 and 405 cm^{-1}. The FTIR spectra of LA (.3, .5, .7 and 1 mol%) doped ADP crystals showed that the peak positions have been moved from lower to higher energy due to the presence of LA in to ADP. For example, the PO_4 vibration of the parent is shifted from 405 to 415 cm^{-1}. Similarly the P-O-H vibrations at 1100 and 925 cm^{-1} of the parent are shifted to 1125 and 975 cm^{-1}.Which confirmed the presence of LA in the lattice of ADP crystals. Similar results L-arginine monohydrochloride (LAHCl) and LA doped with ADP crystals found by Dhanaraj et. al [11].

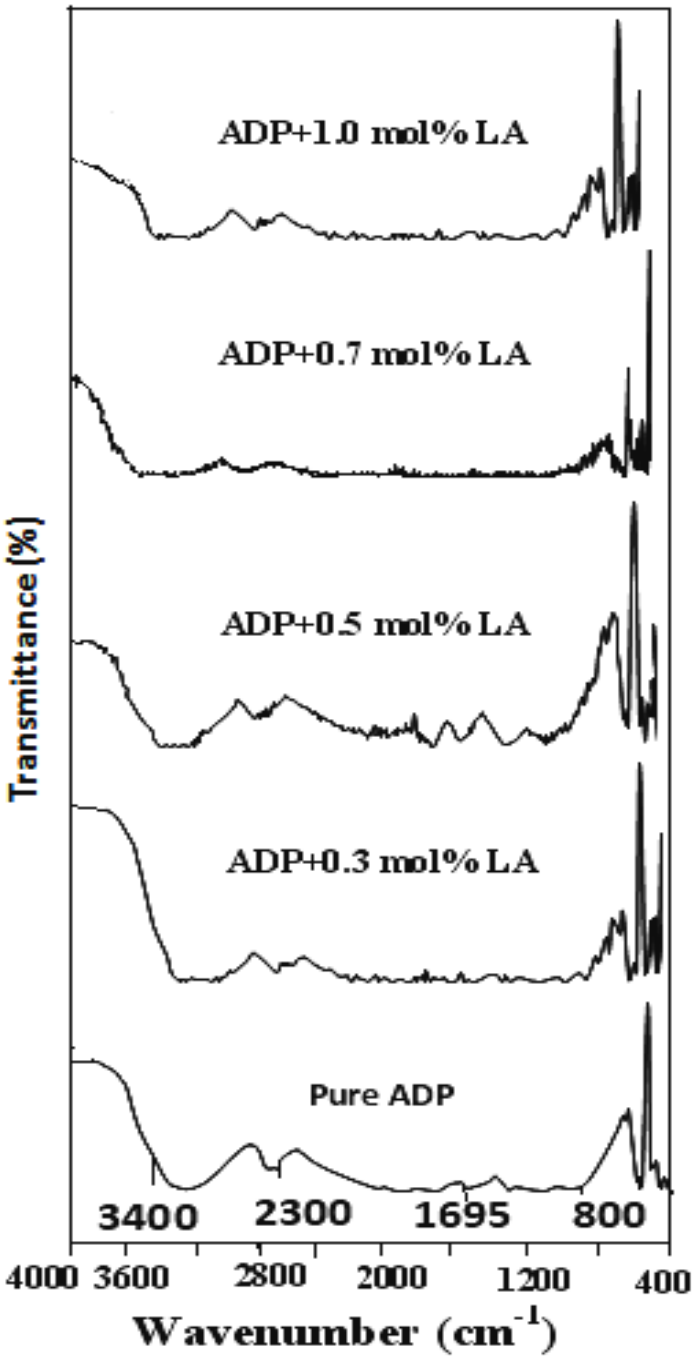

Fig. 4.3 FTIR spectra of pure and LA doped ADP crystals

Table 4.1 Vibrational frequencies obtained for pure and doped ADP crystals through FTIR studies

Calculated frequencies (cm^{-1})	Observed IR frequencies (cm^{-1})					Assignments
Literature data	Pure ADP	ADP+0.3 mol% LA	ADP+0.5 mol% LA	ADP+0.7 mol% LA	ADP+1.0 mol% LA	
3640-3160	3100	3000	3000	3005	3075	O-H stretching
3400-2800	2850	2850	2860	2850	2875	N-H stretching of NH_4
2830-2300	2300	2300	2380	2375	2300	Combination band of stretching
1700-1580	1695	1550	1700	1550	1575	N-H bending of NH_4
1650-1400	1400	1400	1400	1410	1475	Bending stretching of NH_4
1340-1020	1295	1300	1310	1305	1325	Combination band of stretching
1250-1020	1100	1115	1125	1125	1150	P-O-H stretching
1000-650	800	775	795	825	795	P-O-H stretching
690-515	546	534	540	550	560	PO_4 stretching
690-400	405	415	415	407	410	PO_4 stretching

4.4.2 Energy Dispersive X-ray Spectroscopy

In order to confirm the presence of the elements of LA into the pure ADP crystal, the sample of grown crystals were subjected to EDX analysis. The atomic percent of the elements of LA are present which are shown in the recorded EDX spectra in fig. 4.4.

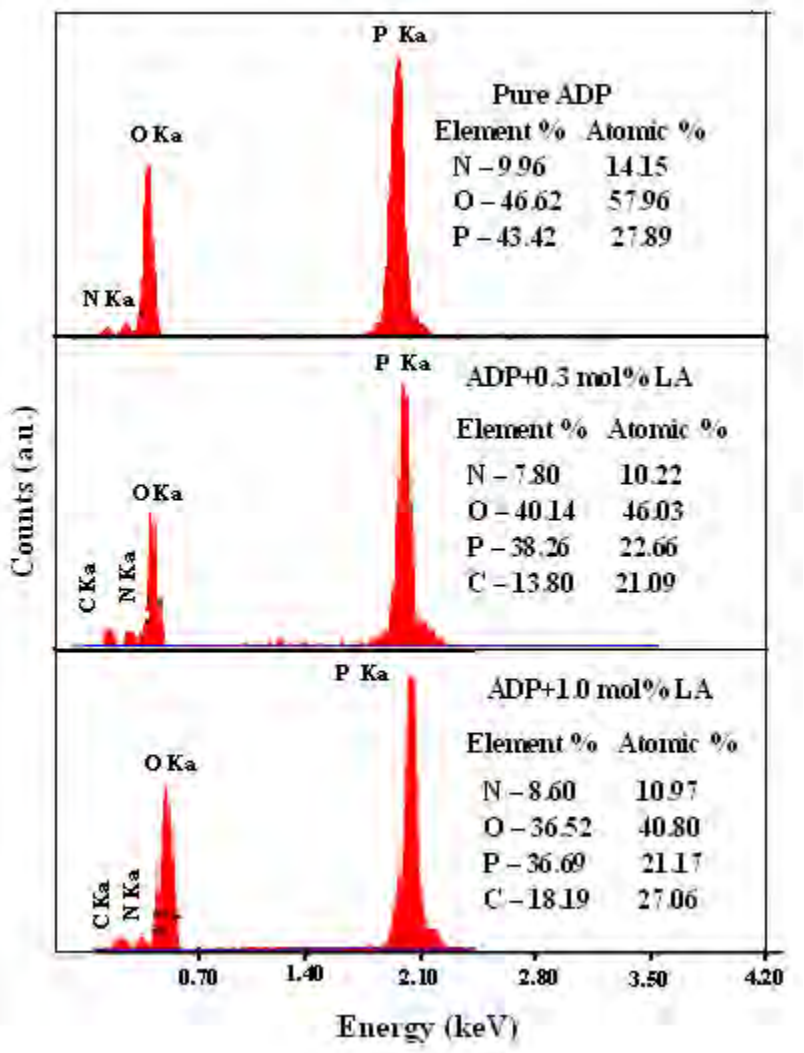

Fig. 4.4 EDX Spectra of pure ADP and LA doped ADP crystals

4.4.3 X-ray Diffraction Analysis

The powder XRD study was conducted to verify the single phase nature of the samples. Figure 4.12, shows the powder XRD patterns of pure and LA doped ADP crystals. Well defined Bragg peaks are obtained at specific 2θ angles indicating that crystals are ordered. The d spacing and hkl values for prominent peaks in the spectrum were identified and compared with ICDD (International Centre for Diffraction Data) data. Using tetragonal crystallographic equation, lattice parameter values are calculated and listed in table 4.2. This suggests that the crystals retain almost the single phase structure and exhibit very slight variation in the unit cell parameters on doping of LA. The variation in the intensities of various diffraction patterns on changing the concentration of doping was observed.

Lattice parameters calculation for Tetragonal pure and LA doped ADP crystal system:

$a = b \neq c$ $\qquad\qquad$ $\alpha = \beta = \gamma = 90^{\circ}$

$$\frac{1}{d_{hkl}} = \sqrt{\frac{h^2 + k^2}{a^2} + \frac{l^2}{c^2}}$$

Table 4.2 Indexed powder diffraction data for pure and LA doped ADP crystals

Sample	(hkl)	$2\theta_{cal}(^0)$	I/I_0 (%)	$2\theta_{exp}(^0)$	$\Delta 2\theta(^0)$
Pure ADP	101	16.797	67.79	16.796	-0.001
	002	23.872	74.42	23.864	-0.008
	112	29.256	78.30	29.258	+0.002
	103	33.911	11.18	33.897	-0.014
	204	45.259	8.06	45.315	+0.056
ADP+0.3 mol% LA	101	16.797	89.82	16.783	-0.014
	002	23.872	100.00	23.778	-0.094
	112	29.256	44.16	29.230	-0.026
	103	33.911	36.55	33.881	-0.030
	204	45.259	28.88	45.241	-0.018
ADP+0.5 mol% LA	101	16.797	100.00	16.764	-0.033
	002	23.872	90.20	23.844	-0.028
	112	29.256	89.75	29.136	-0.120
	103	33.911	19.22	33.842	-0.069
	204	45.259	26.82	45.362	+0.103
ADP+0.7 mol% LA	101	16.797	55.13	16.754	-0.045
	002	23.872	80.00	23.828	-0.044
	112	29.256	100.00	29.230	-0.026
	103	33.911	14.28	33.844	-0.067
	204	45.259	21.26	45.321	+0.062
ADP+1.0 mol% LA	101	16.797	100.00	16.539	-0.258
	002	23.872	74.51	23.862	-0.010
	112	29.256	52.68	29.258	+0.002
	103	33.911	37.02	33.795	-0.116
	204	45.259	42.62	45.254	-0.005

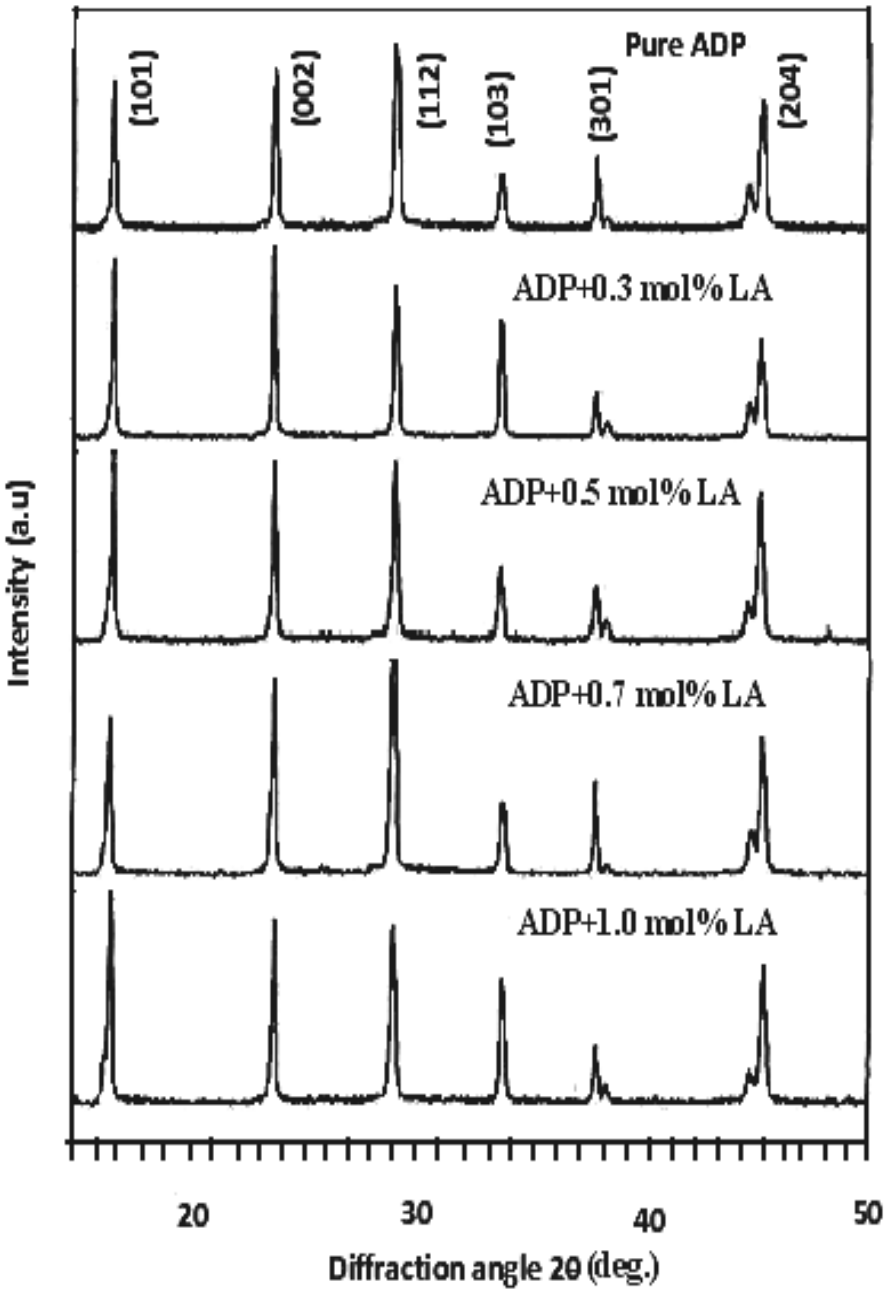

Fig. 4.5 XRD patterns of pure and LA doped ADP crystals

Table 4.3 Unit cell parameters, Optical Transmittance, Band gap energy of pure and doped ADP crystals

Sample	Lattice parameters a = b, c (Å)	Cell Volume $(Å)^3$	Crystal system	Optical Transmission (%)	Band gap energy, E_g(eV)
Pure ADP	7.473, 7.457	416.491	Tetragonal	80	4.80
ADP+0.3 mol% LA	7.458, 7.484	416.282	Tetragonal	83	4.87
ADP+0.5 mol% LA	7.495, 7.464	419.274	Tetragonal	86	4.95
ADP+0.7 mol% LA	7.499, 7.469	420.027	Tetragonal	88	5.05
ADP+1.0 mol% LA	7.479, 7.458	417.166	Tetragonal	95	5.15

4.4.4 Optical Transmission Analysis

The UV-Vis optical transmission spectra of pure and LA doped ADP crystals are shown in fig. 4.5. It is clear from the figure that the percentage of optical transmission increases with the increase of the concentration of LA in ADP crystals. All of them have sufficient transmission in the entire visible and near IR region. The UV transparency cut-off limits decreases with the doping concentration. Similar results have been obtained in the case of doping of LA in KDP [13] and also lithium doped LA crystals [14]. Absorption in the near ultraviolet region arises from electronic transitions associated within the sample. Hence, it could be concluded that the LA doping play a key role in improving the optical quality of ADP crystals. This is the most desirable property of materials possessing NLO activity.

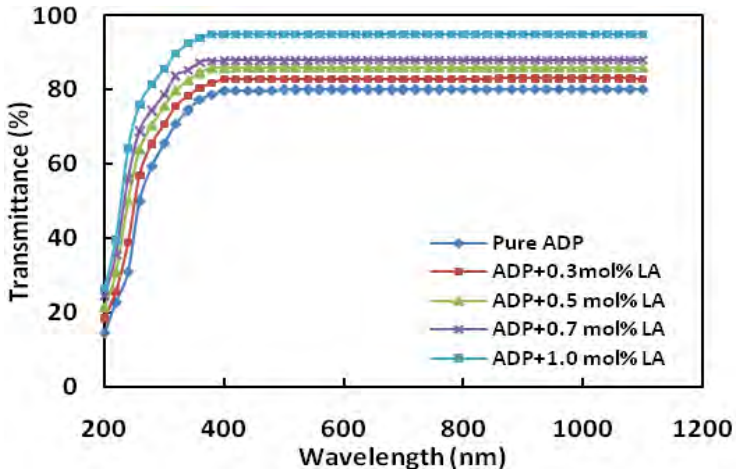

Fig. 4.6 Transmission spectra of pure and LA doped ADP crystals

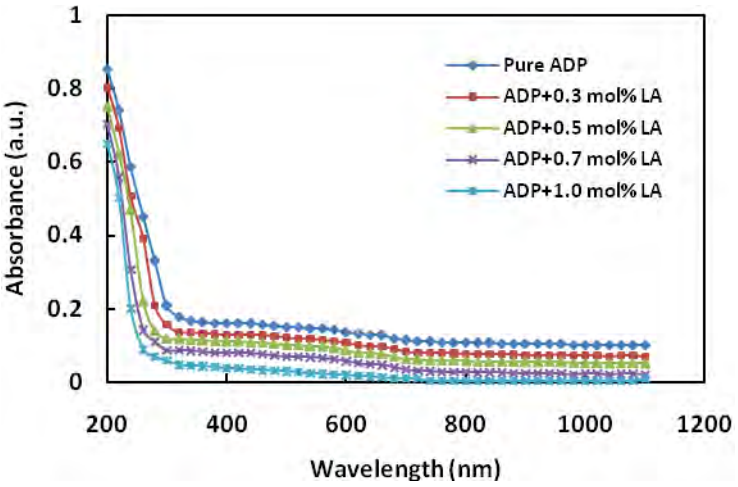

Fig. 4.7 Absorption spectra of pure and LA doped ADP crystals

4.4.5 Optical Parameters Calculation

The dependence of optical absorption coefficient with the photon energy helps to study the band structure and the type of transition of electrons. The α was calculated from the transmittance using the following relation

$$\alpha = [2.3026 \log (1/T)]/d$$

Where T is the transmittance and d is the thickness of the sample. For a direct band gap material, the α is related to light frequency according to the following formula.

$$\alpha h\nu = A(h\nu - E_g)^{1/2}$$

Where A is a constant, E_g is the optical band gap energy, h is the Planck"s constant and ν is the frequency of the incident photons. The band gap energy of the sample can be estimated by plotting $(\alpha h\nu)^2$ versus hν and by extrapolating the linear portion near the onset of absorption edge to the energy axis. The *K* calculated from the following relation.

$$K = \frac{\alpha\lambda}{4\pi}$$

where λ is the wavelength. The n calculated from the reflectance data using,

$n = [-(R+1)\pm 2\sqrt{R}]\ /(R-1)$.

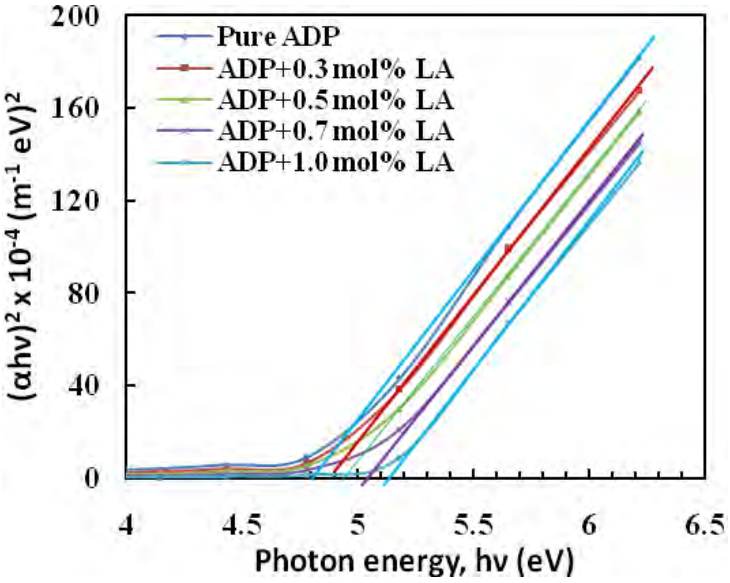

Fig. 4.8 Photon energy vs $(\alpha h\nu)^2$ x 10^{-4}

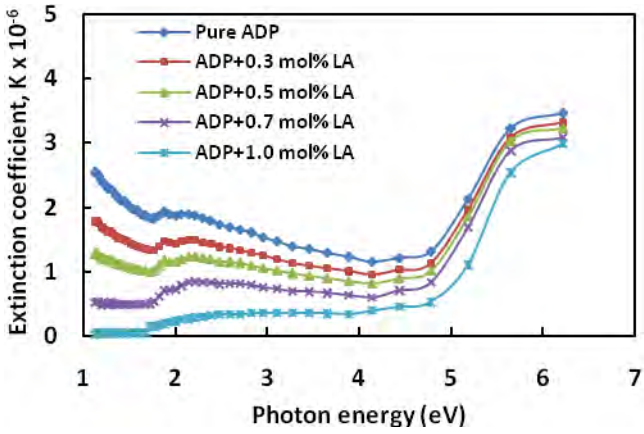

Fig. 4.9 Plot of photon energy vs extinction coefficient, K

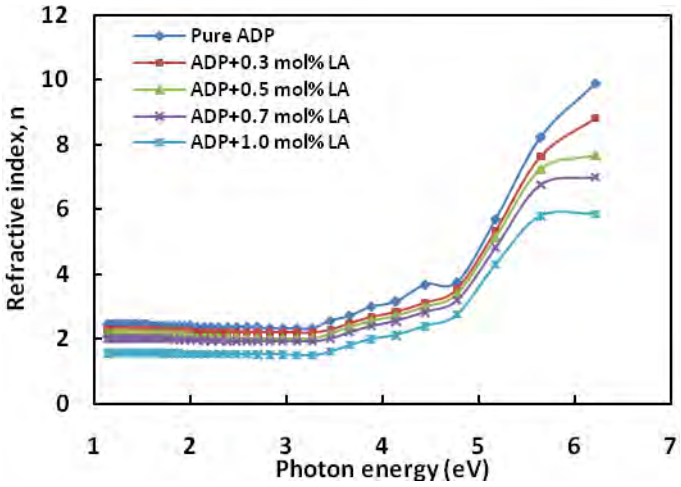

Fig. 4.10 Plot of photon energy vs refractive index, n

4.4.6 Dielectric Studies

The study of dielectric constant of a material gives an outline about the nature of atoms, ions and their bonding in the material. The dielectric constant (ε_r) and dielectric loss (tanδ) depend on frequency of applied field. The real ε_r and imaginary ε_i parts of the dielectric constant calculated by using the relations $\varepsilon_r = n^2 - k^2$ and $\varepsilon_i = 2nk$, Dielectric loss was calculated using the formula: $\tan\delta = \varepsilon_i/\varepsilon_r$.

Figure 4.10. shows the variation of dielectric constant with photon energy. The value of dielectric constant decreases as the frequency increases and it becomes independent of frequency at higher frequency region. The high value of dielectric constant in the low frequency region may be due to the contributions of electronic, ionic, dipolar, and space charge polarizations [12]. The electronic exchange of the number of ions in the crystal gives local displacement of electron in the direction of the applied field, which in turn give rise to polarization. Continuous and gradual decrease in dielectric constant suggests that pure ADP and doped ADP crystals like any normal dielectric may possess domains of different size and varying relaxation times. It is evident that the lower value of dielectric constant is a suitable parameter for the enhancement of SHG coefficient [13]. Figure 4.11 shows the variation of dielectric loss with photon energy of applied field at room temperature. The behavior of variation is similar to that of dielectric constant with frequency. This is the normal behavior observed earlier [8,14]. The dielectric loss is a measure of the energy absorbed by dielectric. Usually the dielectric has a resistance R and reactance $1/\omega C$. Which are related to the phase angle $\tan\delta = 1/\omega CR$, where C is a capacitance. So the low dielectric loss at high frequency reveals the superior optical quality of the crystals with lesser defects, and this parameter is of vital importance for various NLO application.

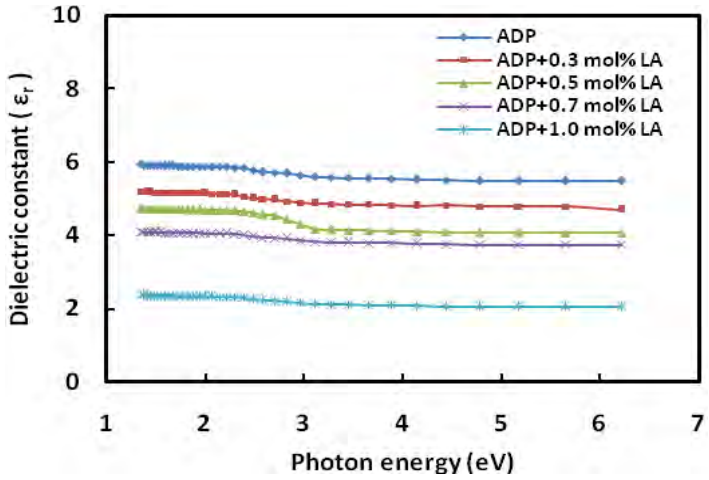

Fig. 4.11 Photon energy vs dielectric constant

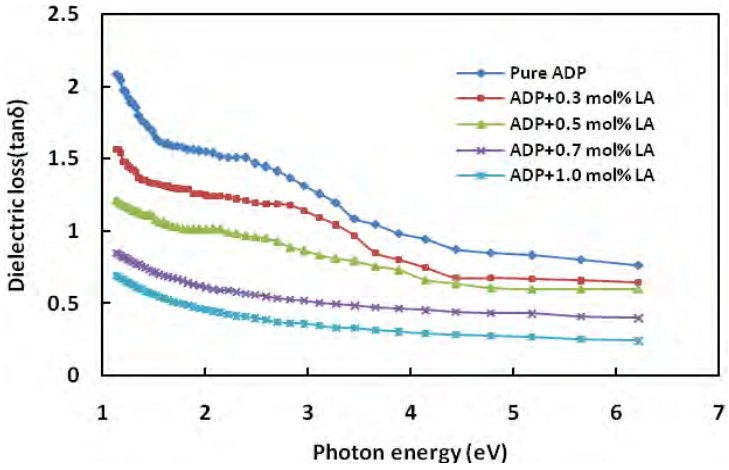

Fig. 4.12 Photon energy vs Dielectric loss

4.4.7 Thermal Analysis

The effect of LA doping on thermal stability of ADP crystals is studied from the simultaneous TG, DTA and DTG curves are shown in the figures 4.13, 4.14 and 4.15. In order to study the influence of dopant on the thermal stability of ADP, the temperature corresponding to the first stage of decomposition is taken into account for comparison. In figure 4.13, the DTA curve shows an endothermic peak at 198.3 ^{0}C for the pure ADP and in figures 4.15, the endothermic peaks of the DTA curves for LA doped ADP crystals is 208.9 ^{0}C. These endothermic peaks correspond to the decomposition temperature of the crystals. The TGA curve exhibited negligible weight loss in the region 40 ^{0}C to 200 ^{0}C as shown in the figures 4.13 and 4.15.The decomposition of pure ADP crystal begins at 188.2 ^{0}C and terminates at 608.7 ^{0}C. The weight loss observed from TGA graph for pure ADP in the temperature range 188.2 ^{0}C to 544.4 ^{0}C is 13.5 %. But for ADP+1.0 mol% LA crystal the decomposition starts at 202.1 ^{0}C and ends at 694.8 ^{0}C. The weight loss observed from TGA graph for ADP+1.0 mol% LA crystal is 9.9%. From this analysis we can see from the TGA/DTA analysis that on increasing the concentration of LA the hydration process starts later and the crystal becomes anhydrous higher than the pure ADP crystal because LA becomes unstable at lower temperature. These results prove that the LA has entered as an impurity into ADP crystals. The similar results have obtained for LA doped KDP [13] and L-arginine doped in KDP [15].

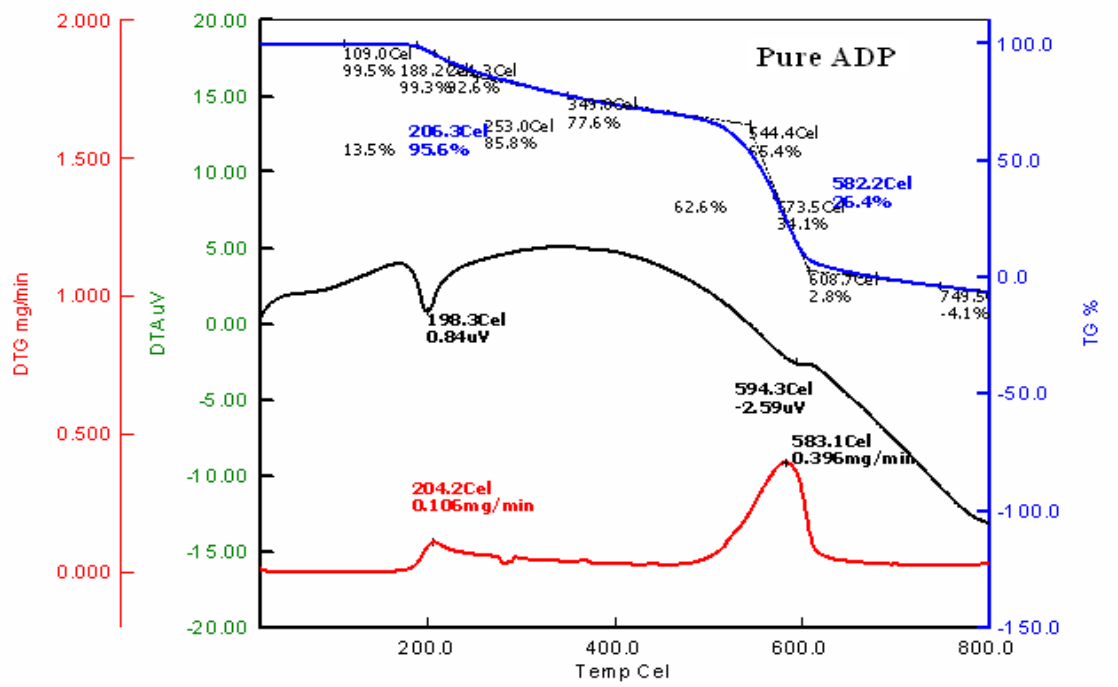

Fig. 4.13 Simultaneous graphs of TGA, DTA and DTG for pure ADP crystal

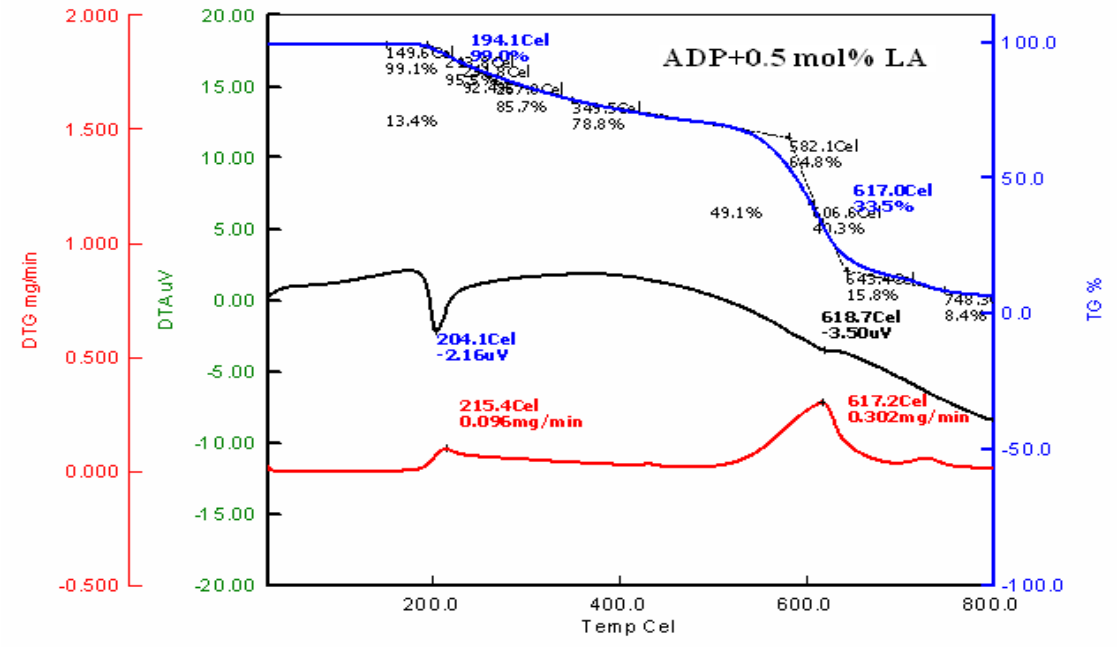

Fig. 4.14 Simultaneous graphs of TGA, DTA and DTG for ADP+0.5 mol% LA crystal

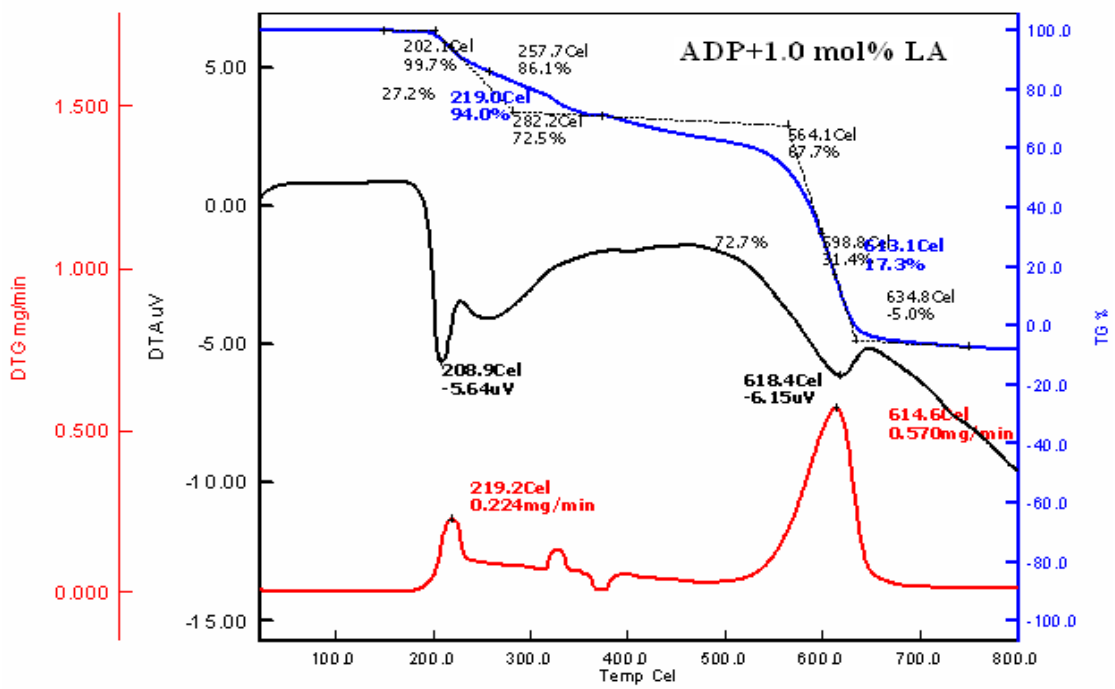

Fig. 4.15 Simultaneous graphs of TGA, DTA and DTG for ADP+1.0 mol% LA crystal

4.4.8 Vicker's Microhardness Analysis

Hardness is an important property to characterize a crystal. Harder crystals are good for device fabrication. Hardness test is useful to find the mechanical hardness of the crystal and to estimate the threshold mechanical stress it can withstand. Vicker"s microhardness measurement of pure and LA doped ADP crystals was taken by varying applied loads 25g, 50g and 100g for indentation time of 7 s. From fig. 4.16 the hardness value of pure and doped crystals were found to decrease with the applied loads because large prominent cracks due to the attainment of the threshold mechanical stress which is comparable with these results [11,14]. The hardness values were calculated using the formula: $H_v = [1.8544 \text{ X } P]/ D^2$ kg-mm^{-2}. Where H_v is the Vicker"s microhardness number, P is the indenter load in kg and D is the diagonal length of the impression in mm. The microhardness value was taken as the average of the several impressions made with both diagonals being measured. In the present study, the hardness of the pure ADP

crystal is higher than LA doped ADP crystals. This is because of the incorporation of the LA ($^{+}NH_3$, COO-) ions into superficial crystal lattice and forming defect centers which generate weak lattice stresses on the surface.

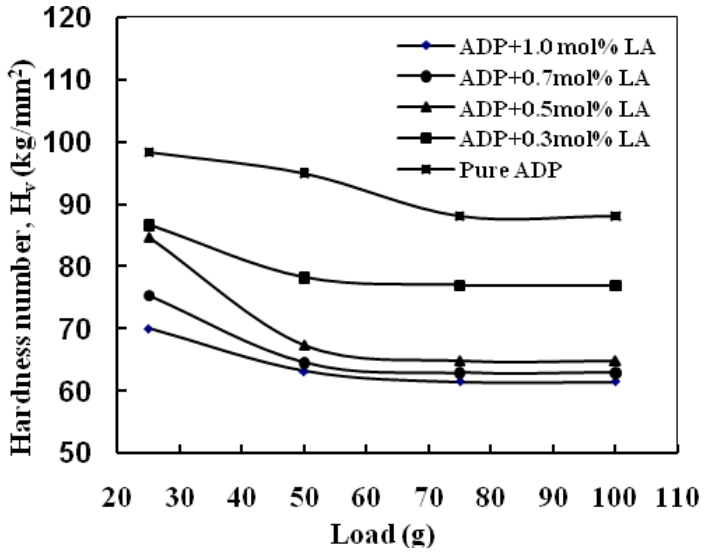

Fig. 4.16 Microhardness curves for pure and LA doped ADP crystals

4.4.9 DC Electrical Conductivity

A graph of DC electrical conductivity vs. temperature of pure and LA doped ADP crystals is plotted in fig.4.17. It is found that conductivity increases exponentially with temperature and also with LA concentration. Similar result has been obtained in the case of doping urea in ADP [9]. Conductivity is found in the order of 10^{-6} mho/m. At low temperature region, conductivity is expected due to the presence of weakly attached impurities and vacancies in the crystal lattice. At high temperature region, the attached water molecule is lost and fracture is developed and conductivity is caused mainly for intrinsic defects. So there were no replacement of either NH_4^+ or $(H_2PO_4)^-$ of ADP with ions of LA lattice. These doping ions of LA may occupy some interstitial positions and create more defects. Due to these interactions between ADP and LA, the conductivity of doped ADP crystals may increased.

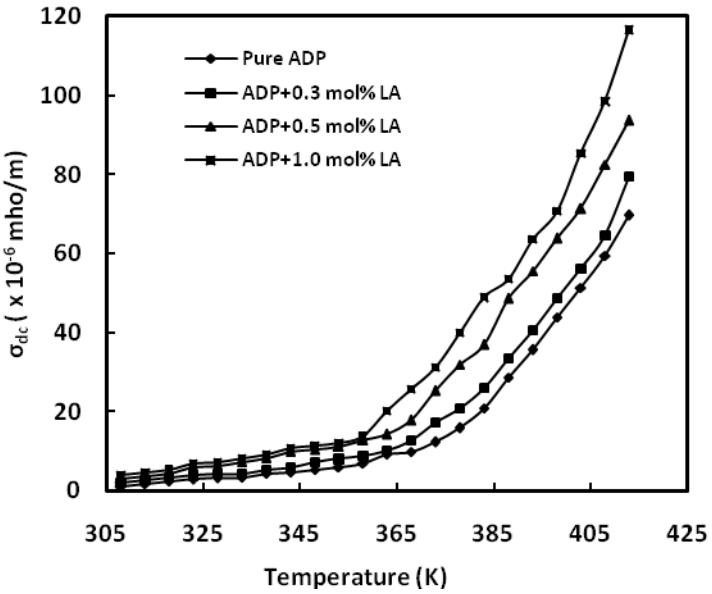

*Fig. 4.17 DC electrical conductivity (ζ_{dc}) vs Temperature (*K*)*

4.4.10 Etching Study

Etching method is a very common and inexpensive technique to reveal dislocations and lattice inhomogenities of the crystals. The chemical etching studies were carried out on the as grown single crystal of pure and LA doped ADP crystals to study the distribution of structural defects in the grown crystal. The surfaces of sample were polished and no scratches markings were visible under an optical microscope. This was then etched in the etching solution (water) at room temperature for 10 s. Then soaked with a filter paper and examined under an optical microscope in reflection. The etching figure Illustrates the typical etch pattern observed on the (100) plane of the pure and LA doped ADP crystal. These etch-pits were formed due to dislocations which were formed during the period of crystal grow. The generation of dislocations was strongly correlated with the formation of inclusions in the crystals. Depending on the shape of the seed crystal, inclusions may also arise. The reason for bulk of the inclusions getting trapped could be due to fluctuations in supersaturation close to the crystal or due to transition from dissolution to growth. A number of parameters such as variation in supersaturation during the growth, non-uniform growth rate, etc., are responsible for the formation of inclusions. The etch pit patterns were shown in fig. 4.18 and fig. 4.19.

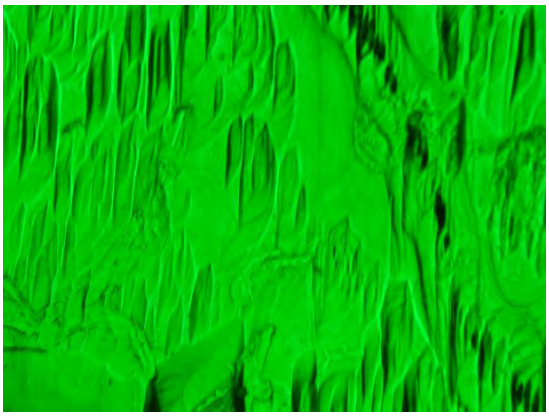

Fig. 4.18 Etch pit pattern of (100) plane for pure ADP crystal

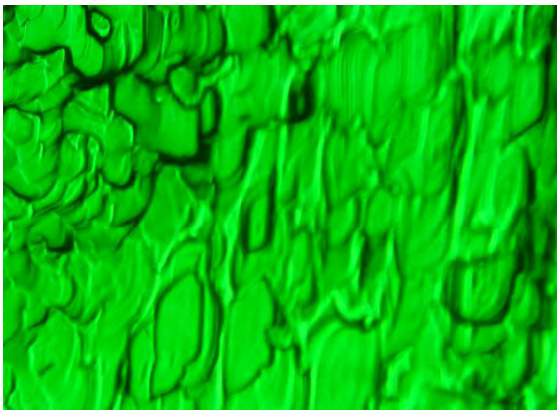

Fig. 4.19 Etch pit pattern of (100) plane for ADP+1.0 mol% LA crystal

4.5 Conclusions

The effect of LA impurity on the growth of ADP from supersaturated solutions has been investigated experimentally by measuring optical transmission, functional groups, DC electrical conductivity, microhardness and decomposition temperatures. The presence of amino acid impurity in ADP solution was found to increase the optical transmission, electrical conductivity with temperature and decomposition temperature. This phenomenon may be attributed due to zwitterionic nature of L-alanine molecule ($^{+}NH_3 - C_2H_4 - COO^{-}$). The enhancement of optical transmission of LA doped ADP crystals highlights their prospects of application as NLO materials.

4.6 References

[1] Marder, R. S., Tiemann, G. B, Perry, W. J. et al., Materials for non-linear optics chemical perspectives (American Chemical Society, Washington), p.280, 1991.

[2] Warren, F. L., " New development in semiorganic nonlinear optical crystals", in Electronic Materials, Our future, proceedings of the Fourth International SAMPE Electronics Conference, (ed.) Allred R.E., Martinez R.J. and Wischmann W.D. Society for the Advancement of Material and Process Engineering, Covina, Ca., Vol. **4**, p.388-396, 1990.

[3] Nicoud, F. J. and Twieg, R.J. " Design and synthesis of organic molecular compounds for efficienty second harmonic generation", in Nonlinear Optical Properties of Organic Molecules and Crystals, D. S. Chemla and J. Zyss, eds. Academic, Orlando, Fla., Vol. **1,** 1986.

[4] Bernal, D. J., " The crystal structure of the natural amino acids and related compounds", Z. Kristallogr. Vol.**78**, p.363-369, 1931.

[5] Simpson, H. J. Jr. and Marsh, R. E., "The crystal structure of L-alanine", Acta. Cryst. Vol. **20**, Part 4, p.550-555, April 1966.

[6] Destro, R., Marsh, R. E. and Bianchi, R., "A low temperature (23K) study of L-alanine", J. Phys. Chem. Vol.**92**, p.966-973, 1988.

[7] Misoguti, L.,Varela, A. T., Nunes, F. D., Bagnato, V. S., Melo, F. E. A., Mendes Filho, J. and Zilio, S. C., "Optical properties of L-alanine organic crystals", Opt. Mater. Vol. **6**, p.147-152, 1996.

[8] Vijayan, N., Rajasekaran, S., Bhagavannarayana, G., Ramesh Babu, R., Gopalakrishnan, R., Palanichamy, M. and Ramasamy, P., " Growth and characterization of nonlinear optical amino acid single crystal: L-alanine", Crystal growth & design, Vol. **6**, no. 11, p.2441-2445, 2006.

[9] Anne Assencia, A. and Mahadevan, C., " D.C. electrical conductivity measurements on ADP single crystals added with simple organic compounds", Bull. Mater. Sci., Vol. **28**, no. 5, p. 415-418, 2005.

[10] Rajesh, N. P., V. Kannan, V., Santhana Raghavan, P., Ramasamy, P. and Lan, C. W.,"Nucleation studies and crystal growth of $(NH_4)H_2PO_4$ doped with thiourea in supersaturated aqueous solutions", Materials Chemistry and Physics, Vol. **76**, Issue 2, p.181-186, 2002.

[11] Dhanaraj, P. V., Bhagavannarayana, G. and Rajesh, N. P.," Effect of amino acid additives on crystal growth parameters and properties of ammonium dihydrogen orthophosphate crystals", Materials Chemistry and Physics, Vol. **112**, Issue 2, p.490-495, 2008.

[12] Meena, M. and Mahadevan, C. K.,“ Growth and electrical characterization of L-arginine added KDP and ADP single crystals”, Cryst. Res. Technol. **43**, no. 2, p.166-172, 2008.

[13] Parikh, K. D., Dave, D. J., Parekh, B. B. and Joshi, M. J.,“ Growth and Characterization of L-alanine doped KDP crystals”, Cryst. Res. Technol., Vol. **45**, 603, p.1-8, 2010.

[14] Suresh Kumar, B., Sudarsana Kumar M. R. and Bajendra Babu, K.,“ Growth and Characterization of pure and Lithium doped L-alanine single crystals for NLO devices”, Cryst. Res. Technol. **43**, no. 7, p.745-750, 2008.

[15] Parikh, K. D., Dave, D. J., Parekh, B. B. and Joshi, M. J., “ Thermal, FT-IR and SHG efficiency studies of L-arginine doped KDP crystals”, Bull. Mater. Sci., Vol. **30**, no. 2, p.105-112, 2007.

CHAPTER 5

GROWTH AND CHARACTERIZATION OF L-ALANINE DOPED POTASSIUM DIHYDROGEN PHOSPHATE (KDP) CRYSTALS

CHAPTER 5

GROWTH AND CHARACTERIZATION OF L-ALANINE DOPED POTASSIUM DIHYDROGEN PHOSPHATE (KDP) CRYSTALS

5.1 Introduction

KDP is a dielectric material well known for its electro optical and nonlinear optical properties. The excellent properties of KDP include transparency in a wide region of optical spectrum, resistance to damage by laser radiation and relatively high nonlinear efficiency [1-2]. The demand for high quality large KDP single crystal increases due to its application as frequency conversion crystal in inertial confinement fusion [3-4]. KDP belongs to scalenohedral (twelve faced) class of tetragonal crystal system [5]. With the aim of improving the second harmonic generation (SHG) efficiency of KDP, research workers have attempted to modify KDP crystals by doping different type of impurities. The NLO and other properties of the crystal have been improved by doping of organic impurities [7-12]. KDP doped with amino acids like α-alanine, β-alanine, α-leucine, α-histidine, α-cystine and α-valine were reported [13]. Kumaresan et al. [14] have grown the amino acids such as L-glutamic acid, L-histidine and L-valine doped KDP crystals. They found improved NLO properties of the KDP crystal, modifications in the structure, optical, mechanical, and electrical properties, too. Parikh el. al [18] and Meena et. al [16] have studied L-arginine doped KDP crystal. They have investigated the effect of the doping on the NLO, thermal, mechanical properties and optical transparencies. Muley et. al [8] has studied thermal, NLO properties of KDP crystal doped with L-arginine and L-alanine. Suresh Kumar et. al [9] studied the effects of L-arginine, L-histidine and glycine on the growth of KDP single crystals and observed that addition of amino acid enhances transparency, thermal stability and NLO efficiency of KDP crystals.

Amino acid family crystals are playing an important role in the field of non-linear optical organic molecular crystal. Among them LA, with chemical formula (CH_3 CH NH_2 COOH) is the smallest, naturally occurring chiral amino acid with a non-reactive hydrophobic methyl group ($^{-}CH_3$) as a side chain. LA has the zwitterionic form ($^{+}NH_3$-

C_2H_4-COO^-) both in crystal and in aqueous solution over a wide range of pH, which favors crystal hardness for device application [21]. It belongs to the orthorhombic crystal system and the unit cell parameters are; a = 6.320 Å, b = 12.343 Å, c = 5.784 Å, $\alpha = \beta = \gamma = 90^0$. Recently, several new complexes incorporating the amino acid LA have been crystallized and their structural, optical and thermal properties have also been investigated [17]. The growth of pure LA crystals was reported [19] and found higher damage threshold than KDP.

In this thesis the effect of LA as impurity was studied (concentration ranging was from 3000 – 10000 ppm, i.e, 0.3 – 1.0 mol%). The grown crystals were characterized by FT-IR, EDX, Optical transmission, XRD, AC electrical conductivity, Dielectric constant, Dielectric loss, etch pits and compared all these results with pure KDP crystal.

5.2 Experiment

5.2.1 Determination of Solubility of Pure and LA Doped KDP

Solubility of the pure and doped KDP in double distilled water was determined gravimetrically in the temperature range 30-50 ^{0}C insteps of 5 ^{0}C using a constant temperature bath of accuracy ±0.01 ^{0}C. 500 mL of the saturated solution of pure KDP salt was prepared gravimetrically at 30 ^{0}C. This solution was stirred well for six hours constantly using magnetic stirrer and then filtered using Whatmann filter paper. This solution was taken in five different beakers of 100 mL and LA was added to each of four beakers as 0.3 mol%, 0.5 mol%, 0.7 mol% and 1.0 mol%. After making supersaturated solution of LA doped KDP, the 5 mL of the solution was pipetted out and poured into a 10 mL beaker of known weight. The solvent was completely evaporated by warming the solution at 50 ^{0}C. The amount of the salt present in 5 mL of the solution was measured by subtracting the empty beaker"s weight. From this the amount of the salt present in 100 mL of the solution was found out. In the same way, the amount of the salt dissolved in 100 mL at 35, 40, 45 and 50 ^{0}C was determined. Fig. 5.1 shows the solubility curves of pure and doped KDP salt. It is observed from the solubility graph that the solubility of pure and doped KDP in water increases as the temperature increases and decreases with

doping concentration increase. From this solubility data it can state that the KDP material has positive temperature coefficient.

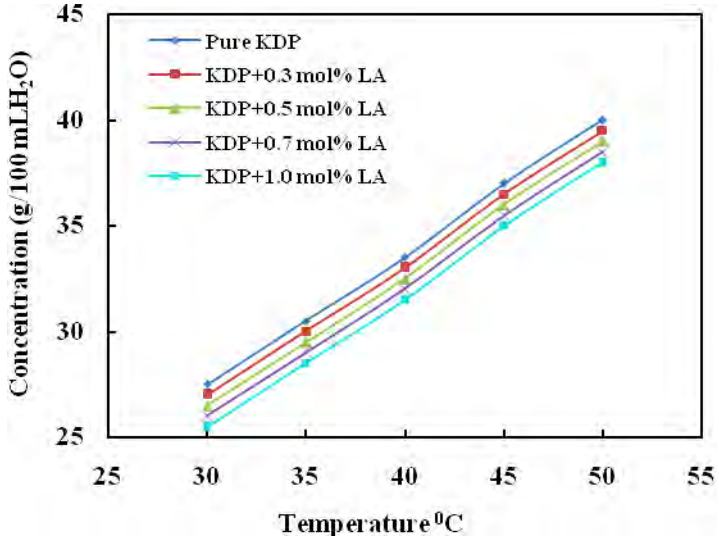

Fig. 5.1 Solubility curves of pure and LA doped KDP

5.2.2 Growth of Pure and LA Doped KDP Crystals

The pure KDP and LA (AR grade chemical from SIGMA) doped KDP crystals were grown using a good quality seed crystal at room temperature by solvent evaporation method. For the preparation of seed crystals saturated solution of KDP was prepared first and then kept in a petri dish covered with a perforated polyethylene and allowed to grow seed crystals within 4-5 days. The pH of the different concentration of LA doped KDP solution was ranged from 4.40 to 4.90. The purity of the crystals was improved by successive recrystallization process. The growth period takes 25-30 days for bigger size. The grown crystals were found color-less and transparent. Fig. 5.2 shows the photographs of solution grown pure and doped KDP crystals.

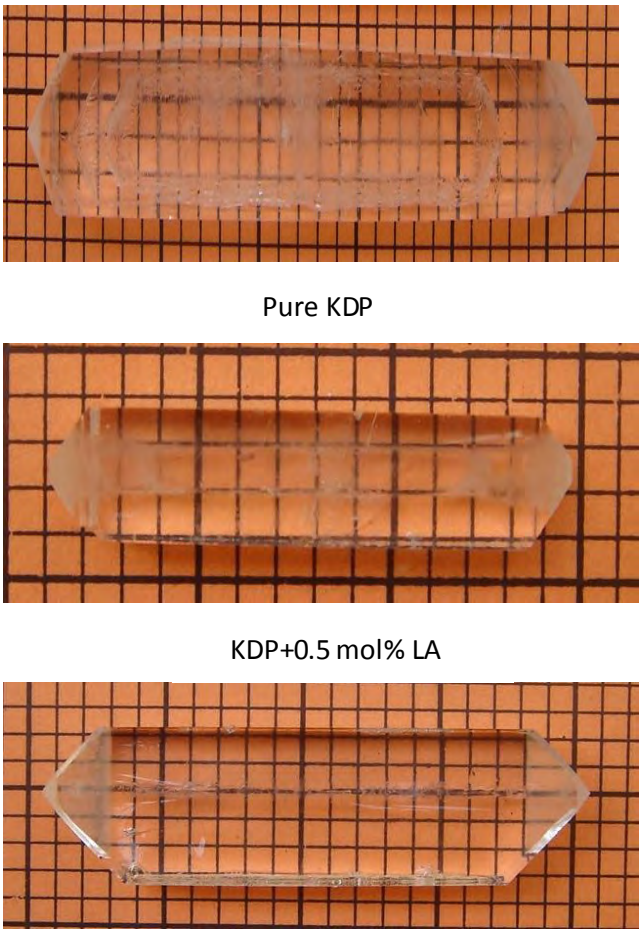

Fig. 5.2 Photographs of pure and LA doped KDP crystals

5.3 Characterization of Pure and LA Doped KDP Crystals

The grown pure and LA doped KDP crystals were characterized structurally, optically, Thermally, Mechanically and AC electrical properties. In order to confirm the presence of functional groups in the crystal lattice, FTIR spectrum was recorded by KBr pellet technique using a Shimadzu FTIR - 8900 spectrometer in the wave number range 400-4000 cm^{-1}. In order to confirm the presence of the elements of the compound of LA into KDP crystals were subjected to EDX. EDX patterns were recorded using a JEOL-6360 Scanning Electron Microscope. The recorded EDX spectrum is shown in fig. 5.4. Powder XRD pattern was recorded using a Philips X pert PRO X-ray diffractometer with CuK_{α} (λ = 1.5418 Å) radiation. The lattice parameters were calculated for pure and doped (0.3,

0.5, 0.7 and 1.0 mole% LA) KDP crystals using XRD data. The optical properties of the grown crystal were studied by the transmission spectra using Shimadzu UV-1601 visible spectrometer in the wavelength region from 200 to 1100 nm. The AC electrical conductivity measurements were carried out along the unique axis c at various temperatures ranging from 35 to 140 ^{0}C. The field is applied to perpendicular to c-axis. The dimensions of the crystals were measured using a travelling microscope. The dielectric properties were studied by using Agilent 4274A LCR meter in the temperature range from 35 to 140 ^{0}C. Dislocation, surface defects and morphology were characterized by chemical etching followed by etch pit examination using optical microscope, SWIFTMASTER II (SWIFT) Tokyo, Japan.

5.4 Results and Discussion

5.4.1 Fourier Transform Infrared Spectroscopy

L-arginine and LA with KDP crystals were studied by FTIR by Muley et.al [8]. The authors confirmed the interaction between KDP and organic amino acid by additional peaks corresponds to the functional groups of L-arginine and LA. In this thesis the FTIR spectra of pure KDP and LA doped KDP crystals are shown in fig. 5.3. In the FTIR spectrum of pure KDP the O-H stretching vibration of water happened at 3239 cm^{-1}, P-O-H stretching at 2249 cm^{-1} , HO-P-OH bending at 749 cm^{-1}, P-OH deformation or K-O stretching at 582 cm^{-1} and PO_4stretching at 416 cm^{-1}. In the FTIR spectrum of 1.0 mol% LA doped KDP crystal, C-H stretching at 2812 cm^{-1} and CH_2 bending at 1237 cm^{-1}have been observed. Table 5.1 shows the vibrational frequencies corresponding to the band assignments of pure and doped KDP crystals. The following vibration assignments showed the hydrogen bonding extends throughout the LA doped KDP molecules. These hydrogen bonding results in the modification of stretching frequencies of O-H group of KDP and the carboxyl group of LA molecules. This confirms the presence of LA into pure KDP crystal.

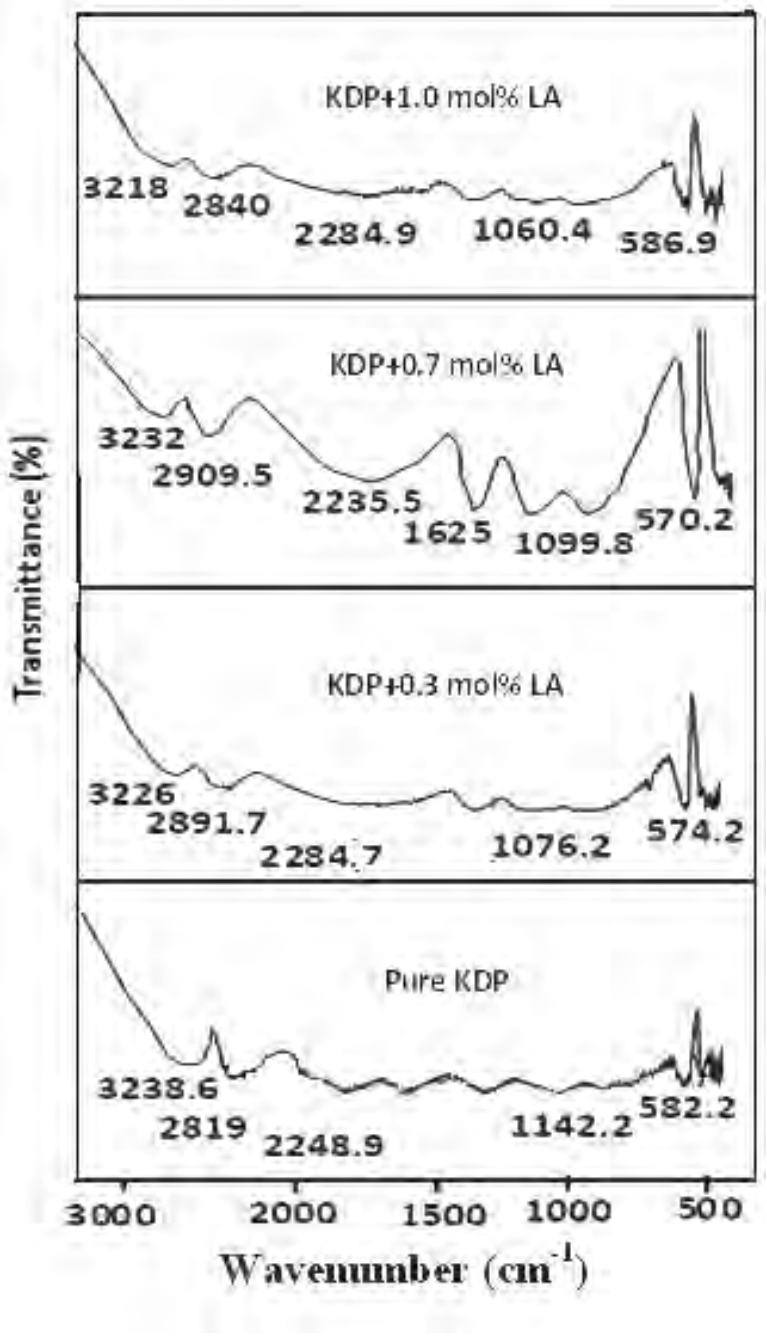

Fig. 5.3 FTIR spectra of pure and LA doped KDP crystals

Table 5.1 Vibrational frequencies obtained for pure and LA doped KDP crystals through FTIR studies

Calculated Frequencies (cm^{-1})	Observed IR frequencies (cm^{-1})				Assignments
Literature data	Pure KDP	KDP+0.3 mol% LA	KDP+0.7 mol% LA	KDP+1.0 mol% LA	
2500-3300	3239	3226	3232	3218	O-H stretching, H-bonded
2750-3200	3072	3115	3156	3121	O-H strtching
2750-3200	2929	2958	2909	2942	O-H stretching
2750-3200	2819	2892	2871	2840	Intermolecular H-bonded-OH stretching
2850-3000	------	2841	2824	2812	C-H stretching
2500-3300	2525	2548	2539	2575	O-H strtching
2050-2250	2249	2285	2235	2285	P-O-H symmetric stretching
1580-1700	1675	1674	1625	1648	O-P-OH symmetric stretching
1350-1550	1463	1384	1369	1373	O-H stretching
1220-1370	1230	1233	1232	1237	CH_2 bending, P=O symmetric stretching
1030-1145	1142	1076	1100	1060	P-O-H symmetric stretching
840-970	866	938	957	949	O=P-OH bending
600-780	749	767	762	651	HO-P-OH bending
300-600	582	574	570	587	P-OH deformation/K-O stretching
300-600	416	455	419	445	PO_4 stretching

5.4.2 Energy Dispersive X-ray Spectroscopy

In order to confirm the presence of the elements of LA into pure KDP crystals, the sample of grown crystals were subjected to Energy Dispersive X-ray analysis using JEOL-6360 Scanning Electron Microscope. Fig. 5.4 shows the EDX result of pure KDP and LA doped KDP crystals. Elements are identified and presented as atomic % in the EDX spectra.

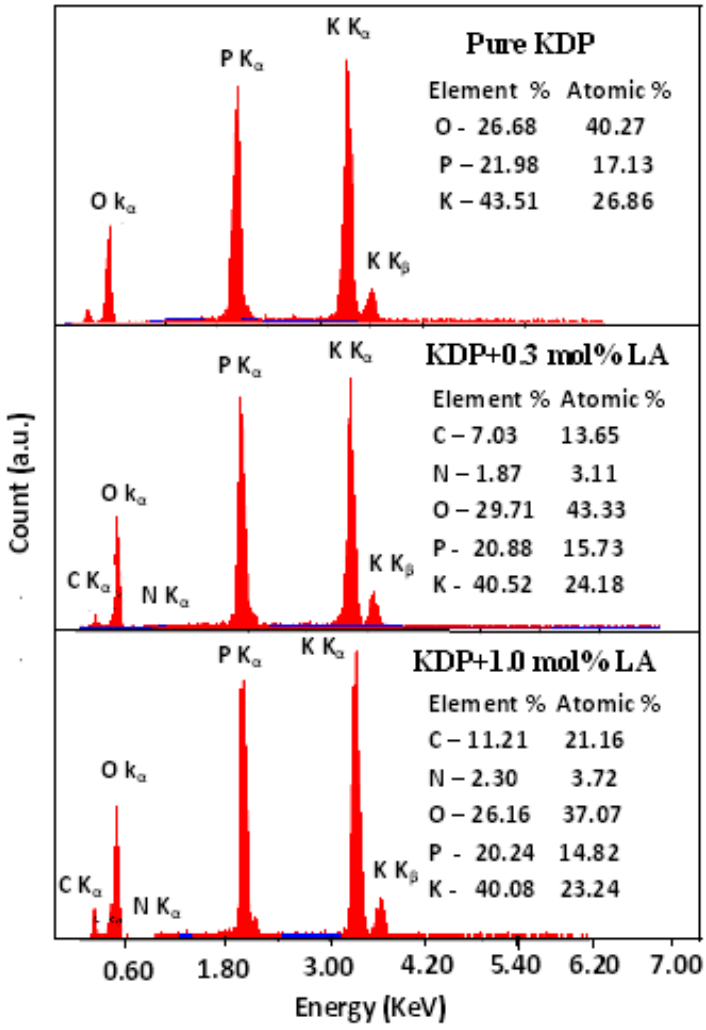

Fig. 5.4 EDX spectra of pure and LA doped KDP crystals

5.4.3 X-ray Diffraction Analysis

The powder XRD study was conducted to verify the single phase nature of the samples. Fig. 5.5 shows the powder XRD patterns of pure and LA doped KDP crystals. Well defined Bragg peaks are obtained at specific 2θ angles indicating that crystals are ordered. The ‚d" spacing and hkl values for prominent peaks in the spectrum were identified and compared with ICDD (International Centre for Diffraction Data) data. Using tetragonal crystallographic equation, lattice parameter values are calculated and listed in table 5.3. This suggests that the crystals retain almost the single phase structure and exhibit very slight variation in the unit cell parameters on doping of LA. The variation in the intensities of various diffraction patterns on changing the concentration of doping was observed.

Lattice parameters calculation for Tetragonal of pure and L-alanine doped KDP crystal system:

$$a = b \neq c \qquad\qquad \alpha = \beta = \gamma = 90^{\circ}$$

$$\frac{1}{d_{hkl}} = \sqrt{\frac{h^2 + k^2}{a^2} + \frac{l^2}{c^2}}$$

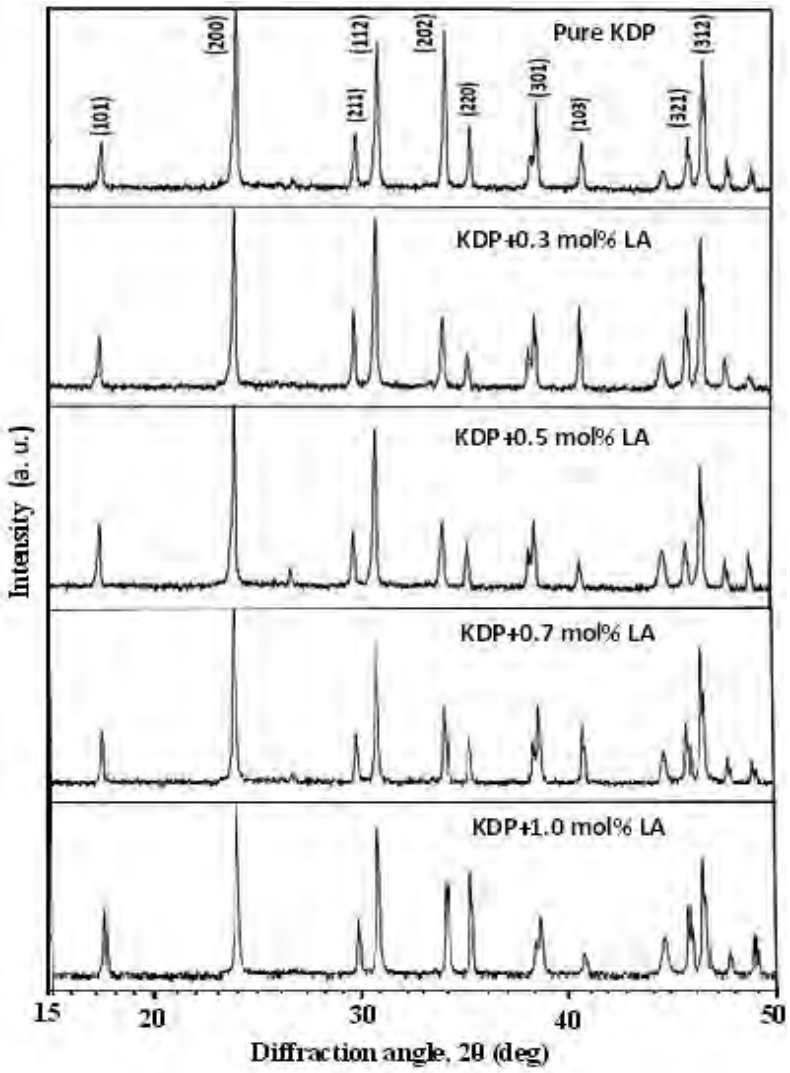

Fig. 5.5 Powder XRD patterns of pure and LA doped KDP crystals

Table 5.2 Indexed powder diffraction data for pure and LA doped KDP crystals

Sample	(hkl)	$2\theta_{cal}(^0)$	I/I_0 (%)	$2\theta_{exp}(^0)$	$\Delta 2\theta(^0)$
Pure KDP	101	17.463	9.42	17.570	+0.107
	200	23.925	100.00	24.019	+0.094
	112	30.783	68.05	30.888	+0.105
	202	32.067	68.05	34.178	+2.111
	301	38.503	5.23	38.279	-0.224
	321	45.801	6.13	46.022	+0.221
	312	46.521	56.43	46.633	+0.112
KDP+0.3 mol% LA	101	17.463	10.64	17.504	+0.041
	200	23.925	100.00	23.966	+0.041
	112	30.783	90.21	30.812	+0.029
	202	32.067	19.30	34.094	+2.027
	301	38.503	21.63	38.531	+0.028
	321	45.801	11.78	45.967	+0.166
	312	46.521	34.56	46.697	+0.176
KDP+0.5 mol% LA	101	17.463	16.33	17.522	+0.059
	200	23.925	100.00	23.979	+0.054
	112	30.783	77.77	30.816	+0.033
	202	32.067	15.84	34.107	+2.04
	301	38.503	17.84	38.535	+0.032
	321	45.801	9.57	45.834	+0.033
	312	46.521	50.82	46.557	+0.036
KDP+0.7 mol% LA	101	17.463	13.02	17.524	+0.061
	200	23.925	100.00	23.964	+0.039
	112	30.783	74.30	30.833	+0.05
	202	32.067	23.11	34.108	+2.041
	301	38.503	23.65	38.536	+0.033
	321	45.801	16.22	45.846	+0.045
	312	46.521	26.66	46.710	+0.189
KDP+1.0 mol% LA	101	17.463	18.73	17.516	+0.053
	200	23.925	100.00	23.976	+0.051
	112	30.783	71.78	30.822	+0.039
	202	32.067	30.45	34.091	+2.024
	301	38.503	13.36	38.518	+0.015
	321	45.801	18.90	45.838	+0.037
	312	46.521	47.43	46.559	+0.038

Table 5.3 Lattice parameters, Optical transmission and Band gap energy of pure and doped KDP crystals

Sample	Calculated values of lattice parameters a = b, c (Å)	Cell volume ($Å^3$)	Reference [11] a=b,c(Å)	Crystal system	Optical Transmission (%)	Band gap energy E_g (eV)
Pure KDP	7.455, 6.975	387.649	7.457, 6.976	Tetragonal	85	4.91
KDP+0.3 mol% LA	7.426, 6.981	384.981	7.453, 6.975	Tetragonal	87	5.09
KDP+0.5 mol% LA	7.422, 6.993	385.216	7.453, 6.975	Tetragonal	90	5.12
KDP+0.7 mol% LA	7.427, 6.979	384.989	Not done	Tetragonal	92	5.17
KDP+1.0 mol% LA	7.423, 6.995	385.415	Not done	Tetragonal	97	5.30

5.4.4 Optical Transmission Analysis

The UV-Vis optical transmission spectra of pure and LA doped KDP crystals are shown in fig. 5.6. It is clear from the figure that the percentage of optical transmission increases with the increase of concentration of LA in KDP crystals. All of them have sufficient transmission in the entire visible and near IR region. The percentage of optical transmission data are tabulated in table 5.3. The UV transparency cut-off limits decreases with the doping concentration. Similar results have been obtained in the case of LA doped KDP [8]. Absorption in the near ultraviolet region arises from electronic transitions associated within the sample. Hence, it could be concluded that the LA doping play a key role in improving the optical quality of KDP crystals. This is the most desirable property of materials possessing NLO activity.

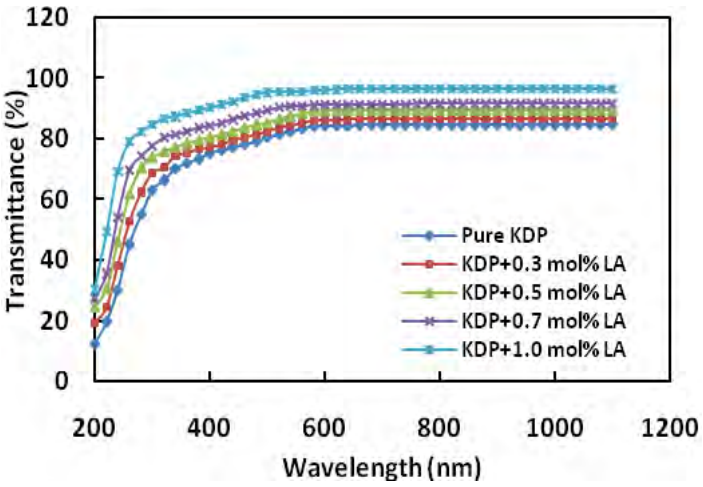

Fig. 5.6 Transmission spectra of pure and LA doped KDP crystals

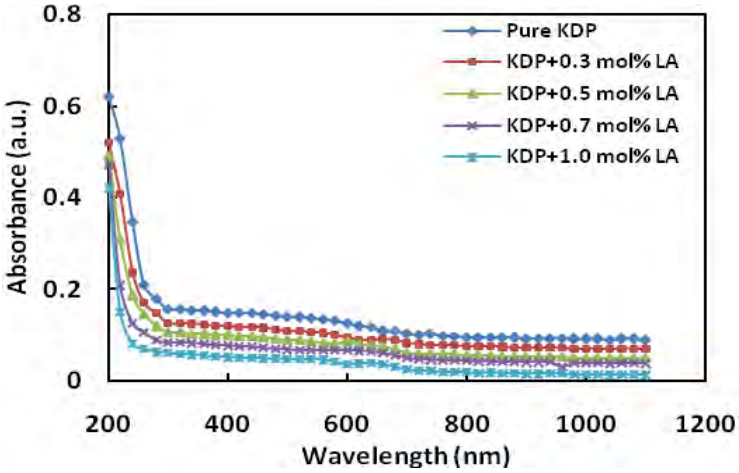

Fig. 5.7 Absorption spectra of pure and LA doped KDP crystals

5.4.5 Optical Parameters Calculation

The dependence of optical absorption coefficient with the photon energy helps to study the band structure and the type of transition of electrons. The optical absorption coefficient (α) calculated from the transmittance using the following relation

$$\alpha = [2.3026 \log (1/T)]/d$$

Where T is the transmittance and d is the thickness of the sample. For a direct band gap material, the absorption coefficient α is related to light frequency according to the following formula.

$$\alpha h\nu = A(h\nu - E_g)^{1/2}$$

Where A is a constant, Eg is the optical band gap energy, h is the Planck‟s constant and ν is the frequency of the incident photons. The band gap energy of the sample can be estimated by plotting $(\alpha h\nu)^2$ versus hν and by extrapolating the linear portion near the onset of absorption edge to the energy axis. The extinction coefficient (K) calculated from the following relation.

$$K = \frac{\alpha\lambda}{4\pi}$$

where λ is the wavelength. The refractive index (n) calculated from the reflectance data using,

$$n = [-(R+1) \pm 2\sqrt{R}] / (R-1)$$

Where R is the reflectance.

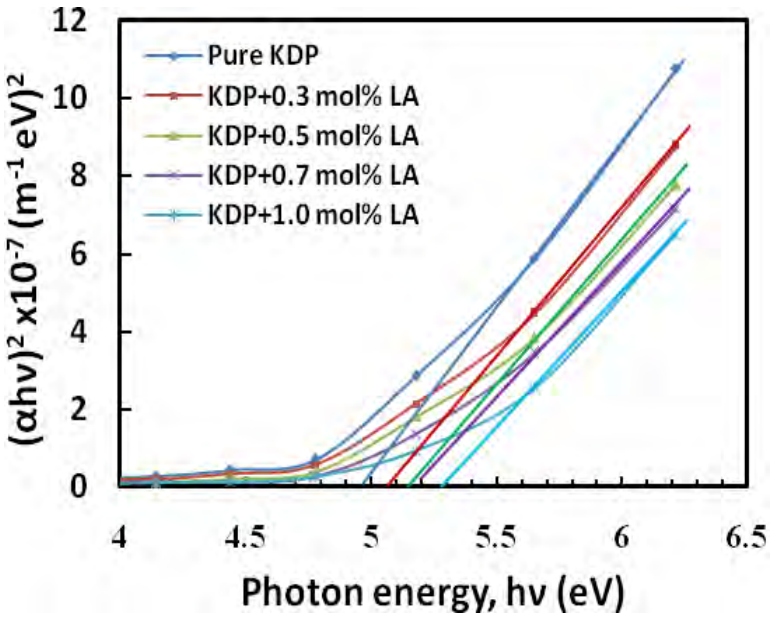

Fig. 5.8 Photon energy vs. $(\alpha h\nu)^2 \times 10^{-7}$

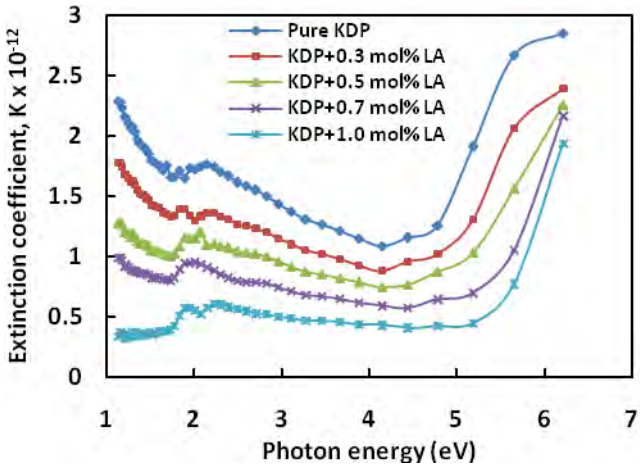

Fig. 5.9 Photon energy vs. extinction coefficient (K) x 10^{-12}

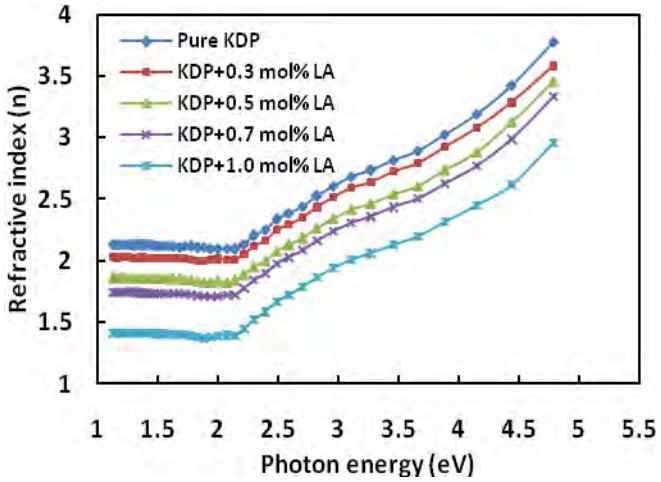

Fig. 5.10 Photon energy vs. refractive index

5.4.6 Dielectric Studies

The study of dielectric constant of a material gives an outline about the nature of atoms, ions and their bonding in the material. The dielectric constant (ε_r) and dielectric loss (tanδ) depend on frequency of applied field. The real ε_r and imaginary ε_i parts of the dielectric constant calculated by using the relations $\varepsilon_r = n^2 - k^2$ and $\varepsilon_i = 2nk$, Dielectric loss was calculated using the formula: $\tan\delta = \varepsilon_i/\varepsilon_r$.

Fig. 5.11. shows the variation of dielectric constant with photon energy. The value of dielectric constant decreases as the frequency increases and it becomes independent of frequency at higher frequency region. The high value of dielectric constant in the low frequency region may be due to the contributions of electronic, ionic, dipolar, and space charge polarizations [12]. The electronic exchange of the number of ions in the crystal gives local displacement of electron in the direction of the applied field, which in turn give rise to polarization. Continuous and gradual decrease in dielectric constant suggests that pure LA crystal like any normal dielectric may possess domains of different size and varying relaxation times. It is evident that the lower value of dielectric constant is a suitable parameter for the enhancement of SHG coefficient [13]. Fig. 4.12 shows the variation of dielectric loss with photon energy of applied field at room temperature. The behavior of variation is similar to that of dielectric constant with frequency. This is the normal behavior observed earlier [8,14]. The dielectric loss is a measure of the energy absorbed by dielectric. Usually the dielectric has a resistance R and reactance $1/\omega C$. Which are related to the phase angle $\tan\delta = 1/\omega CR$, where C is a capacitance. So the low dielectric loss at high frequency reveals the superior optical quality of the crystals with lesser defects, and this parameter is of vital importance for various NLO application.

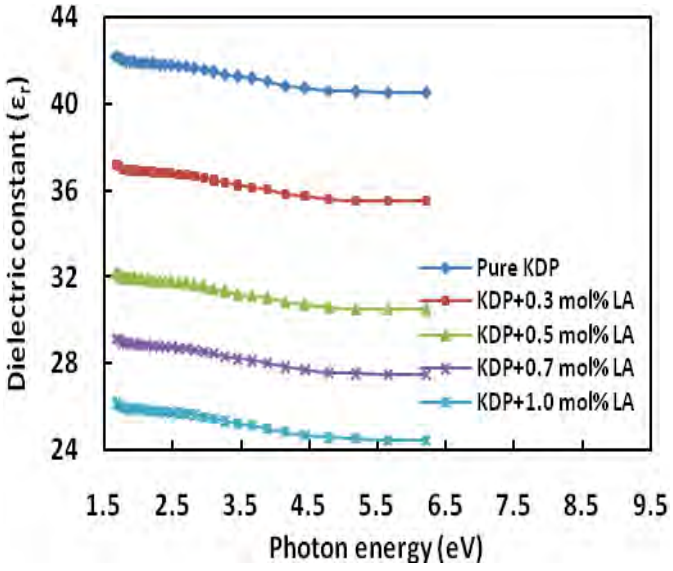

Fig. 5.11 Variation of dielectric constant (ε_r) with photon energy

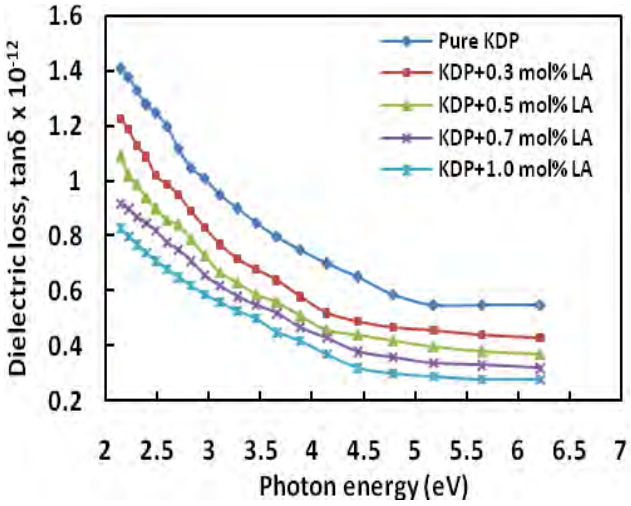

Fig. 5.12 Variation of dielectric loss (tanδ) with photon energy

5.4.7 Thermal Analysis

The effect of LA doping on thermal stability of KDP crystals is studied from the simultaneous TG, DTA and DTG curves are shown in the fig. 5.13, 5.14 and 5.15. In order to study the influence of dopant on the thermal stability of KDP, the temperature corresponding to the first stage of decomposition is taken into account for comparison. In fig. 5.13, the DTA curve shows an endothermic peak at 229.4 ^{0}C for the pure KDP and in fig. 5.15, the endothermic peaks of the DTA curves for LA doped KDP crystals is 232.8 ^{0}C. These endothermic peaks correspond to the decomposition temperature of the crystals. The TGA curve exhibited negligible weight loss in the region 40 ^{0}C to 193 ^{0}C as shown in the fig. 4.13 and 5.15.The decomposition of pure KDP crystal begins at 192.5 ^{0}C and terminates at 395.3 ^{0}C. The weight loss observed from TGA graph for pure KDP in the temperature range 192.5 ^{0}C to 395.3 ^{0}C is 13.7%. But for KDP+1.0 mol% LA crystal the decomposition starts at 274.1 ^{0}C and ends at 370.7 ^{0}C. The weight loss observed from TGA graph for KDP+1.0 mol% LA crystal is 17.4%. From this analysis we can see from the TGA/DTA analysis that on increasing the concentration of LA the hydration process starts later and the crystal becomes anhydrous higher than the pure KDP crystal because LA becomes unstable at lower temperature. These results prove that

the LA has entered as an impurity into KDP crystals. The similar results have obtained for LA doped in KDP [11], and L-arginine doped in KDP and ADP [16].

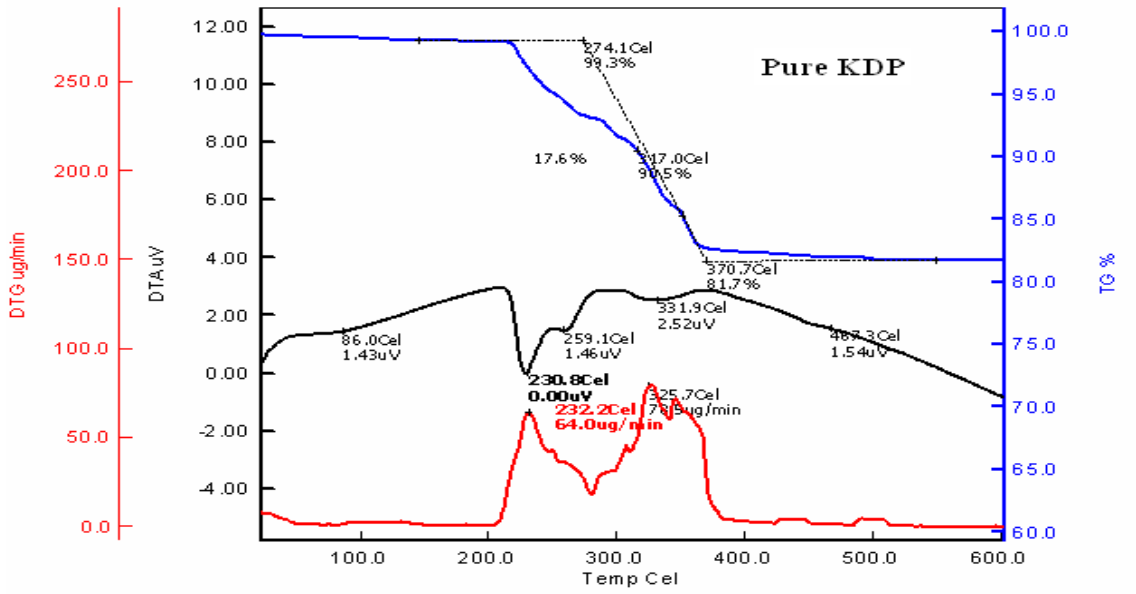

Fig. 5.13 Simultaneous TGA, DTA and DTG curves of pure KDP crystal

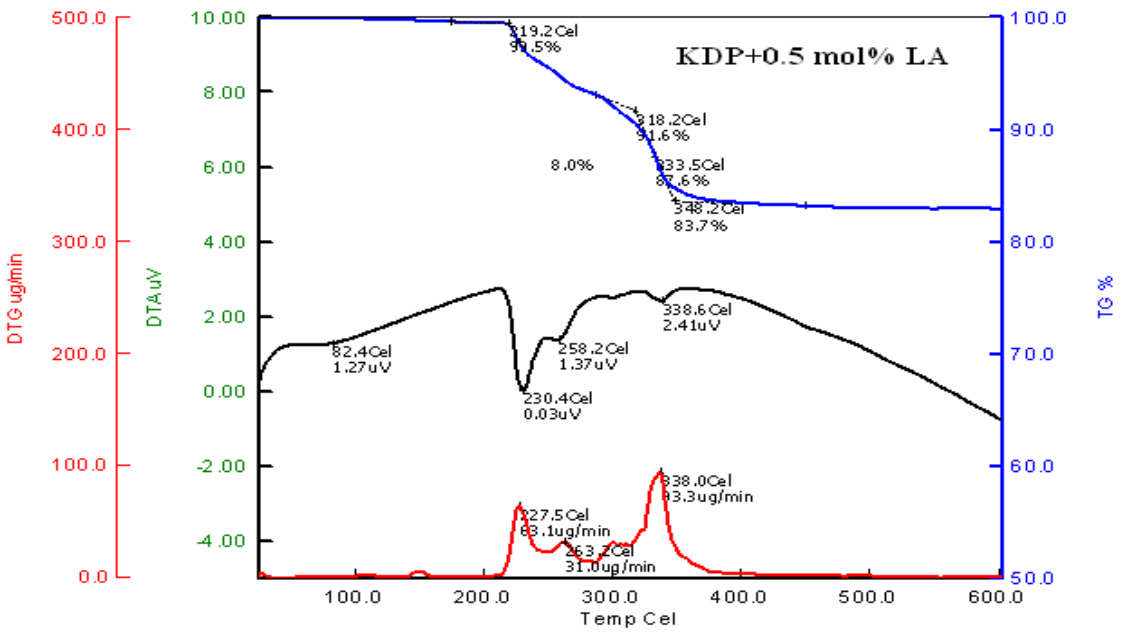

Fig. 5.14 Simultaneous TGA, DTA and DTG curves of KDP+0.5 mol% LA crystal

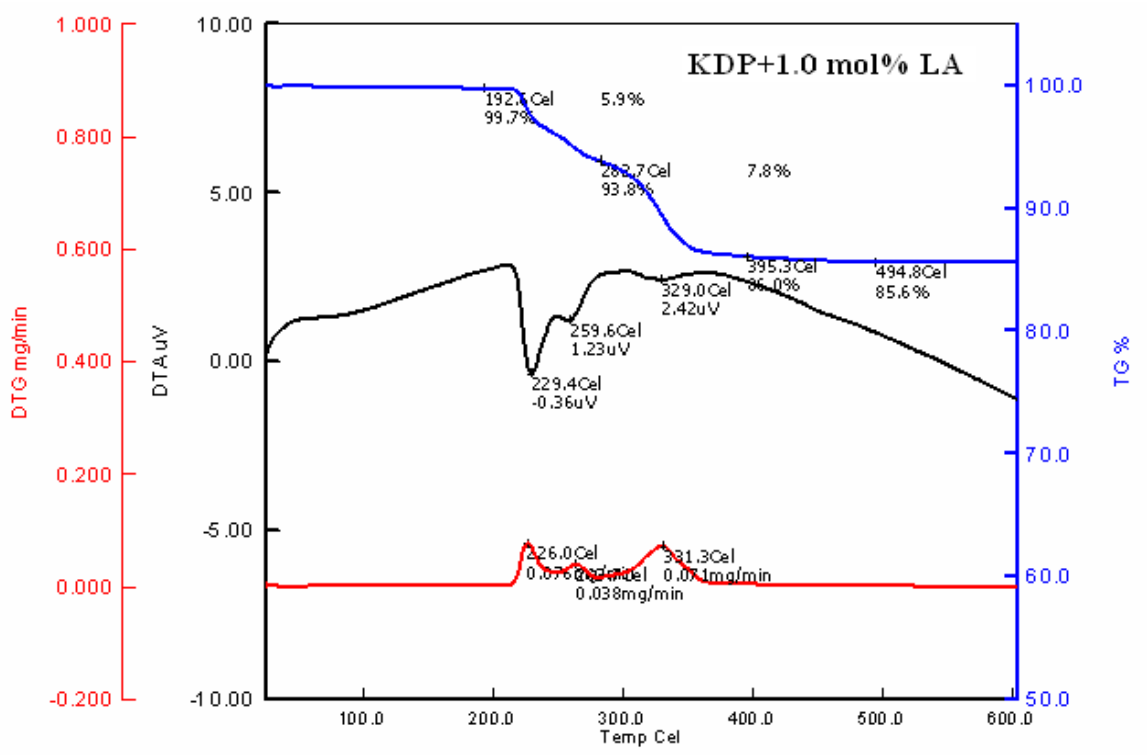

Fig. 5.15 Simultaneous TGA, DTA and DTG curves of KDP+1.0 mol% LA crystal

5.4.8 Vicker's Microhardness Analysis

Hardness is an important property to characterize a crystal. Harder crystals are good for device fabrication. Hardness test is useful to find the mechanical hardness of the crystal and to estimate the threshold mechanical stress it can withstand. Vicker"s hardness measurement of pure and LA doped KDP crystals was taken by varying applied loads 25, 50, 75 and 100 g for indentation time of 7 s. From fig. 4.16 the hardness value of pure and doped crystals were found to decrease with the applied loads because large prominent cracks due to the attainment of the threshold mechanical stress which is comparable with these results [11,14]. The hardness values were calculated using the formula: $H_v = [1.8544 \text{ X } P]/D^2$ kg-mm^{-2}. Where H_v is the Vicker"s microhardness number, P is the indenter load in kg and D is the diagonal length of the impression in

mm. The micro hardness value was taken as the average of the several impressions made with both diagonals being measured. In the present study, the hardness of the pure KDP crystal is higher than LA doped KDP crystals. This is because of the incorporation of the LA ($^{+}NH_3$, COO-) ions into superficial crystal lattice and forming defect centers which generate weak lattice stresses on the surface.

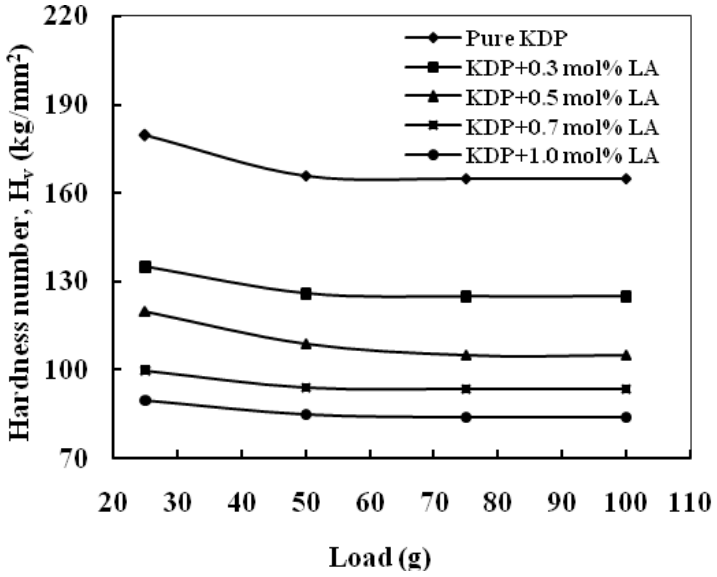

Fig. 5.16 Hardness number (H_v) vs. Load (g)

5.4.9 AC electrical conductivity and Dielectric Studies

The AC conductivity (ζ_{ac}), dielectric constant (ε_r) and dielectric loss (tanδ) of pure KDP and LA doped KDP crystals were carried out at different temperatures ranging from 35 °C to 140 °C at a particular frequency 1 kHz by LCR meter. The samples were cut and polished using wet cloth polishing sheet. The sample dimensions were 8mm x 6mm surfaces area and 2mm thickness. The sample was electrode on either side with silver paste to make it behaves like parallel plate capacitor. Silver paste electrodes on opposite sides ensure good electrical contacts. The resistance, capacitance, and dissipation factor values were directly measured from LCR meter. From the values of capacitance and dissipation factor, the dielectric constant and dielectric loss of the samples were calculated. The dielectric constant (ε_r) of the all KDP crystals were calculated through the capacitance by the fundamental equation, $\varepsilon_r = C\ t / 0.0885\ A$, Where C is the capacitance,

t is the thickness and A is the area of the samples. The dielectric loss (tanδ) of the samples were calculated by the relation, tanδ = dissipation factor x ε_r. The AC conductivity (ζ_{ac}) has been calculated using the expression: $\zeta_{ac} = 2\pi fCt / A$, where f is the frequency of applied field. The AC conductivity, dielectric constant and dielectric loss at different temperatures of pure and LA doped KDP crystals have been shown in figs. 17, 18 and 19. The AC conductivity is found to increase with the increase in temperature but decreases with LA concentrations. Electrical conductivity of the KDP group crystals is determined by the proton transport within the framework of hydrogen bonds [20]. The mechanism can be considered here is identical to the conductivity mechanism in ice also containing hydrogen bonds. It is assumed that the conductivity of ice is determined by the simultaneous presence of positive and negative ions and orientational defects-vacant hydrogen bonds (L-defects) and doubly occupied hydrogen bonds (D-defects). Other possible defects are vacancies and defect associates. The experimental data and especially the character of the temperature dependence of conductivity allow us to state that the conductivity of KDP crystals is determined by both thermally generated L-defects and foreign impurities incorporated into the lattice and generating L-defects there [20]. As the conduction in KDP is protonic and mainly due to the anion $(H_2PO_4)^-$ and not the cation (K^+) for KDP, the additional hydrogen bonds created may reduce the L-defects and consequently obstruct the movement of protons. This may be the reason for the decrease in conductivity value with the increase in impurity concentration. The nature of variations of dielectric constant with temperature indicates the contribution of ionic, electronic, orientational and space charge polarization. Generally the low value of dielectric loss indicates that the sample possesses good crystalline quality with fewer defects. The lower value of dielectric constant is a suitable parameter for the enhancement of SHG signals.

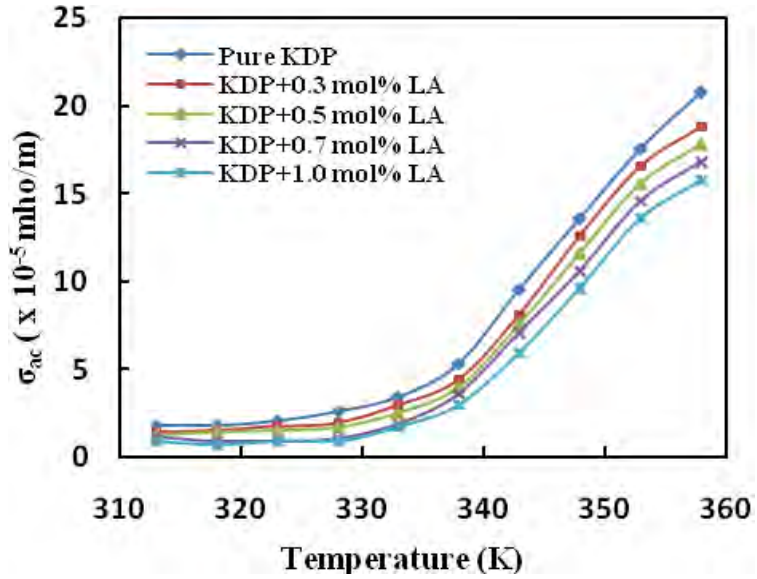

*Fig. 5.17 AC electrical conductivity versus temperature (*K*)*

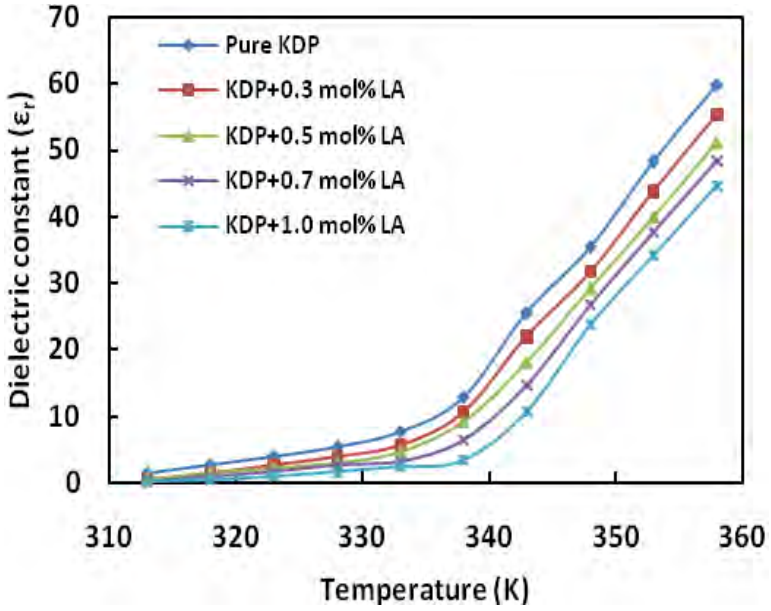

Fig. 5.18 Dielectric constant versus temperature

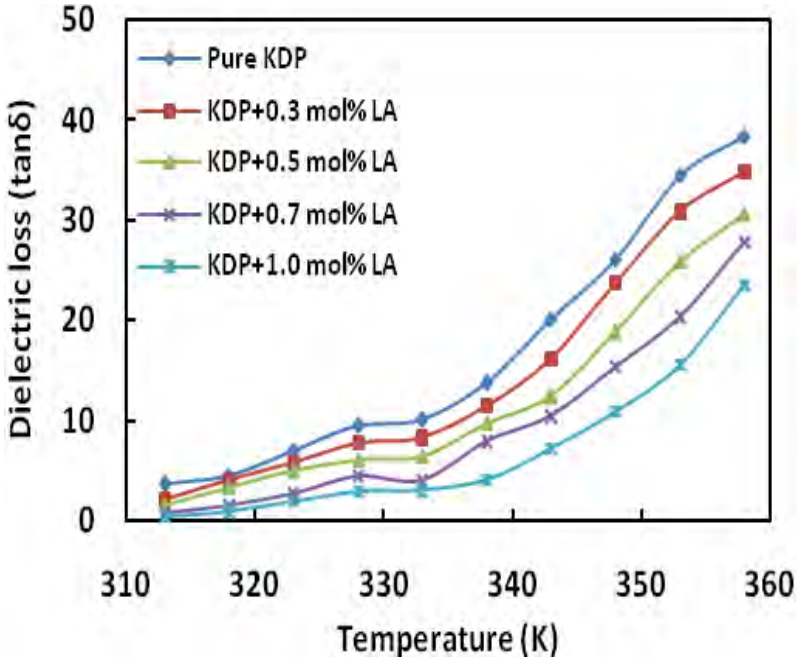

Fig. 5.19 Dielectric loss versus temperature

5.4.10 Etching Study

Etching is the selective dissolution of the crystal which reveals the crystal symmetry and lattice defects [22]. Patterns observed on surface like spirals, hillocks and step pattern, etc yield considerable information on the growth process and growth mechanism of the crystal. When a surface is etched, well defined etch patterns are produced at the dislocation sites. The chemical etching studies were carried out on the as grown crystals of pure KDP and LA doped KDP crystals to investigate the distribution of structural defects in the grown crystals. The surfaces of samples were polished and then etched in the etching solution (water) at room temperature for 10 s. Then soaked with a filter paper and examined under an optical microscope in reflection mode. Fig.5.20. illustrate the typical etch patterns observed on the (001) plane of the pure KDP and LA doped KDP crystals. When the crystals were etched in water, the triangular type etch pits were observed and the etch-pit density (EPD) for pure KDP crystal was found 2.5 x 10^2 cm^{-2} and for LA doped KDP crystal was 14.28 x 10^2 cm^{-2}. Usually, these etching pits are considered as outcrop of dislocation lines. The shape of these etching pits is determined

by the lattice structure and symmetry [23]. This is also evident from the fact that the bottom of the crystal is flat. It means that the crystals are grown from the bottom of the beaker /container and not in the middle of the solution. The presence of dislocations strongly influences many of the properties of crystals. The generation of dislocations is strongly correlated with the formation of inclusions in the crystals. The formation of inclusions destroys the normal build of lattices, which results in stress and lattice mismatch in crystal. In order to relax the stress and adjust the lattice mismatch, lots of dislocations were produced. That‟s why so many dislocation etching pits are observed in doped KDP crystal.

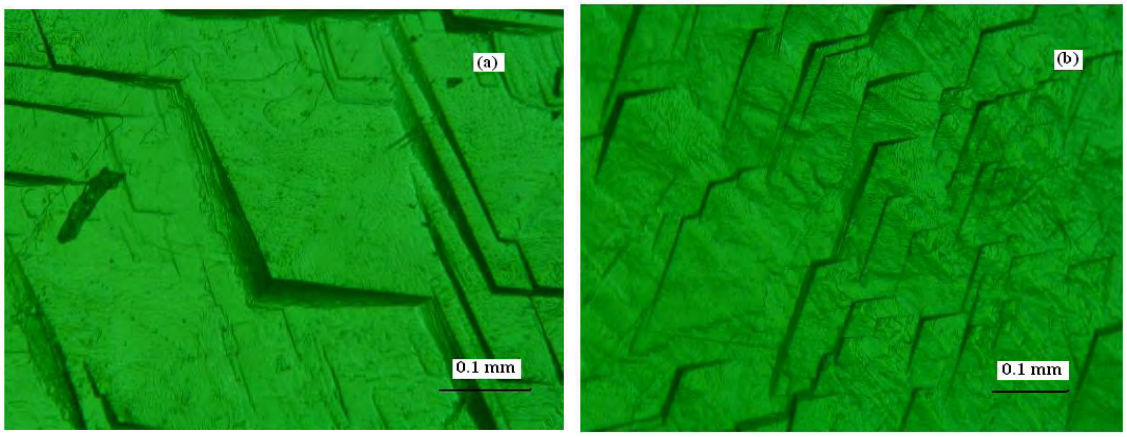

Fig. 5.20 Etch pit patterns on (001) plane of (a) pure KDP and (b) 1.0 mol% LA doped KDP crystals

5.5 Conclusions

Amino acid, LA doped KDP crystals have been grown by employing the slow evaporation solution growth technique. The study of cell parameters calculated by powder X-ray diffraction analysis which confirmed that the crystal structure of KDP does not change by doping LA. The doping of LA in the sample was confirmed by EDX analysis. The FTIR analysis confirmed the presence of all functional groups. The absence of absorption and excellent transmission in entire visible region makes this crystal a good candidate for optoelectronic application. The thermal study of grown LA doped crystals indicated that these crystals can be exploited for NLO applications up to the temperature of 193 ^{0}C.

5.6 References

[1] Zaitseva N.,and Carman, L., "Rapid Growth of KDP-Type Crystals", [J]. Prog. Cryst. Growth Ch., **43**, p.1-118, 2001.

[2] De Vries, S. A. and Goedtkindt,P., et al, "X-ray diffraction Studies of Potassium Dihydrogen Phosphate (KDP) Crystal Surface", J. Cryst. Growth, **205**, p.202-214, 1999.

[3] Xin-guang Xu, Xun Sun, Zheng-ping Wang, Gui-bao Xu, Zong-shu Shao, Zhang-shou Gao, **"**Supernormal optical characteristics in doped quaternary ammonium salt KDP crystals", Optical Materials, Vol. **23**, Issues 1-2, p. 409-414, 2003.

[4] Zaitseva N., Carman L. and Smolsky, I., J. Cryst. Growth, "Habit control during rapid growth of KDP crystals", **241**, p.363, 2002.

[5] Wyckoff R. W. G., " Crystal Structure", Vol. **3**, 2nd edn., Interscience, New York, 1960.

[6] Franken P. A., Hill A. E. and Petess, C. W., Phys. Rev. Lett, **7**, p.118, 1961.

[7] Podder J., "The Study of Impurities Effect on the Growth and Nucleation Kinetics of Potassium Dihydrogen Phosphate", J. Cryst. Growth, **70**, p.237-239, 2002.

[8] Muley G. G., Rode M. N. and Pawar, B. H., "FT-IR, Thermal and NLO Studies on Amino Acid (L-arginine and L-alanine) Doped KDP Crystals", Acta Physica Polonica A, Vol.**116**, p.1033-1038, 2009.

[9] Suresh Kumar B. and Rajendra Babu,K., "Effect of L-arginine, L-histidine and Glycine on the Growth of KDP Single Crystals and Their Characterization", Indian Journal of Pure and Applied Physics, Vol.**46**, p.123-126, 2008.

[10] Gunasekaran S. and Ramkumaar,G. R.,"Analysis on Suitability of Pure and α-histidine Doped KDP Crystals in High Speed Applications", Indian Journal of Physics, **83**(11), p.1549-1555, 2009.

[11] Parikh, K. D., Dave, D. J., Parekh B. B. and Joshi, M. J., "Growth and Characterization of L-alanine Doped KDP Crystals", Cryst. Res. Technol. **45**, N0.6, p.603-610, 2010.

[12] Priya, M., Padma, C. M., Freeda, T. H., Mahadevan C. and Balasingh, C.,"Electrical Conductivity Measurements on Gel Grown KDP Crystals Added With Urea and Thiourea", Bull. Mater. Sci., Vol.**24**, No.5, p.511-514, 2001.

[13] Kumaresan,P., Moorthy Babu S. and Anbarasan, P. M.,,Influence of dopants (L-Glutamic acid,L-Histidine and L-Valine) on the performance of KDP crystals, 4th DAE-BRNS laser symposium, ISBN No.81-903321-0-3, Vol. **4**, p.521-522, 2005a.

[14] Kumaresan,P., Moorthy Babu, B. S. and Anbarasan, P. M., " Thermal Dielectric Studies on pure and Amino Acid (L-glutamine, L-histadine, L-valine) Doped KDP Single Crystals", Opt. Mater., Vol. **30**, Issue-9, p.1361-1368, 2008.

[15] Dhanaraj, P. V., Bhagavannarayana, G. and Rajesh, N. P., " Effect of amino acid additives on crystal growth parameters and properties of ammonium dihydrogen orthophosphate crystals", Materials Chemistry and Physics, Vol. **112**, Issue 2, p.490-495, 2008.

[16] Meena, M. and Mahadevan,C. K.," Growth and electrical characterization of L-arginine added KDP and ADP single crystals", Cryst. Res. Technol. **43**, no. 2, p.166-172, 2008.

[17] Suresh Kumar, B., Sudarsana Kumar M. R. and Bajendra Babu,K.," Growth and Characterization of pure and Lithium doped L-alanine single crystals for NLO devices", Cryst. Res. Technol. **43**, no. 7, p.745-750, 2008.

[18] Parikh, K. D., Dave, D. J., Parekh, B. B. and Joshi,M. J.," Thermal, FT-IR and SHG efficiency studies of L-arginine doped KDP crystals", Bull. Mater. Sci., Vol. **30**, no. 2, p.105-112, 2007.

[19] Vijayan, N., Rajasekaran, S., Bhagavannarayana, G., Ramesh Babu, R., Gopalakrishnan, R., Palanichamy, M. and Ramasamy, P.," Growth and characterization of nonlinear optical amino acid single crystal: L-alanine", Crystal growth & design, Vol. **6**, no. 11, p.2441-2445, 2006.

[20] Harris,L. B. and Vella, G. J., "Conductivity of single crystals of potassium dihydrogen phosphate," J. Chem. Phys., Vol. **10**, 1964, p. 4294.

[21] Nicoud, J. F. and Twieg, R. J., "Design and Synthesis of Organic Molecular Compounds for Efficienty Second Harmonic Generation," In: D. S. Chemla and J. Zyss, Ed., *Nonlinear Optical Properties of Organic Molecules and Crystals*, Academic, Orlando, Vol. **1**. 1986.

[22] Sangwal, Keshra, "Etching of crystals: Theory, experiment, and application", North-Holland (Amsterdam and New York, NY, USA), Vol **15**, p.497, 1987.

[23] Sangwal, K. and Owczarek**,** I., **"**On the formation of etch grooves at impurity striations and growth sector boundaries in crystals grown from solutions", J. Cryst. Growth, Vol.**129**, p.640-652, 1993.

CHAPTER 6

GROWTH AND CHARACTERIZATION OF L-ALANINE DOPED POTASSIUM ACID PHTHALATE (KAP) CRYSTALS

CHAPTER 6

GROWTH AND CHARACTERIZATION OF L-ALANINE DOPED POTASSIUM ACID PHTHALATE (KAP) CRYSTALS

6.1 Introduction

KAP with chemical formula $K(C_6 H_4 COOH.COO)$, crystallized into the orthorhombic form with four molecules per unit cell. It is well known material for its application in the production of crystal analyzers for long-wave X-ray spectrometers [1-2]. KAP crystal possesses piezo-electric, pyro-electric, elastic and non-linear optical properties [3-7]. It is a fine model in studying the crystallization process especially the spiral growth mechanism in crystals [6]. They have excellent physical properties and have a good record for long term stability in devices [8-10]. It exhibits excellent cleavage and the planes are comparable to that of mica. Single crystals of KAP exhibit a rare blend of ionic and molecular properties and have wide application potential by virtue of their polar nature [11]. Contribution from the polarizable aromatic rings of phthalate ions to the non-linear susceptibility of KAP, renders KAP similar to some of the well explored non-linear optical organic molecular crystal.

Amino acid family crystals are playing an important role in the field of non-linear optical organic molecular crystal. Among them LA, with chemical formula (CH_3 CH NH_2 COOH) is the smallest, naturally occurring chiral amino acid with a non-reactive hydrophobic methyl group ($^{-}CH_3$) as a side chain. LA has the zwitterionic form ($^{+}NH_3$-C_2H_4-COO^{-}) both in crystal and in aqueous solution over a large range of pH, which favors crystal hardness for device application. It is an efficient organic amino acid nonlinear optical material. It belongs to the orthorhombic crystal system and the unit cell parameters are; a = 6.320 Å, b = 12.343 Å, c = 5.784 Å, $\alpha = \beta = \gamma = 90^0$.

Several new complexes incorporating the amino acid LA have been recently crystallized and their structural, optical and thermal properties have been investigated [12-15]. The growth of pure LA crystals was reported by Vijayan et. al [16] and found higher damage

threshold than KDP. It is also reported that the addition of some of the amino acids as dopant enhances the NLO and ferroelectric properties of semi organic materials [17,18]. So LA doped semi organic material, KAP will be of special interest as a fundamental building block to develop many complex crystals with improved NLO properties.

In this thesis we have studied the pure KAP and the effect of LA as impurity with concentration ranging from 3000 – 10000 ppm, i.e, 0.3 – 1.0 mol% added separately in to the parent KAP saturated solution at 30 ^{0}C which were used for the growth of crystals by slow evaporation at room temperature. The effect of this impurity on the structure, optical, mechanical, electrical and thermal properties have been studied and reported.

6.2 Experiment

6.2.1 Determination of the Solubility of Pure and LA Doped KAP

The solubility of pure and LA doped KAP materials in double distilled water was determined in the temperature range 30-50 ^{0}C insteps of 5 ^{0}C using a constant temperature bath of accuracy ±0.01 ^{0}C. 500 mL of the saturated solution of pure KAP salt was prepared gravimetrically at 30 ^{0}C. This solution was stirred well for six hours constantly using magnetic stirrer, then solution was filtered using Whatmann filter paper. This solution was taken in five different beakers of 100 ml and the amino acid LA was added to each four beaker as 0.3 mol%, 0.5 mol%, 0.7 mol% and 1 mol%. Each beaker separately with LA doped KAP solution was stirred well for six hours constantly at 30 ^{0}C using magnetic stirrer. After making doped supersaturated solution of KAP, the 5 ml of the solution was pipetted out and poured into a 10 mL beaker of known weight. The solvent was completely evaporated by warming the solution at 50 ^{0}C. The amount of the salt present in 5 mL of the solution was measured by subtracting the empty beaker's weight. From this the amount of the salt present in 100 mL of the solution was found out. In the same way, the amount of the salt dissolved in 100 mL at 35, 40, 45 and 50 ^{0}C was determined. Fig. 6.1 shows the solubility curves of pure and doped KAP salt. It is observed from the solubility graph that the solubility of pure and doped KAP in water increases as the temperature increase and decreases with doping concentration increase.

From this solubility data we can say that the KAP material has positive temperature coefficient.

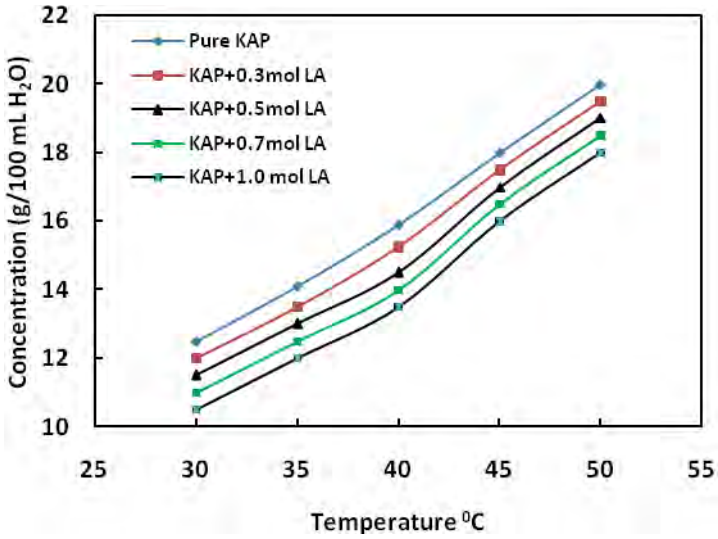

Fig. 6.1 Solubility curves of pure and LA doped KAP salt

6.2.2 Growth of Pure and LA Doped KAP Crystals

The pure KAP (AR grade) and LA (chemical from SIGMA) doped KAP crystals were grown by dissolving purified KAP, and LA powders in appropriate amount in double distilled water at 30 ^{0}C with continuous stirring using magnetic stirrer for two hours to form a supersaturated mother solution. The solution is then filtered using Whatmann filter papers and kept in a petri dish covered with a perforated polyethylene and tied it by a rubber band, place it in a dust free place to harvest the seed crystals within 4-5 days. The pH of the solution was ranged from 3.93 to 3.97. The same process was used to prepare the solutions for the bulk crystal growth. Pure and LA doped KAP solution was used for the growth of crystal by slow evaporation method at room temperature using a good quality seed crystal. The purity of the crystals was improved by successive recrystallization process. Grown the crystals of bigger size within 25-30 days. Grown crystals were found color-less and transparent. Fig. 6.2 shows photographs of pure and doped KAP crystals.

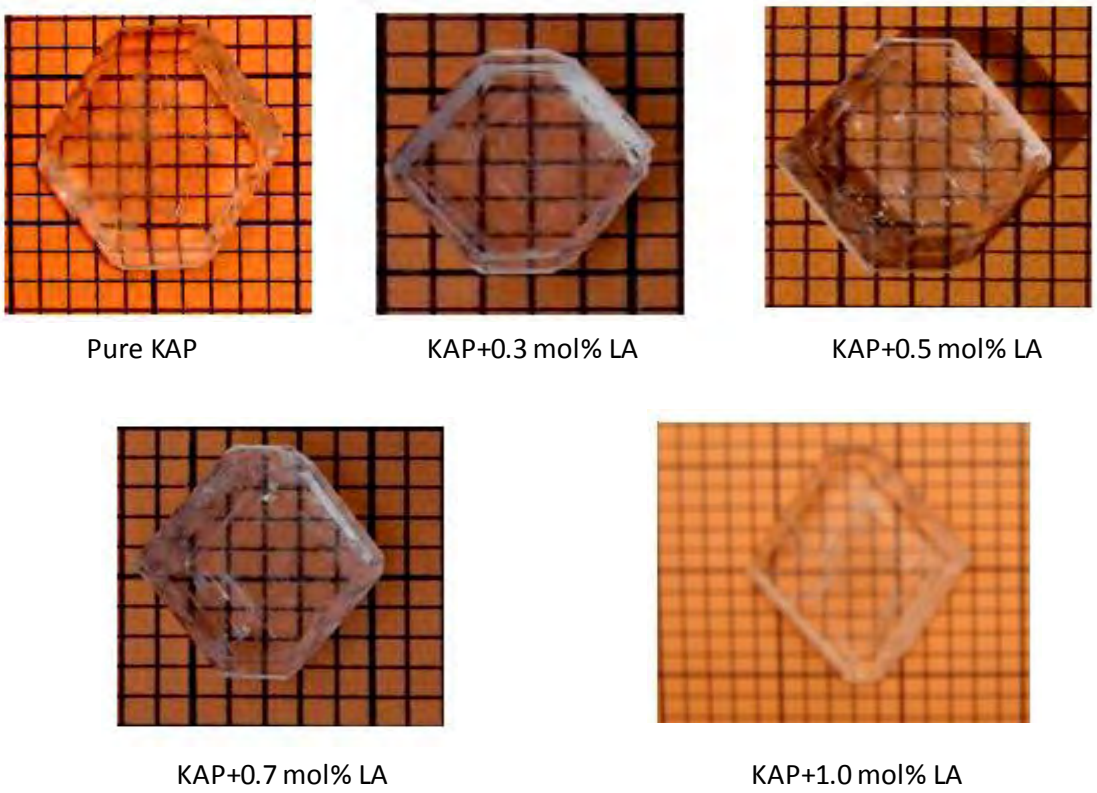

Fig. 6.2 Photographs of pure and LA doped KAP crystals

6.3 Characterization of LA Doped KAP Crystals

The grown pure and doped KAP crystals were characterized by EDX, Powder XRD, FTIR, Optical Transmission Spectrum, TGA, DTA, Vicker"s microhardnes, surface morphology by etching in water and compare all these results with pure KAP crystal.

In order to confirm the presence of LA into KAP crystals was subjected to EDX. EDX spectra were recorded using a JEOL-6360 Scanning Electron Microscope. The recorded EDX spectra shown in fig.6.4. Powder XRD was recorded using a Philips X pert PRO X-ray diffractometer with CuK_α (λ = 1.5418Å) radiation. The XRD spectra shown in fig. 6.11.The lattice parameters were calculated from the XRD data and tabulated in table 6.2. In order to confirm the presence of functional groups in the crystal lattice, FTIR spectrum was recorded by KBr pellet technique using a Shimadzu FTIR-8900 spectrometer in the wave number range 400-4000 cm^{-1}. The FTIR spectra of pure and LA doped KAP

crystals shown in fig. 6.3. The optical properties of the grown crystals were studied by the transmission spectra using Shimadzu UV-1601 visible spectrometer in the wavelength region from 200 to 1100 nm. The transparent crystals with 2 mm thickness samples were used and mounted in a standard manner so that equal area of samples was exposed to the radiation. Thermal analysis was conducted on pure and LA doped KAP crystals using simultaneous TGA, and DTA using thermal analyzer (model no.TG/DTA- 6300) from 40 ^{0}C to 700 ^{0}C at heating rate of 15 ^{0}C/min in nitrogen atmosphere. Crystals with high transparency and large defect-free with the dimensions of 8 mm x 6 mm x 2 mm were cut into a rectangular size and surfaces were coated with silver paint to give good electrical contact between the electrodes; were selected for the electrical conductivity measurements. The DC electrical conductivity measurements were carried out along the unique axis (c-) using the conventional two-probe technique using a million ohmmeter at various temperatures ranging from 35 to 140 ^{0}C. The field is applied to perpendicular to c- axis. The dimensions of the crystals were measured using a travelling microscope. The ζ of the crystal was calculated using the relation $\zeta = d/(RA)$, where R is the measured resistance, d is the thickness of the sample crystal and A is the area of the face of the crystal in contact with the electrode. Vicker"s microhardness number of pure and LA doped crystals was studied using the HMV-2T, Shimadzu, Japan. Dislocation, surface defects and morphology were characterized by chemical etching followed by etch pit examination using optical microscope, SWIFTMASTER II (SWIFT) Tokyo, Japan.

6.4 Results and Discussion

6.4.1 Fourier Transform Infrared Spectroscopy

The FTIR spectra of pure and doped KAP crystals are shown in fig. 6.3. The frequencies with their relative intensities obtained in FTIR of pure and doped with different concentrations of LA into KAP crystals and their most probable assignments are presented in table 6.1. The hydrogen bonding extends throughout the molecule of KAP. This hydrogen bonding result in the modification of stretching frequencies of O-H and the carboxyl groups. Absorption band in the region which was less than 900 cm^{-1} appears due to C-H bending vibrations. The asymmetric and symmetric stretching modes of C-O

(with vertical double bond of oxygen on carbon) are observed at 1535 and 1350 cm^{-1}. Aromatic ring group appears around the frequency 1481 cm^{-1}. Carbonyl group C=O presents in the range 1535-1650 cm^{-1}. C-H stretching vibration appears between 3095 and 2480 cm^{-1}. Carboxylic O-H stretching vibration produced resolved multiple bands between 2200 and 3800 cm^{-1}. It was clearly illustrated that the strong hydrogen bonding interaction of C-OH group and the corresponding C-OH in plane and out of plane bands are observed as weak bands at 1443 and 960 cm^{-1}. All these observations confirmed the presence of the functional groups of all grown crystals.

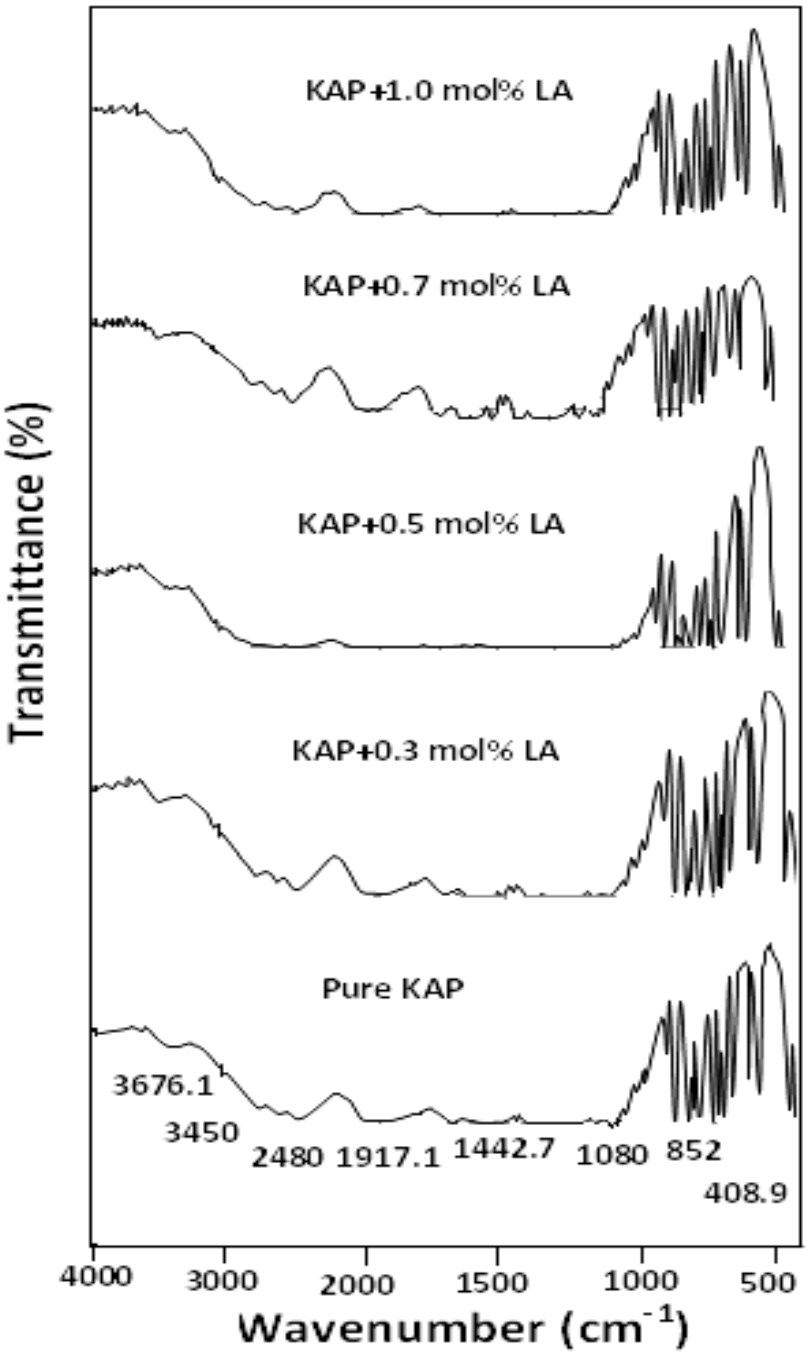

Fig. 6.3 FTIR spectra of pure and LA doped KAP crystals

Table 6.1 Vibrational frequencies obtained for pure and LA doped KAP crystals

Calculated Frequency (cm^{-1})	Observed IR frequencies (cm^{-1})					Assignments
Literature data	Pure KAP	KAP+0.3 mol% LA	KAP+0.5 mol% LA	KAP+0.7 mol% LA	KAP+1.0 mol% LA	
3500-3200	3450	3495	3495	3450	3450	O-Hstretching
3300-2500	3300	3325	3323	3325	3322	O-Hstretching
3100-3000	3095	3095	3095	3095	3095	C-Hstretching
3100-3000	3025	3025	3025	3025	3025	C-Hstretching
2830-2695	2750	2750	2800	2779	2779	H-C=O; C-H stretching
2830-2695	2600	2600	2600	2621	2621	H-C=O; C-H stretching
2830-2400	2480	2478	2460	2480	2482	-C-H aromatic stretching
2000-1600	1917	1919	2025	1917	1911	O-H hydrogen bonded
2000-1600	1801	1801	1800	1801	1800	=C-H out of plane bending
2000-1600	1650	1675	1650	1674	1720	C=O symmet. stretching
1600-1500	1535	1600	-------	1545	1600	C=O arom.stre.
1600-1475	1481	1485	--------	1485	1485	C=C ring stret.
1470-1450	1443	1443	--------	1443	1450	O-H in plane bending
1370-1290	1350	1325	--------	1385	1300	-C=O Carboxylate ion=O symmetr.
1335-1250	1225	1220	---------	1254	--------	C-COO stretch.
1300-1150	1038	1038	1038	1038	1038	C-H in plane bending
1000-650	961	961	961	961	961	C-C=stretching
1000-650	887	887	887	887	887	C-C-O stret.
1000-650	811	------	812	-----	812	C-H out of plane bending
1000-650	791	791	791	791	791	-C-H bending

6.4.2 Energy Dispersive X-ray Spectroscopy

In order to confirm the presence of the elements of LA into the pure KAP crystal, the sample of grown crystals were subjected to EDX analysis. The recorded EDX spectra are shown in fig. 6.4. The doping of LA into KAP crystals was confirmed by the atomic percent of the elements of LA.

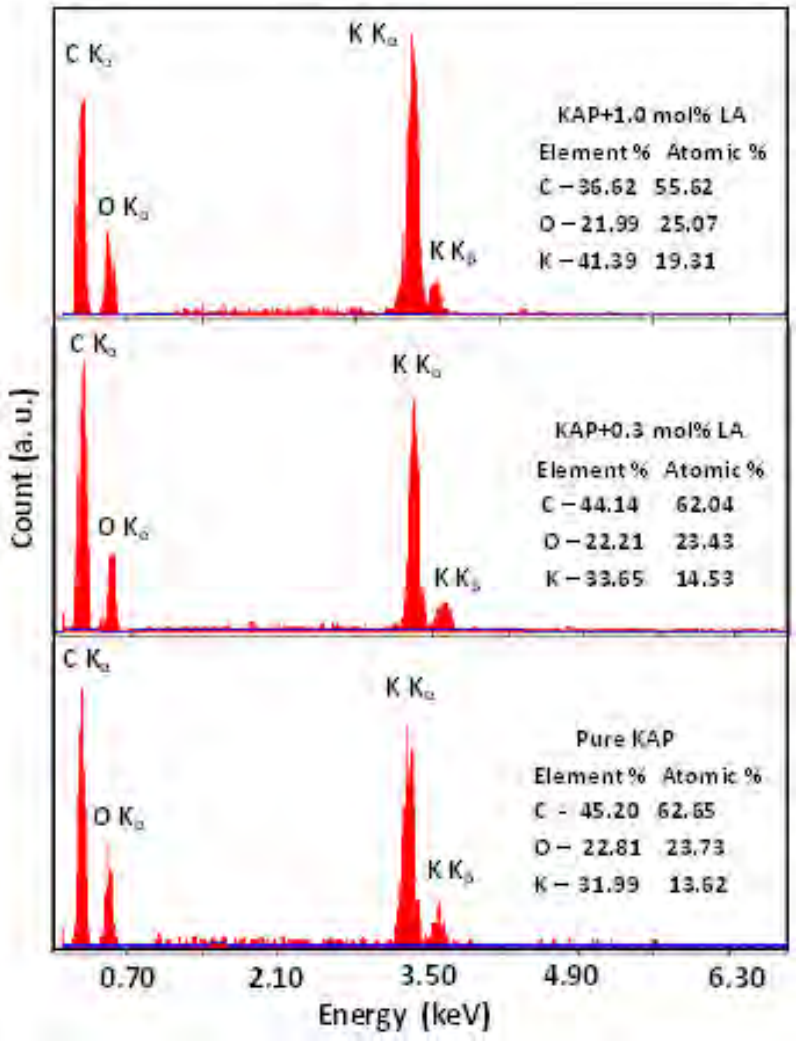

Fig. 6.4 EDX spectra for pure and LA doped KAP crystals

6.4.3 X-ray Diffraction Analysis

Powder XRD patterns were recorded for pure and LA doped KAP crystals and are presented in the fig. 6.5. The respective experimental data for pure and doped KAP of the XRD analysis viz., 2θ value and relative intensity for corresponding hkl values are presented in table 6.2. The lattice parameters and cell volume of pure and doped KAP crystals had shown in table 6.3. It was observed that the lattice parameters and cell volume of LA doped KAP crystals slightly differ from those of pure KAP, which may be attributed to the presence of LA doping in KAP crystals. Calculated cell parameters from the powder XRD analysis confirmed that the crystal structure (orthorhombic) of KAP had not changed by doping of LA

Lattice parameters calculation for Orthorhombic crystal system of KAP and LA doped KAP crystals

$$a \neq b \neq c \qquad \alpha = \beta = \gamma = 90^{\circ}$$

$$\frac{1}{d_{hkl}} = \sqrt{\frac{h^2}{a^2} + \frac{k^2}{b^2} + \frac{l^2}{c^2}}$$

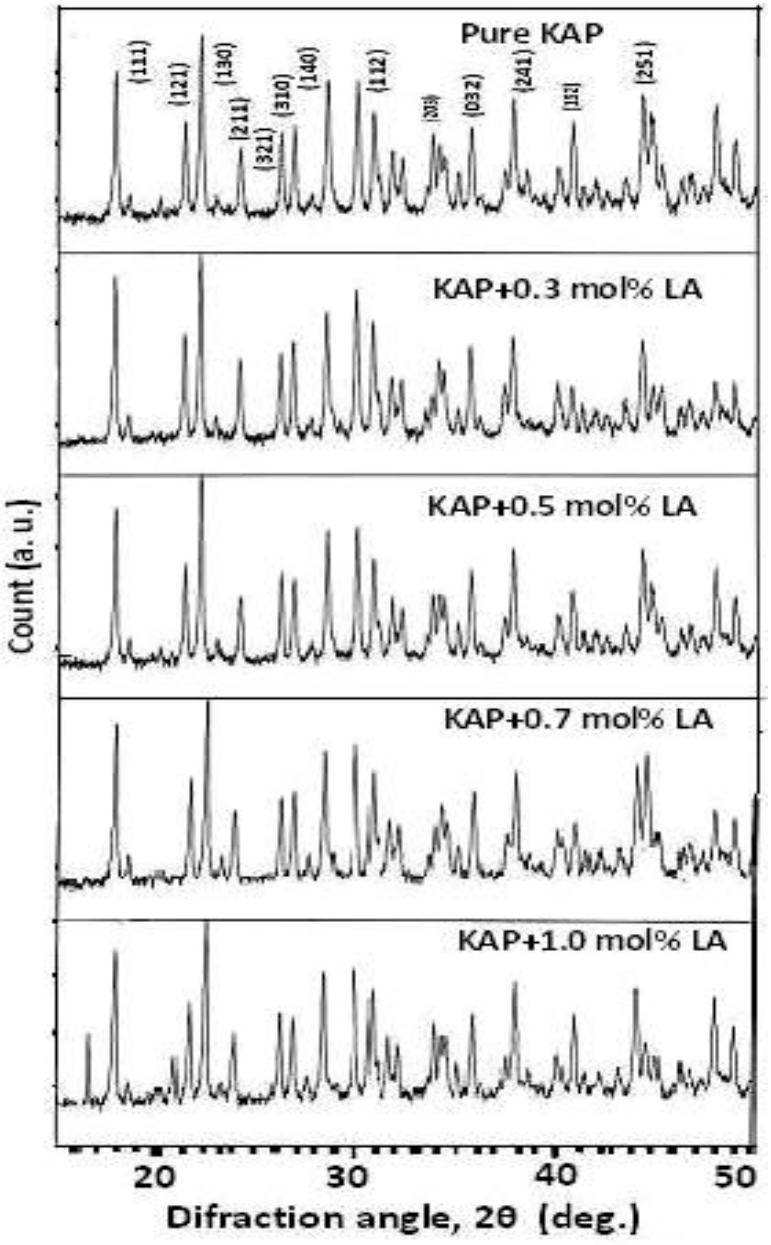

Fig. 6.5 XRD patterns for pure and LA doped KAP crystals

Table 6.2 Indexed powder diffraction data for pure and LA doped KAP crystals

Sample	(hkl)	$2\theta_{cal}(^0)$	I/I_0 (%)	$2\theta_{exp}(^0)$	$\Delta 2\theta$ (^{0}0
Pure KAP	111	17.97	67.01	17.938	-0.032
	121	21.38	28.29	21.387	+0.007
	130	22.38	100.00	22.184	-0.196
	211	24.13	21.31	24.118	-0.012
	002	26.83	31.45	26.823	-0.007
	310	28.48	60.18	28.485	+0.005
	112	29.99	59.40	30.001	+0.011
	320	30.82	38.27	30.806	-0.014
	032	34.11	22.69	34.113	+0.003
	241	35.71	29.56	35.716	+0.006
	410	37.78	47.23	37.804	+0.024
	251	44.25	49.99	44.251	+0.001
KAP+0.5 mol% LA	111	17.97	71.44	17.913	-0.057
	121	21.38	34.02	21.352	-0.028
	130	22.38	100.00	22.154	-0.230
	211	24.13	18.01	24.097	-0.033
	002	26.83	26.57	26.784	-0.046
	310	28.48	53.39	28.454	-0.026
	112	29.99	55.77	29.958	-0.032
	320	30.82	36.45	30.787	-0.033
	032	34.11	19.15	34.114	+0.004
	241	35.71	28.03	35.685	-0.025
	410	37.78	43.01	37.779	-0.001
	251	44.25	42.90	44.236	-0.014
KAP+1.0 mol% LA	111	17.97	73.90	17.942	-0.028
	121	21.38	36.49	21.371	-0.009
	130	22.38	100.00	22.181	-0.199
	211	24.13	21.02	24.120	-0.010
	002	26.83	28.27	26.813	-0.017
	310	28.48	54.86	28.474	-0.006
	112	29.99	56.90	29.981	-0.009
	320	30.82	44.30	30.812	-0.008
	032	34.11	19.65	34.117	+0.007
	241	35.71	29.93	35.711	+0.001
	410	37.78	48.85	37.795	+0.015
	251	44.25	44.93	44.257	+0.007

Table 6.3 Unit cell parameters of pure and LA doped KAP crystals

Crystal	Crystal system	a(Å)	b(Å)	c(Å)	Volume ($Å^3$)
Pure KAP	Orthorhombic	9.749	12.905	6.647	836.265
KAP+0.3 mol% LA	Orthorhombic	9.774	12.873	6.663	838.343
KAP+0.5 mol% LA	Orthorhombic	9.767	12.849	6.659	835.278
KAP+0.7 mol% LA	Orthorhombic	9.768	12.863	6.656	836.293
KAP+1.0 mol% LA	Orthorhombic	9.754	12.869	6.650	834.757

6.4.4 Optical Transmission Analysis

The UV-Vis optical transmission and absorption spectra of pure and doped KAP crystals had been shown in fig. 6.6 and fig. 6.7 respectively. This spectral study might assist in understanding electronic structure of the optical band gap of the crystals. It was clear from the fig.6.6 that the percentage of optical transmission increases with the increase of the concentration of LA in KAP crystals. All of them have sufficient transmission in the entire visible and near IR (infrared) region. This is the most desirable property of materials possessing NLO activity. There is a strong absorption at 280 nm. Absorption in the ultraviolet region arises from electronic transitions associated within the sample. Using the formula $E_g = hc/\lambda$, the band gap energy was found to be 4.428 eV. Hence, it could be concluded that the LA doping plays a key role in improving the optical quality of KAP crystals.

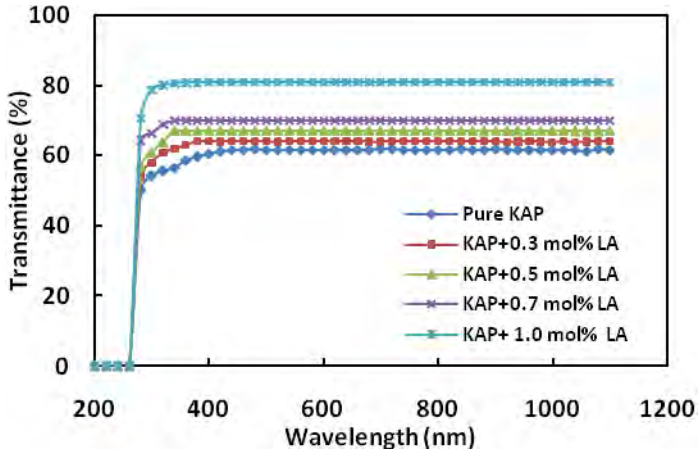

Fig. 6.6 Transmission spectra for pure and LA doped KAP crystals

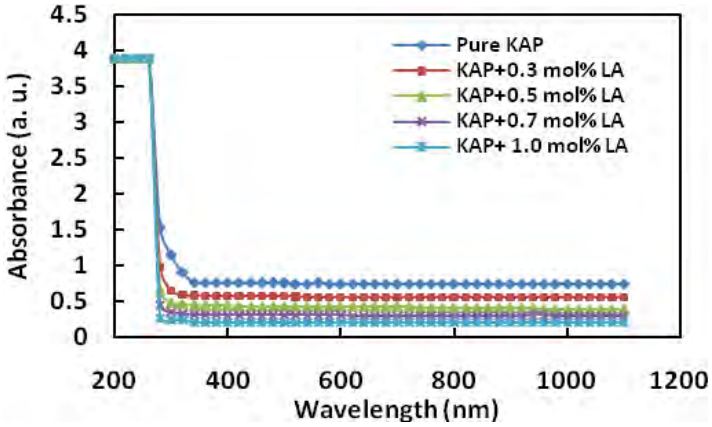

Fig. 6.7 Absorption spectra for pure and LA doped KAP crystals

6.4.5 Optical Parameters Calculation

The optical absorption coefficient (α) can be calculated from the transmittance using the following relation

$$\alpha = [2.3026 \log (1/T)]/d$$

Where T is the transmittance and d is the thickness of the sample. For a direct band gap material, the absorption coefficient (α) is related to light frequency according to the following formula.

$$\alpha h\nu = A(h\nu - E_g)^{1/2}$$

where A is a constant, E_g is the optical band gap energy, h is the Planck's constant and ν is the frequency of the incident photons. The band gap energy of the sample can be estimated by plotting $(\alpha h\nu)^2$ versus hν and by extrapolating the linear portion near the onset of absorption edge to the energy axis. *K* can be obtained from the following relation.

$$K = \frac{\alpha\lambda}{4\pi}$$

where λ is the wavelength. The reflectance (R) in terms of absorption coefficient can be written as: R = [exp(-αt)±√exp(-αt)-exp(-3αt)T +exp(-2αt)T] / exp(-αt)+exp(-2αt)T

The refractive index (n) can also be derived as

$$n = [-(R+1)\pm 2\sqrt{R}] /(R-1)$$

The variation of *K* and n with hν for pure and doped KAP crystals are shown in the figs. 6.8 and 6.9.

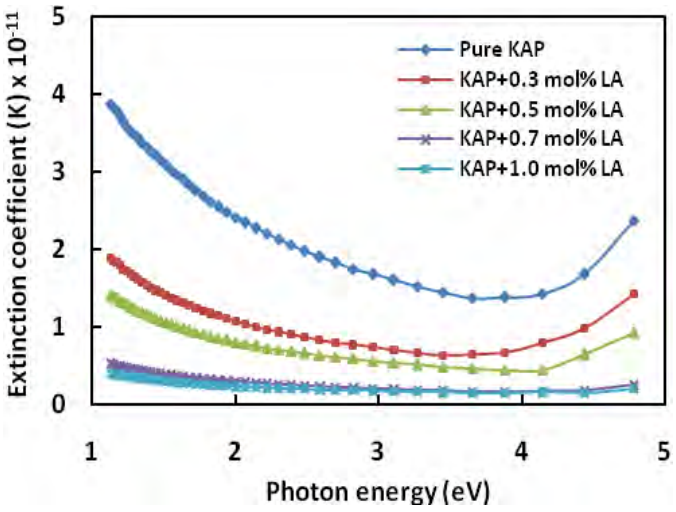

Fig. 6.8 Variation of extinction coefficient with photon energy

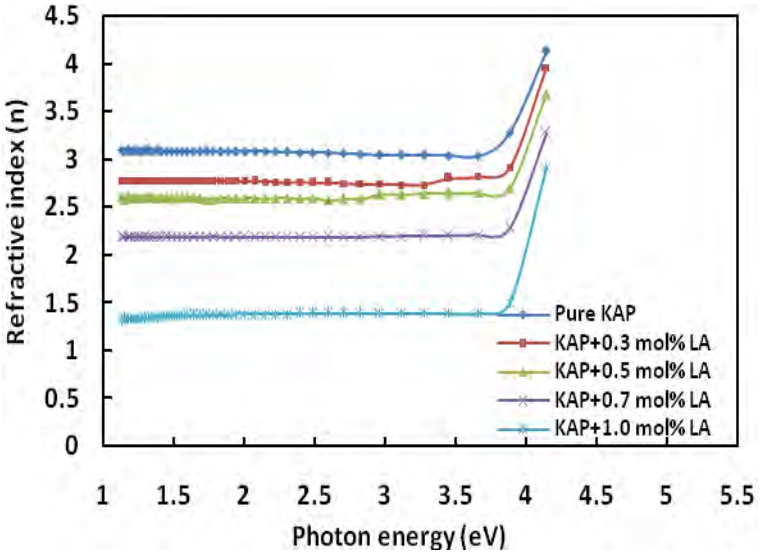

Fig. 6.9 Variation of refractive index with photon energy

6.4.6 Dielectric Studies

The study of dielectric constant (ε_r) of a material gives an outline about the nature of atoms, ions and their bonding in the material. The ε_r and tanδ depend on frequency of applied field. The real ε_r and imaginary ε_i parts of the dielectric constant can be determined using the formula $\varepsilon_r = n^2 - k^2$ and $\varepsilon_i = 2nk$. Dielectric loss was calculated using the formula $\tan\delta = \varepsilon_i/\varepsilon_r$.

Fig. 6.10 shows the variation of dielectric constant with photon energy. The value of dielectric constant decreases as the frequency increases and it becomes independent of frequency at higher frequency region. The high value of dielectric constant in the low frequency region may be due to the contributions of electronic, ionic, dipolar, and space charge polarizations. The electronic exchange of the number of ions in the crystal gives local displacement of electron in the direction of the applied field, which in turn give rise to polarization. Continuous and gradual decrease in dielectric constant suggests that pure and doped KAP crystals like any normal dielectric may possess domains of different size and varying relaxation times. It is evident that the lower value of dielectric constant is a suitable parameter for the enhancement of SHG coefficient. Fig. 6.11 shows the variation

of dielectric loss with photon energy at room temperature. This is the normal behavior observed earlier [1,2]. The dielectric loss is a measure of the energy absorbed by a dielectric. Usually the dielectric has a resistance R and reactance $1/\omega C$, which are related to the phase angle $\tan\delta = 1/\omega CR$, where C is a capacitance. So the low dielectric loss at high frequency reveals the superior optical quality of the crystals with lesser defects, and this parameter is of vital importance for various NLO application.

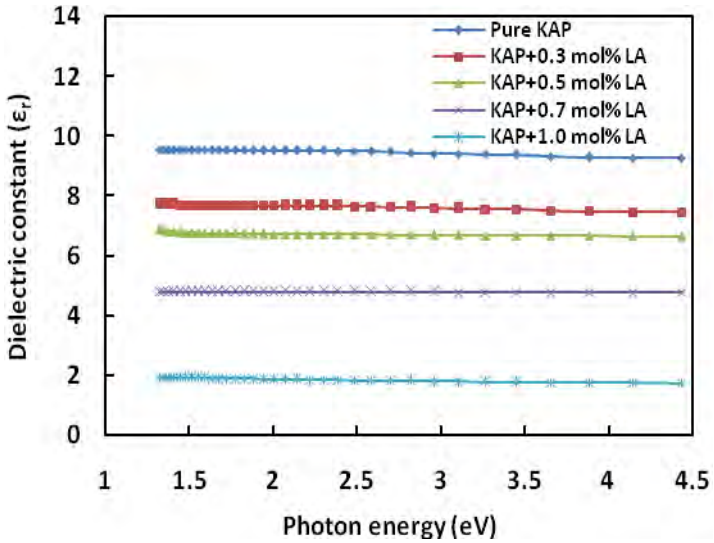

Fig. 6.10 Variation of dielectric constant with photon energy

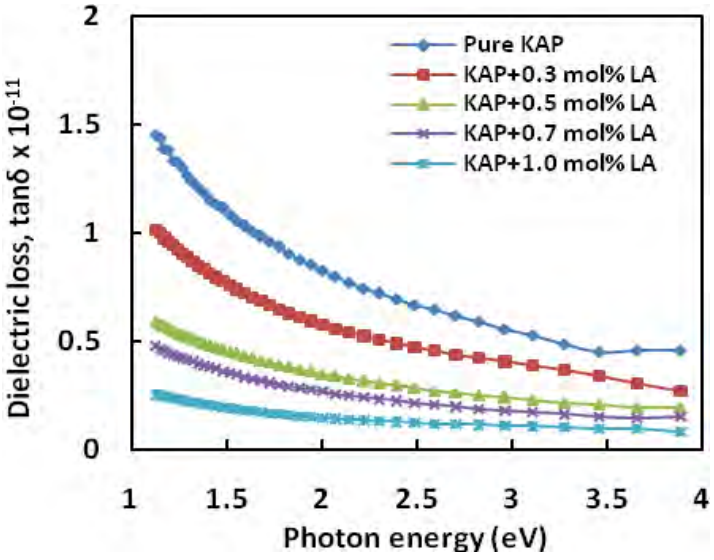

Fig. 6.11 Variation of dielectric loss with photon energy

6.4.7 Thermal Analysis

In this work, the effect of LA doping on thermal stability of KAP crystals was studied by employing TGA and DTA. Fig. 6.12 indicated thermo gram and differential thermal analysis for pure KAP crystal. The TGA trace showed the different stages of decomposition. The first stage of decomposition started at 281.0 ^{0}C and at about 302.5 ^{0}C it appeared to be the major stage of decomposition. So it was observed that initially crystal lost water of hydration and then became anhydrous and remained in that form up to the end of the analysis. But there is no weight loss below 281.0 ^{0}C. The DTA curve of pure KAP showed an endothermic peak at 296.8 ^{0}C. This endothermic peak corresponded to the decomposition temperature of the crystal. The TGA/DTA curves for LA doped Potassium acid phthalate were presented in figure 6.13 and fig. 6.14. The DTA curve of doped KAP+1mol% LA crystal showed an endothermic peak at 298.2 ^{0}C. The major stage of decomposition started at 303.6 ^{0}C. It was confirmed that there is no phase transition for pure and doped KAP crystals up to temperature range 30 ^{0}C to 201 ^{0}C.

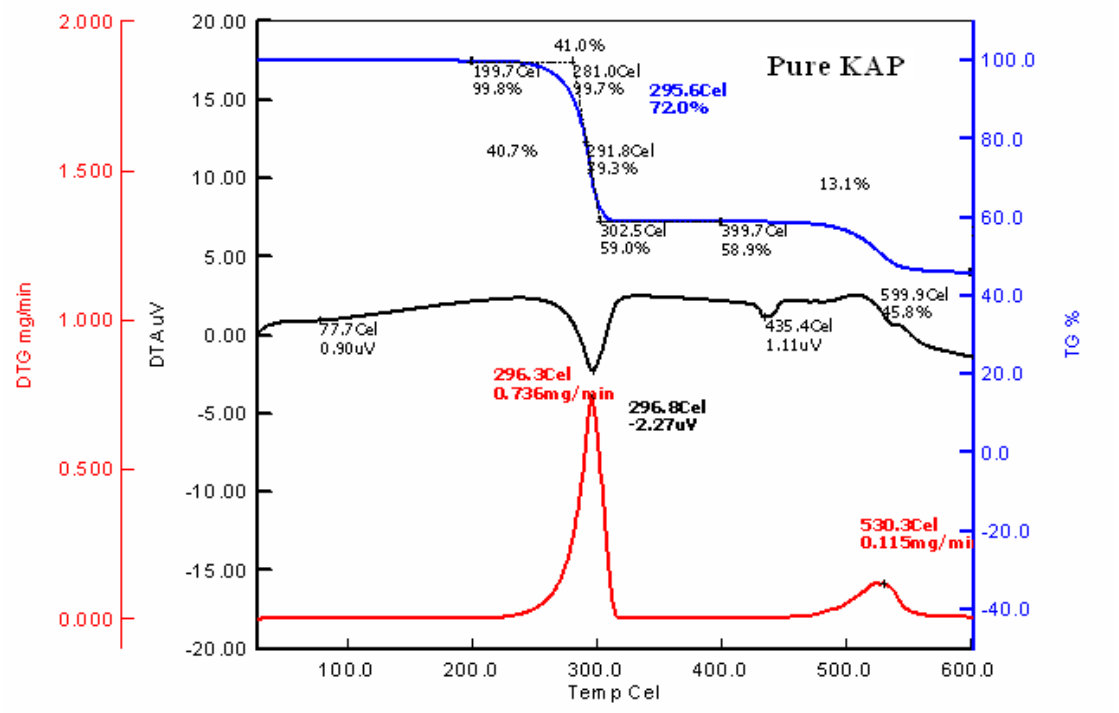

Fig. 6.12 Simultaneous TG, DTA and DTG curves for pure KAP crystal

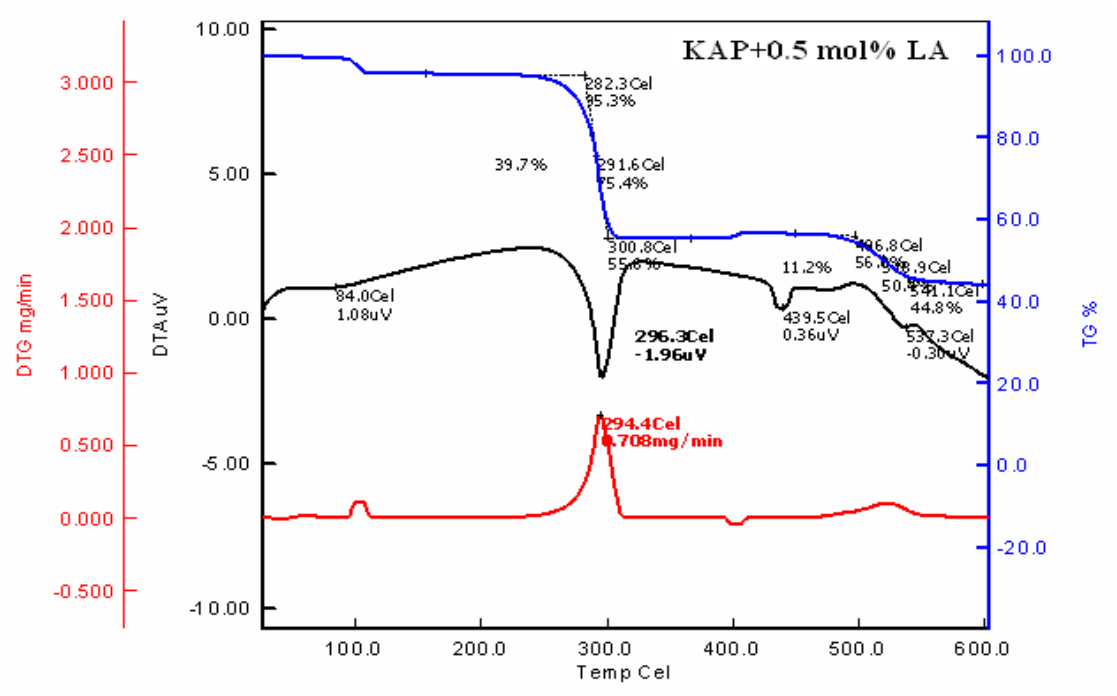

Fig. 6.13 Simultaneous TG, DTA and DTG curves for LA doped KAP crystals

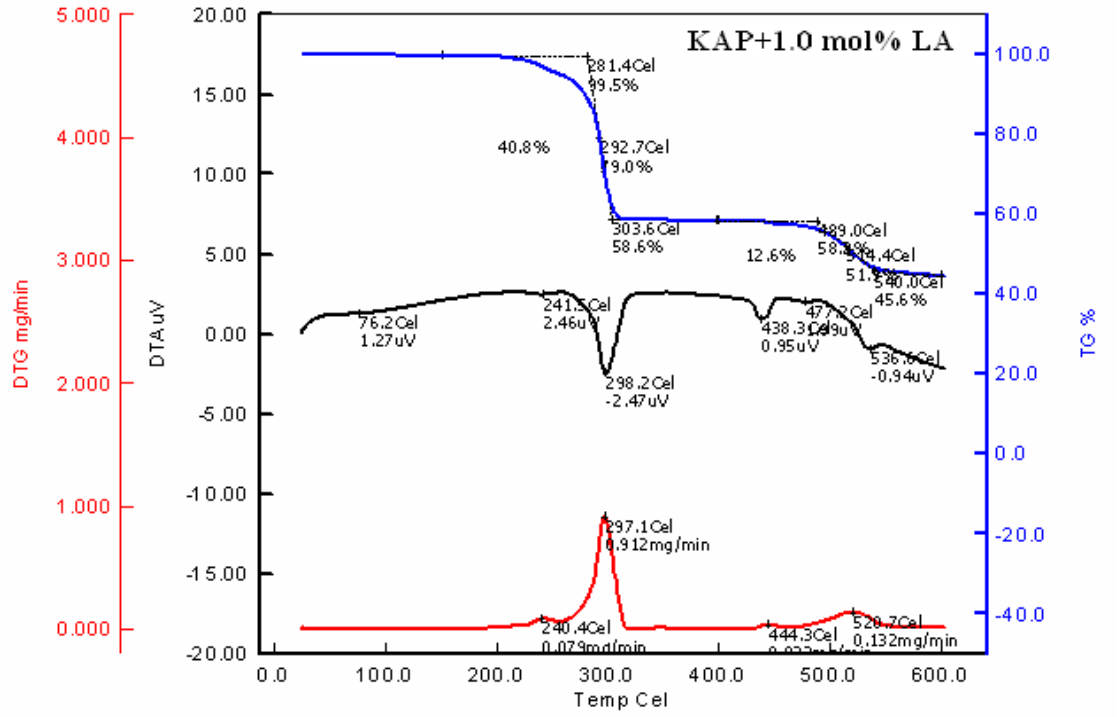

Fig. 6.14 Simultaneous TG, DTA and DTG curves for LA doped KAP crystals

6.4.8 Vicker's Microhardness Analysis

Hardness is an important property to characterize a crystal. Harder crystals are good for device fabrication. Hardness test is useful to find the mechanical hardness of the crystal and to estimate the threshold mechanical stress it can withstand. Vicker"s microhardness measurement of pure and LA doped KAP crystals was taken by varying applied loads 25, 50, 75 and 100 g for indentation time of 7 s. From fig. 6.15 the hardness value of pure and doped crystals were found to decrease with the applied loads because large prominent cracks due to the attainment of the threshold mechanical stress which is comparable with these results[11,21]. The hardness values were calculated using the formula: $H_v = [1.8544 \text{ X } P]/ D^2$ kg-mm^{-2}. Where H_v is the Vicker"s hardness number, P is the indenter load in kg and D is the diagonal length of the impression in mm. The microhardness value was taken as the average of the several impressions made with both diagonals being measured. In the present study, the hardness of the pure KAP crystal is higher than LA doped KAP crystals. This is because of the incorporation of the LA ($^{+}NH_3$, COO-) ions into superficial crystal lattice and forming defect centers which generate weak lattice stresses on the surface.

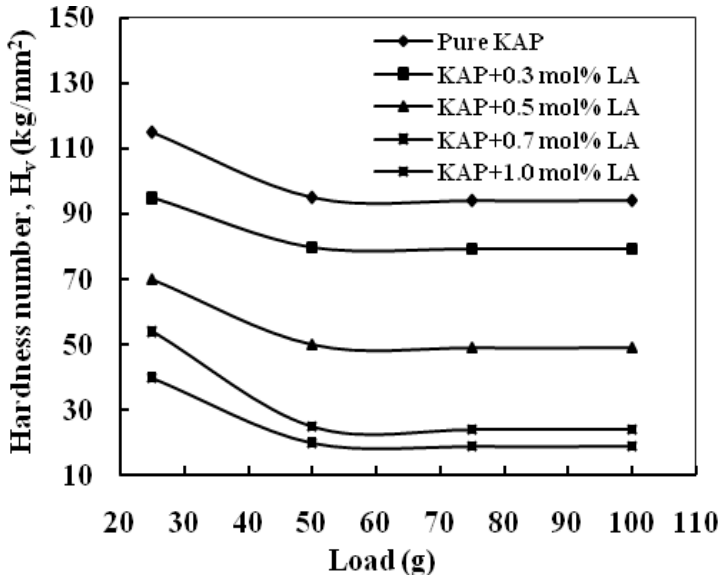

Fig. 6.15 Hardness number vs. load (g) of pure and LA doped KAP crystals

6.4.9 DC electrical Conductivity

A graph of DC conductivity vs. temperature of pure and LA doped KAP crystals is plotted in fig. 6.16. It is found that conductivity increases with temperature and also with LA concentration. Similar result has been obtained in the case of doping urea in KAP [9]. DC electrical conductivity is found in the order of 10^{-3} mho/m. At low temperature region, conductivity is expected due to the presence of weakly attached impurities and vacancies in the crystal lattice. At high temperature region, the attached water molecule is lost and fracture is developed and conductivity is caused mainly for intrinsic defects. These doping ions of LA may occupy some interstitial positions and create more defects. Due to these interactions between KAP and LA, the conductivity of doped KAP crystals may increased.

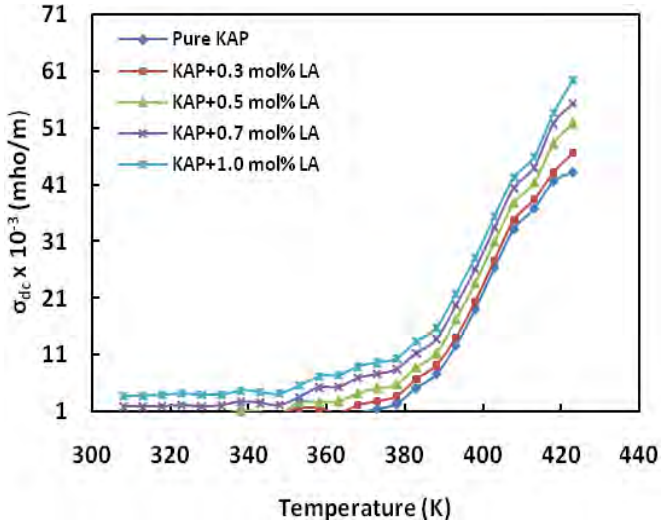

Fig. 6.16 DC electrical conductivity with temperature

6.4.10 Etching Study

Etching method is a very common and inexpensive technique to reveal dislocations and lattice inhomogenities of the crystals. The chemical etching studies were carried out on the as grown single crystal of pure and LA doped KAP crystals to study the distribution of structural defects in the grown crystal. The surfaces of sample were polished and no scratches markings were visible under an optical microscope. This was then etched in the

etching solution (water) at room temperature for 10 s. Then soaked with a filter paper and examined under an optical microscope in reflection. The etching figure Illustrates the typical etch pattern observed on the (010) plane of the pure and LA doped KAP crystal. These etch-pits were formed due to dislocations which were formed during the period of crystal grow. The generation of dislocations was strongly correlated with the formation of inclusions in the crystals. Depending on the shape of the seed crystal, inclusions may also arise. The reason for bulk of the inclusions getting trapped could be due to fluctuations in supersaturation close to the crystal or due to transition from dissolution to growth. A number of parameters such as variation in supersaturation during the growth, non-uniform growth rate, etc., are responsible for the formation of inclusions. The etch pit patterns are shown in the figs. 6.17 and 6.18.

Fig. 6.17 Etch pit patterns on (010) plane of pure KAP crystal

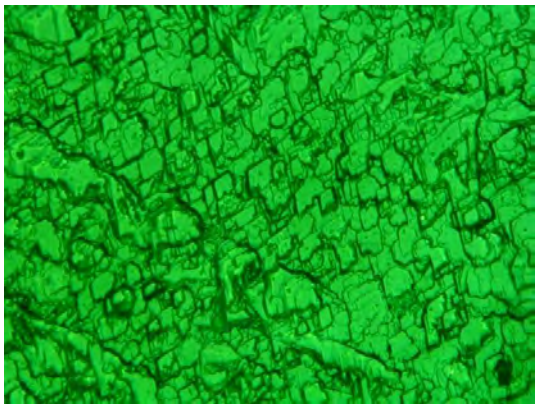

Fig. 6.18 Etch pit patterns on (010) plane of 1.0 mol% LA doped KAP crystal

6.5 Conclusions

Good quality pure and LA doped KAP crystals were successfully grown by using the slow solvent evaporation technique at room temperature. Solubility test was carried out which indicates double distilled water as a suitable solvent for growing pure and LA doped crystals. The doping of LA in the KAP crystal was confirmed by EDX analysis. The cell parameters of the crystals were calculated from powder X-ray diffraction data. XRD data confirmed that the crystal structure (orthorhombic) of pure KAP did not change by doping of LA. The FTIR analysis confirmed the presence of all functional groups of KAP and LA. The absence of absorption and excellent transmission in the entire visible region makes these crystals a good candidate for optoelectronic applications. The thermal study of grown LA doped crystals indicated that these crystals can be exploited for NLO applications up to the temperature of 281 ^{0}C. Thus LA doped KAP crystals are going to play a vital role in the field of optoelectronics and laser technique.

6.6 References

[1] Krishnan, S., Justin Raj, C., Dinakaran, S. and Jerome Das, S.,"Investigation of optical band gap in potassium acid phthalate single crystal", Cryst. Res. Technol. **43**, No. 6, p.670-673, 2008.

[2] Benedict, J. B., P.M. Wallace, P.J. Reid and Jang, S.H., "Optically nonlinear single crystals of potassium hydrogen phthalate", Adv. Mater., **15,** p.1068-1070, 2003.

[3] Bernal, J.D., Zeitschrift fuer Kristallographie, Kristallphysik, Kristallchemie, **78,** p.363-369, 1931.

[4] Destro, R., Marsh, R.E. and Bianchi, R., "A low-temperature (23K) study of L-alanine", J. Phys. Chem., **92 (4),** p.966-973, 1988.

[5] Halfpenny, E.G.R., J. Cryst. Growth, **187,**p. 111, 1998.

[6] Lorin, K.F., Le Moigne, A. and Szpunar, J., Acta Phys. Pol. A **87**, p.713, 1995.

[7] Miyashita, Y. O., Murakami, A., Aoki, K., and Yamaguchi, S., Proc. SPIE Int. Soc. Opt. Eng. **1503**, p. 463, 1991.

[8] Misoguti, L., Varela, A. T., Nunes, F. D., Bagnato, V. S., Melo, F. E. A., Mendes Filho, J. and Zilio, S. C., "Optical properties of L-alanine organic crystals", Opt. Mater. **6**, p.147-152, 1996.

[9] Meera, K., Muralidharan, R., Jeyavel, R. and Ramasamy, P., J. Cryst. Growth **263,** p. 510, 2004.

[10] Uthayarani, K., Sankar, R. and Shashidharan Nair, C. K., "Growth, Spectral and thermal properties of KAP single crystals in the presence of DL-alanine and L-methionine amino acid dopants", Cryst. Res. Technol. **43**, No. 7, p.733-739, 2008.

[11] Jones, L., Paschen, K. W. and Nicholson, J. B.,"Comparison between pure and deuterated potassium acid phthalate", J. Appl. Opt. **2,** p. 955, 1963.

[12] Stemmler, B. L.and Legrand, P., Rev. Sci. Instr. **66,** p.1601, 1995.

[13] Srinivasan, K. N., "Temperature-dependent refractive index of KAP", Opt. Mat. **27,** p.389, 2004.

[14] Simpson Jr., H. J., and Marsh, R. E., "Micro-transitions or breathers in L-alanine", Acta. Cryst. **8,** p.550, 1966.

[15] Varma, K. B. R. and Shankar, M. V., "Piezoelectric resonance in KAP single crystals", Ferroelectrics Lett., **21**, 55-59,1996.

[16] Vijayan, N., Rajasekaran, S., Bhagavannarayana, Ramesh Babu, R., Gopalakrishnan, R., Palanichamy, M., and Ramasamy,P., Crystal Growth & Design, Vol. **6**, No. 11, p. 2441-2445, 2006.

[17] Mohan Kumar, R., Muraliddharan, R., Rajan Babu, D., Rajendiran, K. V., Jayavel, R., Jayaraman, D., and Ramasamy,P., J. Cryst. Growth **229**, p.568, 2001.

[18] Bartkiewicz, M.A., Adv. Mater. Opt. Electron. **2**, p.157, 1993.

[19] Aggarwal, M.D., J. Stephens, A.K. Batra and Lal,R. B., "Bulk crystal growth and characterization of semiorganic nonlinear optical materials", J. Optoelectron. Adv. Mater., **5**, p.555-562, 2003.

[20] Kejalakshmy, N. and Srinivasan, K., "Electro-optic properties of potassium hydrogen phthalate crystal and its application as modulators", J. Phys. D: Applied Phys., **36**, p.1778-1782, 2003.

[21] Kajzar, F., A. Lorin, J. Le Moigne and Szpunar, J**., "**Habit modification of KAP single crystals by impurities", Acta Phys. Pol. A **87**, p.713, 1995.

[22] Vijayan, N., S. Rajasekaran, G. Bhagavannarayana, R.R. Babu, R. Gopalakrishnan, M. Palanichamy and Ramasamy, P., "Growth and characterization of nonlinear optical amino acid single crystal: l-alanine", Cryst. Growth Design, **6**, p.2441-2445, 2006.

[23] Vasudevan, G.,AnbuSrinivasan, P., Madhurambal, G. and Mojumdar, S. C., "Thermal analysis, Effect of dopants, Spectral Characterization and Growth Aspects of KAP Crystals", Journal of Thermel Analysis and Calorimetry, Vol. **96**, 1, p.99-102, 2009.

Chapter 7

Summary and Suggestions for Future Work

Chapter 7

Summary and Suggestions for Future Work

7.1 Summary

KDP, ADP, KAP and LA NLO crystals have wide applications in microelectronics, optoelectronics and also in satellites. To improve the quality of the crystals, the addition of small amount of impurities always plays a vital role. LA has been used as dopant in this research work to modify the nucleation behavior and to improve the quality of the technologically important crystals like ADP, KDP, and KAP.

Growth conditions of pure and LA doped ADP, KDP, KAP and pure LA crystals have been investigated. An investigation has been made on the basic growth parameters such as solubility and nucleation. The solubility of pure LA, pure and doped ADP, KDP, and KAP was determined at different fixed temperatures (viz. 30, 35, 40, 45 and 50 ^{0}C) in a constant temperature bath maintained with an accuracy of ±0.01 ^{0}C. It has been found that the solubility increased with temperature but reduced with doping concentration. Large size NLO crystals viz. pure ADP, KDP, KAP, LA and doped ADP, KDP, KAP were successfully grown from supersaturated solutions by solvent evaporation method.

The functional groups present in the grown crystals were confirmed by FTIR spectral analysis. The frequencies with their relative intensities obtained in FTIR of pure and doped ADP, KDP and KAP crystals are discussed. The peak positions have been moved from lower to higher energy due to the presence of LA in to ADP and KDP crystals. For example, the PO_4 vibration of the parent is shifted from 405 to 415 cm^{-1} for ADP and from 416 to 445 cm^{-1} for KDP crystals. In the case of KAP crystal C-COO vibration of the parent is shifted from 1225 to 1254 cm^{-1}. All these results confirmed the presence of LA in to ADP, KDP and KAP crystals.

The presence of doping elements in to pure ADP, KDP and KAP has been analyzed by EDX spectroscopy. The presence of the atomic percent of C element in the EDX spectrum confirmed the presence of LA into pure ADP and KDP crystals. The increase of

atomic percent of C in the EDX spectrum of KAP crystal confirmed the presence of pure KAP crystal.

Crystalline quality and the structures of pure LA, pure and LA doped ADP, KDP and KAP crystals are analyzed through powder XRD. The XRD reflections were indexed using the conventional procedures and lattice parameters were calculated. The values are found to be in good agreement with standard data. The XRD results confirmed the orthorhombic crystal structure of pure LA and KAP crystals. Tetragonal structure of pure and doped ADP and KDP crystals was confirmed from XRD data. The presence of LA dopants has marginally altered the lattice parameters without affecting the basic structure of crystals.

UV-Vis spectra for pure and LA doped crystals have sufficient transmission in the entire visible region. The percentage of transmission of pure crystals increases with doping concentration from 80 to 95% for ADP, 85 to 97% for KDP and 61 to 81% for KAP crystals. It is happened due to the presence of LA ($^{+}NH_3$, COO^{-}) ions. The dielectric constant and dielectric loss have been calculated from transmission data. It is found that both dielectric constant and dielectric loss are decreased with doping concentration and also with frequency.

Decomposition temperature, weight loss and transition temperature of all crystals are confirmed by TGA and DTA analysis. The decomposition temperature 272 ^{0}C of pure LA was found from DTA graph. The increasing decomposition temperatures due to the presence of LA from 198 to 209 ^{0}C for ADP, 229 to 231 ^{0}C for KDP and 297 to 298 ^{0}C for KAP crystals were observed in the DTA graphs.

Vicker"s microhardness measurement of pure LA, pure and LA doped ADP, KDP and KAP crystals was taken by varying applied loads 25, 50, 75 and 100 g for indentation time of 7 s. The hardness value of pure and doped crystal was found to decrease with the applied loads because large prominent cracks start due to the attainment of the threshold mechanical stress. It is found that the hardness of the pure crystals is higher than LA doped crystals. This is because of the incorporation of the LA ($^{+}NH_3$, COO^{-}) ions into

superficial crystal lattice and forming defect centers which generate weak lattice stresses on the surface.

DC electrical conductivity was measured at different temperatures ranging from 35 to 140 ^{0}C by conventional two probe method. It is found that the conductivity has increased from 0.02 x 10^{-6} to 3.97 x 10^{-6} mho/m for pure to doped ADP crystals with temperatures and also with doping concentration. Similar result has been found from 0.15 x 10^{-3} to 3.86 x 10^{-3} mho/m in the case KAP crystals. The AC electrical conductivity has been decreased from 1.79 x 10^{-5} to 0.92 x 10^{-5} mho/m with doping concentration and increased with temperature for KDP crystals. As the conduction in KDP is protonic and mainly due to the anions [$(H_2PO_4)^+$] and not the cations (K^+) for KDP, the additional hydrogen bonds created may reduce the L-defects (vacant hydrogen bonds) and consequently obstruct the movement of protons. This may be the reason for the decrease in conductivity value with the increase in impurity concentration. Both dielectric constant and dielectric loss have been decreased with temperatures and also with doping concentration.

Surface morphology of all crystals has been characterized by etching in water for 10 s at room temperature on (001) plane of pure LA on (001) plane of pure and doped KDP and ADP and on (010) plane of KAP crystals. The middle portion of the etched surface of LA crystal is more or less smooth and show uniform growth bands. Towards the edge of the crystal, more number of defects is seen. Which reveal the layer growth mechanism of LA crystal. The triangular type etch pits on the etched surfaces of pure and doped KDP, ADP and KAP crystals reveal that their surfaces possess high and low growth steps.

The results obtained from the present investigations indicate that the optically transparent colorless large size doped ADP, KDP and KAP crystals can be grown by solvent evaporation method. From the experimental data it is found that all crystals have sufficient transmittance in the visible region but the transmittance of the ADP crystal has increased more than KDP and KAP crystals. The thermal stability and DC electrical conductivity of ADP crystals have also been increased.

7.1 Comparison data between pure and LA doped KDP, ADP, KAP and pure LA crystals

Properties	Pure LA	Pure KDP	1.0 mol% LA doped KDP	Pure ADP	1.0 mol% LA doped ADP	Pure KAP	1.0 mol% LA doped KAP
Transmittance (%)	80	85	97	80	95	62	81
Decomposition Temp. (^{0}C)	272.00	229.40	230.80	198.30	208.90	296.80	298.20
Electrical conductivity (mho/m)	2.00 x 10^{-8}	1.79 x 10^{-5}	0.92 x 10^{-5}	0.95 x 10^{-6}	3.97 x 10^{-6}	1.15 x 10^{-3}	5.20 x 10^{-3}
Microhardness at 25 g	74.50	179.50	90.00	98.40	70.00	115.00	40.00
Band gap energy (eV)	2.75	4.91	5.30	4.80	5.15	4.43	4.43

7.2 Suggestions for future work

Efforts can be made to grow large size LA doped crystals by changing the crystal growth technique, pH of the solution, using different solvent or using the mixed solvent. Growth kinetics such as metastable zone width, induction period, interfacial energy, critical free energy, critical nucleus etc. of LA doped crystals can be done in future.

Due to lack of facilities, second harmonic generation study could not carry out on the growth LA doped crystals. Optical characterization like second harmonic efficiency of the fabricated SHG optical elements from the LA doped ADP, KDP and KAP crystals may be carried out with high power fundamental laser source. This will lead to the judge of maximum conversion efficiency of the optical elements. Fabrication of SHG cell and the device characteristics studies will be of great interest from the application point of view. The efficiencies of the fabricated third, fourth and fifth harmonic generation elements may also be studied. The fabricated electro-optic modulation elements may be utilized for a voice modulation process.

Publications

(a) Journals

[1] **Ferdousi Akhtar**, and Jiban Podder, "Structural, Optical, Electrical and Thermal Characterizations of Pure and L-alanine Doped Ammonium Dihydrogen Phosphate Crystals", Journal of Crystallization Process and Technology, Vol. 1, No. 2, pp.18-25, 2011.

[2] **Ferdousi Akhtar** and Jiban Podder, "Studies on the Effect of L-alanine on the Structural, Optical and Thermal Properties of Potassium Acid Phthalate Crystals", Journal of Applied Sciences, 11 (16), p.2974-2983, 2011.

[3] **Ferdousi Akhtar** and Jiban Podder, "A Study on Growth, Structural, Optical and Electrical Characterization of L-alanine Single Crystal for Optoelectronic Devices" (Communicated to the "Journal of Applied Sciences").

[4] **Ferdousi Akhtar** and Jiban Podder, "A Study on Structural, Optical, Electrical and Etching Characteristics of Pure and L-alanine Doped Potassium Dihydrogen Phosphate Crystals", Journal of Crystallization Process and Technology, Vol. 3, pp. 55-62, 2011.

(b) Contributed Research Presentation in the Conferences:

(Published in the Abstract Book)

[1] **Ferdousi Akhtar** and Jiban Podder, "Growth and Optical Characterization of Pure and L-alanine doped Potassium Acid Phthalate (KAP) Crystals", National Conference on Physics for Developmant, organized by Bangladesh Physical Society, Abstract Book-paper no. CW-II-B 02, February 10-11, 2011.

[2] **Ferdousi Akhtar** and Jiban Podder, "Growth, EDX, FTIR, Electrical and Thermal Characterization of Amino Acid (L-alanine) Crystals", National Conference on Physics for Developmant, organized by Bangladesh Physical Society, Abstract Book-paper no. CW-II-B 05, February 10-11, 2011.